Vol. 296, No. 2, October 10, 1994 ISSN 0003-2670

ANALYTICA CHIMICA ACTA

An international journal devoted to all branches of analytical chemistry

ELSEVIER

ANALYTICA CHIMICA ACTA

Scope. *Analytica Chimica Acta* publishes original papers, rapid publication letters and reviews dealing with every aspect of modern analytical chemistry. Reviews are normally written by invitation of the editors, who welcome suggestions for subjects. Letters can be published within **four months** of submission. For information on the Letters section, see inside back cover.

Submission of Papers

Americas

Prof. Harry L. Pardue
Department of Chemistry
1393 BRWN Bldg, Purdue University
West Lafayette, IN 47907–1393
USA

Tel:(+1-317) 494 5320
Fax:(+1-317) 496 1200

Computer Techniques

Prof. J.T. Clerc
Universität Bern
Pharmazeutisches Institut
Baltzerstrasse 5, CH-3012 Bern
Switzerland

Tel:(+41-31) 6314191
Fax:(+41-31) 6314198

Prof. Sarah C. Rutan
Department of Chemistry
Virginia Commonwealth University
P.O. Box 2006
Richmond, VA 23284-2006
USA
Tel:(+1-804) 367 7517
Fax:(+1-804) 367 8599

Other Papers

Prof. Alan Townshend
Department of Chemistry
The University
Hull HU6 7RX
Great Britain

Tel:(+44-482) 465027
Fax:(+44-482) 466410

Prof. Willem E. van der Linden
Laboratory for Chemical Analysis
Department of Chemical Technology
Twente University of Technology
P.O. Box 217, 7500 AE Enschede
The Netherlands
Tel:(+31-53) 892629
Fax:(+31-53) 356024

Prof. Paul Worsfold
Dept. of Environmental Sciences
University of Plymouth
Plymouth PL4 8AA
Great Britain

Tel:(+44-752) 233006
Fax:(+44-752) 233009

Submission of an article is understood to imply that the article is original and unpublished and is not being considered for publication elsewhere. *Anal. Chim. Acta* accepts papers in English only. There are no page charges. Manuscripts should conform in layout and style to the papers published in this issue. See inside back cover for "Information for Authors".

Publication. *Analytica Chimica Acta* appears in 16 volumes in 1994 (Vols. 281–296). *Vibrational Spectroscopy* appears in 2 volumes in 1994 (Vols. 6 and 7). Subscriptions are accepted on a prepaid basis only, unless different terms have been previously agreed upon. It is possible to order a combined subscription (*Anal. Chim. Acta* **and** *Vib. Spectrosc.*).
Our p.p.h. (postage, packing and handling) charge includes surface delivery of all issues, except to subscribers in the U.S.A., Canada, Australia, New Zealand, China, India, Israel, South Africa, Malaysia, Thailand, Singapore, South Korea, Taiwan, Pakistan, Hong Kong, Brazil, Argentina and Mexico, who receive all issues by air delivery (S.A.L.–Surface Air Lifted) at no extra cost. For Japan, air delivery requires 25% additional charge of the normal postage and handling charge; for all other countries airmail and S.A.L. charges are available upon request.

Subscription orders. Subscription prices are available upon request from the publisher. Subscription orders can be entered only by calendar year and should be sent to: Elsevier Science B.V., Journals Department, P.O. Box 211, 1000 AE Amsterdam, The Netherlands. Tel: (+31-20) 5803 642, Telex: 18582, Telefax: (+31-20) 5803 598, to which requests for sample copies can also be sent. Claims for issues not received should be made within six months of publication of the issues. If not they cannot be honoured free of charge. Readers in the U.S.A. and Canada can contact the following address: Elsevier Science Inc., Journal Information Center, 655 Avenue of the Americas, New York, NY 10010, U.S.A. Tel: (+1-212) 633 3750, Telefax: (+1-212) 633 3990, for further information, or a free sample copy of this or any other Elsevier Science journal.
Advertisements. Advertisement rates are available from the publisher on request.

US mailing notice – Analytica Chimica Acta (ISSN 0003-2670) is published 3 times a month (total 48 issues) by Elsevier Science B.V. (Molenwerf 1, Postbus 211, 1000 AE Amsterdam). Annual subscription price in the USA US$ 3035.75 (valid in North, Central and South America), including air speed delivery. Second class postage paid at Jamaica, NY 11431. *USA Postmasters*: Send address changes to Anal. Chim. Acta, Publications Expediting, Inc., 200 Meacham Av., Elmont, NY 11003. Airfreight and mailing in the USA by Publication Expediting.

ANALYTICA CHIMICA ACTA

An international journal devoted to all branches of analytical chemistry

(Full texts are incorporated in CJELSEVIER, a file in the Chemical Journals Online database available on STN International; Abstracted, indexed in: Aluminum Abstracts; Anal. Abstr.; Biol. Abstr.; BIOSIS; Chem. Abstr.; Curr. Contents Phys. Chem. Earth Sci.; Engineered Materials Abstracts; Excerpta Medica; Index Med.; Life Sci.; Mass Spectrom. Bull.; Material Business Alerts; Metals Abstracts; Sci. Citation Index)

VOL. 296 NO. 2 CONTENTS OCTOBER 10, 1994

ELSEVIER

Analytica Chimica Acta 296 (1994) 115–117

ANALYTICA CHIMICA ACTA

Letter

Simultaneous determination of iron(II)/iron(III) by sorbent extraction with flow-injection atomic absorption detection

S. Krekler [a], W. Frenzel [a,*], G. Schulze [b]

[a] *Institut für Technischen Umweltschutz, Technische Universität Berlin, Str. des 17. Juni 135, D-10623 Berlin, Germany*
[b] *Institut für Anorganische und Analytische Chemie, Technische Universität Berlin, Str. des 17. Juni 135, D-10623 Berlin, Germany*

Received 29 July 1994

Abstract

Flow-injection atomic spectrometry with sorbent extraction preconcentration is applied to the simultaneous determination of iron(II) and iron(III). Upon injection of a sample containing iron in both oxidation states, iron(III) is directly carried to the flame atomic absorption spectrometer whereas the iron(II)–ferrozine complex formed in-line is temporarily retained on a C_{18}-modified silica column placed between the injection valve and spectrometer and is subsequently eluted with methanol.

Keywords: Atomic absorption spectrometry; Flow injection; Iron; Preconcentration; Sorbent extraction

1. Introduction

On-line separation and preconcentration in flow-injection analysis (FIA) has received considerable attention during recent years and is widely applied for selectivity and sensitivity enhancement [1]. The capabilities of this approach for speciation studies have been exploited using subsequent determination of the individual species with parallel and serial arrangement of detectors, determination of one species and the total amount and subtraction of results, and separation of the species by temporary ion-exchange retention of one compound with sequential determination [2–5].

In this letter the use of FIA with sorbent extraction [4] is examined for simultaneous determination of iron(II) and iron(III) with flame atomic absorption spectrometric detection. The proposed technique makes possible the direct determination of iron in the two oxidation states, avoiding the neccessity of subtracting results.

2. Experimental

2.1. Apparatus

The arrangement of the flow system is depicted in Fig. 1. A Varian SpectrAA-400 atomic spectrometer with air–acetylene flame and 10-cm slit burner was used. Optimal conditions for determination of iron were set according to the manufacturer's instructions. The flow system was composed of a multichannel peristaltic pump, two six-port injection valves, Kel-F mixing tees and PTFE-tubing of 0.5 mm I.D. for interconnections. The microcolumns were made of small pieces of Tygon-tubing (ca. 15

* Corresponding author.

SSDI 0003-2670(94)00369-6

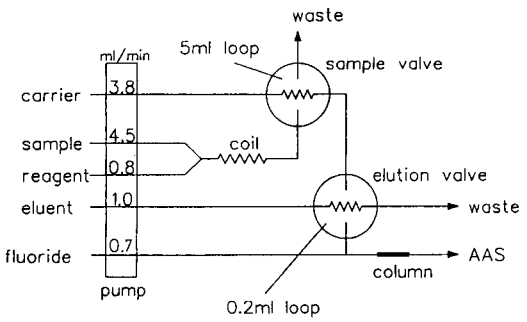

Fig. 1. Optimized FI manifold for iron speciation using sorbent extraction with atomic absorption spectrometric (AAS) detection. For procedural details see text.

mm long and 2 mm I.D.) filled with C_{18}-modified silica (Bakerbond, 40-μm particles).

2.2. Reagents and solutions

Deionized, doubly distilled water was used for all solution preparations and served as the carrier stream. The reagent solution contained 0.05% ferrozine (Ferrospectral, Merck, Cat. No. 11613) and 12% sodium acetate in 10^{-3} mol l^{-1} hydrochloric acid (pH 4.5). Methanol was used as eluent. Iron standards in the two oxidation states were prepared from ammonium iron(II) and iron(III) sulphate by serial dilution of stock solutions (1 g l^{-1} Fe each) with 1% (w/v) hydrochloric acid.

2.3. Procedure

The flow system used is described in Fig. 1. Initially the carrier stream is continuously pumped into the atomic spectrometer and the baseline absorbance is set to zero. Blank, standards and sample solutions are successively aspirated, merged with ferrozine reagent, mixed in the reaction coil and fed into the 5-ml loop of the sample valve. Then the valve is switched and the contents are transferred through the microcolumn into the atomic spectrometer. Iron(III) is not retained, and gives a broad plateaux signal (Fig. 2) the height of which is taken for signal evaluation. After return to baseline (i.e. passage of the 5-ml sample plug), 200 μl of methanol are injected via the elution valve which readily desorbs the iron(II)–ferrozine complex giving rise to a sharp iron signal (Fig. 2).

3. Results and discussion

Iron(II) forms stable, coloured complexes with many organic reagents such as phenanthroline derivates and certain triazine compounds. To be applied for sorbent extraction preconcentration a high partition coefficient of the complex between the solid absorber and the aqueous sample is desirable and fast removal from the column must be possible using a suitable eluent. Experimental investigations

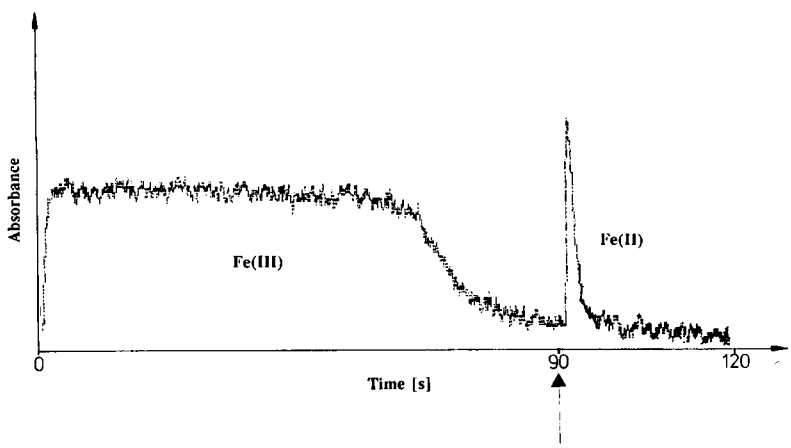

Fig. 2. Typical recorder trace obtained for the determination of mixed iron(II)/iron(III) standards using the manifold shown in Fig. 1. The concentration of iron(III) and iron(II) was 1.5 mg l^{-1} iron(III) and 75 μg l^{-1} iron(II). The arrow indicates the moment of methanol injection.

revealed that the Fe(II)–ferrozine complex is well suited for this purpose and methanol can be used for instant elution. With a 5-ml sample volume (corresponding to about 80 s preconcentration time) the linear working range for iron(II) determination is 5–500 $\mu g\ l^{-1}$ Fe. The relative standard deviation of repetitive measurements is typically $< 5\%$. Iron(III) determination was carried out in the range 0.25–10 $mg\ l^{-1}$. The comple procedure takes < 2 min (Fig. 2). In the simultaneous determination of iron(II) and iron(III), their mutual interference, i.e. partial breakthrough of iron(II) or partial retention of iron(III) on the column was investigated. Complete retention of iron(II) was found even for excessively long preconcentration times and relatively high flow-rates. Some of the iron(III), however, is obviously retained on the column because a small concentration-dependent signal generally occurred upon elution with methanol when pure iron(III) standards were assayed. The addition of fluoride through an extra channel (see Fig. 1) was found to eliminate this interference without having any adverse effects on the iron(II) determination.

4. Conclusions

The proposed method permits the quasi-simultaneous determination of iron(II) and iron(III). The concentration range for iron(III) determination is similar to that of conventional sample aspiration (i.e. 0.25–10 $mg\ l^{-1}$) whereas for iron(II) the detectability depends on the sample volume injected. With a 5-ml sample the determination of low $\mu g\ l^{-1}$ levels is feasible with a sampling frequency of 30 h^{-1}.

References

[1] Z. Fang, Flow Injection Separation and Preconcentration, VCH Publishers, Weinheim, 1993.
[2] T.P. Lynch, N.J. Kernoghan, J.N. Wilson, Analyst, 109 (1984) 839 (Part I) and 843 (Part II).
[3] G.E. Pacey and P.B. Bubnis, Int. Lab., Sept. (1984) 26.
[4] A.G. Cox, I.G. Cook and C.W. McLeod, Analyst, 110 (1985) 331.
[5] A.T. Faizullah and A. Townshend, Anal. Chim. Acta, 167 (1985) 225.
[6] J. Ruzicka and A. Arndal, Anal. Chim. Acta, 216 (1989) 243.

ELSEVIER

Analytica Chimica Acta 296 (1994) 119–128

ANALYTICA CHIMICA ACTA

Determination of metal ions complexed with 2,6-diacetylpyridine bis(*N*-methylenepyridiniohydrazone) by capillary electrophoresis

Andrei R. Timerbaev [a,*], Olga P. Semenova [a], Guenther K. Bonn [a], James S. Fritz [b]

[a] *Department of Analytical Chemistry, Johannes Kepler University, A-4040 Linz, Austria*
[b] *Ames Laboratory, US Department of Energy and Department of Chemistry, Iowa State University, Ames, IA 50011, USA*

Received 15 February 1994

Abstract

Metal ions were determined quantitatively and selectively by complexation with 2,6-diacetylpyridine bis(*N*-methylenepyridiniohydrazone) (H_2dapmp) and separation of the metal ion complexes formed using capillary zone electrophoresis. The effect of various alkyltrimethylammonium ions added to the running electrolyte on the migration behaviour of cationic chelate complexes was examined. As a result, some evidence was obtained that both electrophoretic migration and micellar partitioning play the major role in the separation mechanism. Optimum resolution of metal–H_2dapmp complexes was achieved with a 10 mM sodium borate buffer (pH 9.0) containing 75 mM tetradecyltrimethylammonium bromide and 10 mM sodium *n*-octanesulfonate as an ion-pairing counterion. With this micellar buffer system, it was possible to separate and determine up to fourteen metal ions in a single run within 12 min using fused-silica capillaries at 15 kV and direct on-column UV detection at 254 nm. Linear calibration ranges of more than two orders of magnitude and detection limits at mid-ppb levels are presented for the metal complexes of Cd(II), Co(II), Cu(II), Fe(III), Hg(II), Mo(VI), Sc(III), U(VI), V(V), Y(III) and Zn(II).

Keywords: Capillary zone electrophoresis; Chelating reagents; Metal ion analysis; Micellar electrophoretic systems

1. Introduction

Some excellent separations of various metal ions by capillary electrophoresis (CE) have recently been demonstrated [1–5]. Often, the separation is facilitated by addition of a weak complexing agent added to the capillary electrolyte to partially complex the sample cations. Another approach has been to complex metal ions completely by adding a strong complexing agent to the sample and then to separate the metal complexes by CE [6–8]. Along with a possibility to detect metal ions by direct absorbance measurements, this approach makes it possible to eliminate largely interferences from complex sample matrices, such as serum [9], pharmaceutical preparations [10], electroplating solutions [11], ores [12], etc. Additionally, sample pretreatment conditions, e.g., decomposition with mineral acids

* Correspondence to: A.R. Timerbaev, Department of Analytical Chemistry, Johannes Kepler University, Altenbergerstrasse 69, A-4040 Linz, Austria. On leave from Mendeleev Russian University of Chemical Technology, Moscow, Russian Federation.

SSDI 0003-2670(94)00216-9

and complexing leaching solutions [13], are well tolerated.

By selecting a chelating ligand that forms stable complexes with many metal cations, the number of ions that can be separated by CE can be increased substantially. A ligand that forms very stable metal ion complexes could also make it possible to avoid the addition of free reagent to the carrier electrolyte, a process that inevitably affects the detection and often the separation. Of those considered, we selected 2,6-diacetylpyridine bis(*N*-methylenepyridiniohydrazone) (H_2dapmp) as a water-soluble chelating reagent that had already demonstrated an attractive selectivity in liquid chromatographic (LC) analysis of metal ions [14,15]. This reagent was additionally interesting because of the positive charge of the metal complexes resulting from the presence of quaternary ammonium groups in the molecule. All previous CE studies have dealt with negatively-charged metal complexes.

In the present work, it is shown that the use of H_2dapmp greatly broadens the scope of the metal complexation CE technique. The effect of the polarity of a CE system and compositional changes in the electrophoretic buffers have been studied, and conditions have been established for the separation and quantification of many metal ions. Also, a mechanism is discussed for the excellent separations obtained in micellar migrating systems.

2. Experimental

2.1. CE studies

CE was performed with a Waters (Milford, MA) Quanta 4000 CE system. Polyamide-coated, fused-silica capillaries (Polymicro Technologies Phoenix, AZ), 50 cm × 75 μm i.d., were used. Detection was carried out by on-column photometric measurements at 254 nm. The separation voltage applied was 15 kV. Electropherograms were recorded and processed with a Hewlett Packard 3359 data acquisition system. Samples were introduced into the capillary by hydrostatic injections for a specified time. To ensure run-to-run reproducibility of migration times in the experiments with surfactant-rich electrolyte concentrations, the 2-min purges of capillary with 0.05 M NaOH and running electrolyte were programmed.

All electrolytes were prepared using doubly distilled water. All reagents for preparing electrolytes were of analytical-reagent grade. pH values indicated below were measured after addition of all electrolyte components. Electroosmotic flow velocity (or the electroosmotic mobility of the bulk solution) was evaluated from the migration time of acetone added to a sample. 1-(2-Pyridylazo)-2-naphthol purchased from Merck (Darmstadt) was used to measure the migration time of the micelle.

2.2. Preparation of stock solutions

2,6-Diacetylpyridine bis(*N*-methylenepyridiniohydrazone) dichloride (H_2dapmp) was synthesized from 2,6-diacetylpyridine (Aldrich, Milwaukee, WI) and Gerard's Reagent P (Aldrich) according to a previously published procedure [14]. Solutions of H_2dapmp were prepared by dissolution in water.

Metal ion standard solutions were prepared from the nitrate salts, except for the following. V(IV) and V(V) stock solutions were made from vanadyl sulfate and ammonium metavanadate, respectively, Fe(II) solutions from the sulfate salt, Mo(VI) solutions from ammonium heptamolybdate, U(VI) solutions from uranyl acetate, Bi(V) solutions from sodium bismuthate, and Sn(IV) and Zr(IV) solutions by dissolving tin dioxide and zirconium oxychloride, respectively, in HNO_3. Stock niobium and tantalum solutions were prepared as reported previously [13].

2.3. Preparation of sample solutions

The samples were prepared by taking an aliquot of metal solution, 0.01 M in HNO_3 and adding enough reagent to make the final sample 1.5–2.5 mM in H_2dapmp. All samples were allowed to stand for at least 10 min before injection.

3. Results and discussion

3.1. Selection of the migration mode

In a recent study [16], a number of separation modes have been pointed out to be used for CE separations of metal complexes. However, in case of negatively charged complexes, all of those are the counterelectroosmotic modes with untreated fused-silica capillaries that present a certain disadvantage in respect of analysis time. As mentioned earlier, the two quaternary ammonium groups impart a 2+ charge to the metal ion complexes of H_2dapmp. This provides a unique possibility to separate these complexes using co-electroosmotic migration in which both electrophoretic and electroosmotic flow are in the same direction (i.e., toward the cathode). In addition, two counterelectroosmotic modes – normal reversed movement and reversed movement with the micellar partitioning [16] that were found to work well for other metal complexes [6–8,13,17] – have been studied in the present investigation.

3.2. Separations using free-solution CE

Accelerated movement of metal ion complexes of H_2dapmp was first accomplished in a CE system with a positive power supply (negative polarity of the detection end) and a phosphate electrophoretic buffer of pH 7. As expected, this results in very short migration times which are comparable with those typically observed in CE of partially in-capillary complexed metal cations. The majority of the complexes was sufficiently stable to give good peaks so that addition of H_2dapmp to the capillary electrolyte was not necessary. Note that this fact is in accord with the behaviour of these complexes in LC [14,15]. On the other hand, the resolution in this migrating system was poor so that only two out of four complexes from a test mixture can be separated, as illustrated in Fig. 1. Cd(II) and Fe(III) are not shown in Fig. 1; they are co-eluted with Cu(II) and Zn(II), respectively. The reagent gives only one first-migrating peak and, as will be shown below, this is also related to the limited resolving power.

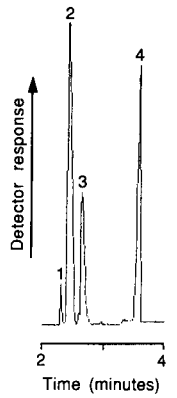

Fig. 1. Separation of metal complexes of H_2dapmp using co-electroosmotic migration. Carrier electrolyte, 10 mM phosphate buffer (pH 7.0); power supply, positive; injection, 10 s. Peaks: 1 = H_2dapmp; 2 = Cu(II); 3 = Zn(II); 4 = acetone.

In order to make a larger migration window for separation, several compositional buffer changes were tried to decrease the electroosmotic flow (EOF). In a recent paper by one of the authors [4], it was noted that when some organic modifier (like methanol) is added to the running electrolyte, the CE separations are usually better. However, both acetonitrile and butanol, as the most hydrophobic water-miscible alcohol (up to 30 and 4%, respectively), caused the migration time to be longer (owing to the reduced EOF) and did not produce any significant change in selectivity.

Next an attempt was made to exploit a pH-dependence of the EOF with borate, phosphate and formate buffers. The observed mobilities decrease when the pH of electrolyte decreases, accompanied by an increase in resolution. However, as seen in Fig. 2, even at the lowest pH of 3 studied, separation of only three test complexes is achieved. Analysis time increases slightly where the selectivity is improved. Furthermore, the formation of many H_2dapmp complexes is impeded in acidic solutions. Fig. 2 also shows three peaks for the excess of H_2dapmp added to the sample. These peaks were due to the *E,E*, *E,Z* and *Z,Z* geometrical isomers of the reagent [14,15].

The separation selectivity was further evaluated by adding tetradecyltrimethylammonium bromide (TDTAB) to the migrating electrolyte

solution. It is well established [18,19] that cationic surfactants have a large effect on the electroosmotic mobility. In fact, increasing the TDTAB concentration produced a gradual decrease in migration velocities of complexes (based on a reduced EOF) until the point when the direction of EOF is reversed. As a result, no peaks could be recorded in a reasonable time with the positive power supply. The reversal of the EOF observed at concentrations from 1×10^{-4} to 10^{-3} M is attributed to the excess positive charges of the adsorbing TDTAB with the formation of hemimicelles, as it has been confirmed recently by Kaneta et al. [19]. It is worth noting that butanol incorporated to the electrolyte along with TDTAB enhances the adsorption of the cationic surfactant on the capillary wall. This causes the net surface charge of the capillary wall to change from negative to positive in the range of lower concentrations of TDTAB.

Reversing the polarity of the CE system (negative injection end) allows one to observe the peaks with TDTAB-containing electrolytes, but migration is accompanied by a number of co-elutions below the critical micellar concentration, which is about 3.6×10^{-3} M [18]. At concentrations $> 5 \times 10^{-3}$ M TDTAB, that guarantee the formation of the micelles in the bulk solution, the resolution, although evidently improved, was still not much different from that in previous experiments (Fig. 3). In contrast, in the CE system with an anodal EOF the complexes of lower electrophoretic mobility migrate first according to the reported regularities of counterelectroosmotic migration [16].

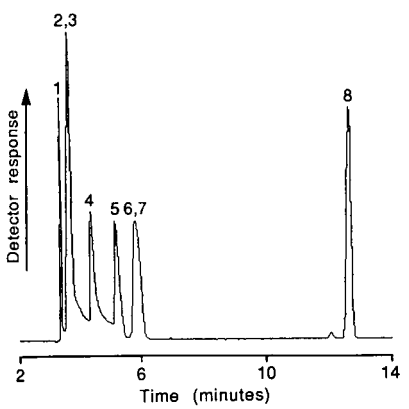

Fig. 2. Separation of metal complexes with acidic carrier electrolyte. Electrolyte, 10 mM formate buffer (pH 3.0). Other operating conditions as in Fig. 1. Peaks: 1 = Cd(II); 2 = Fe(III); 3 = Zn(II); 4–6 = H_2dapmp; 7 = Cu(II); 8 = acetone.

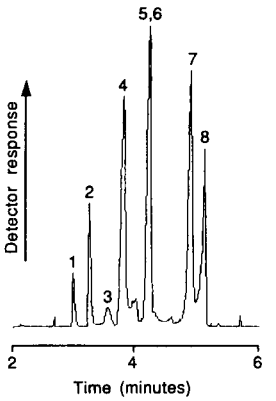

Fig. 3. Separation of metal complexes under counter-electroosmotic conditions. Electrolyte, 10 mM borate buffer (pH 9.0), 7.5 mM TDTAB; power supply, negative; injection, 10 s. Peaks: 1 = acetone; 2–4 = H_2dapmp; 5 = Fe; 6 = Zn; 7 = Cd; 8 = Cu.

3.3. Micellar CE

Since the resolution of closely related complexes was not improved in free-solution CE, it was decided to continue investigations in micellar CE. Micellar electrophoretic systems can be successfully applied to the separation of charged metal complexes provided the solutes possess a rather hydrophobic nature that can be solubilized by surfactant micelles [13]. An optimization of major conditions was carried out for separation of the same test mixture of iron(III), copper(II), cadmium(II) and zinc(II) complexes. These conditions included pH, the nature and concentration of a surfactant, and the kind of ion-pairing anion.

pH of the micellar electrolyte

Some experiments were performed to further investigate the effect of pH on the resolution with micellar electrolytes containing 50 mM dodecyltrimethylammonium bromide (DDTAB) surfactant. The pH of micellar DDTAB solutions

was varied over the pH range 5.0 to 9.0 using acetate, phosphate and borate buffers. With such electrolytes, the migration window stayed practically unchanged while the migration order varied to a larger extent, thus allowing some manipulation of the resolution. For example, in the phosphate buffers the Cu(II) peak appears between those of Fe(III) and Zn(II) whereas in acetate and borate buffers the copper complex elutes the first and the last of the test complexes, respectively. This behaviour was assumed to be related to the effect of ion-pairing association between the solute and anionic component of the buffer that may differ for the electrolytes studied (see also below). For further experiments a borate buffer of pH 9.0 was selected providing a satisfactory separation with shorter migration times as well as a good detectability (owing to the complete complexation).

Effect of the surfactant nature

It was essential for optimization of the separation to investigate the effects of using various cationic surfactants. A series of alkyltrimethylammonium surfactants having different alkyl chain lengths was evaluated: decyltrimethylammonium bromide (DTAB), DDTAB, TDTAB and cetyltrimethylammonium bromide (CTAB), at a constant concentration of 75 mM in the electrolyte, where all surfactants should exist in the micellized form. The length of the alkyl chain is believed to be a significant factor in regulating the separation since it determines the hydrophobic character of a micellar CE system.

The results obtained are presented in Fig. 4. First, the changes in the EOF and the migration time of the micelle, although different in the magnitude, were found to correspond well to the observations of Crosby and El Rassi [18] with the similar micellar systems. Plots of migrations times of the complexes versus the number of carbon atoms in the surfactant molecule are also shown in Fig. 4. They demonstrate the decreased retention when going from a C_{10} to a C_{16} surfactant. It should be noted that these findings contradict the literature data on MEKC of various neutral solutes for which an opposite character of the above dependences was observed [18].

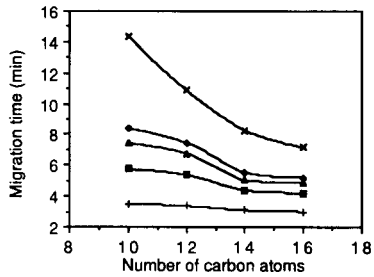

Fig. 4. Migration times of (+) neutral marker, H_2dapmp complexes of (■) iron, (▲) zinc and (◆) copper, and (×) the micelle as a function of the alkyl chain length of the alkyltrimethylammonium surfactants. Electrolyte, 10 mM borate buffer (pH 9.0) containing 75 mM surfactant.

Since the electroosmotic mobility hardly changes with increasing the length of the alkyl chain it was considered that reduced migration times can be attributed to certain changes in effective mobilities. In fact, very recently we demonstrated that the electrostatic repulsion between similarly charged complexes and headgroups of micelles can play an important role in micellar CE [13,16]. The overall charge of the micelle reflecting the degree of repulsion is proportional to the aggregation number that is a linear function of the carbon atom for the surfactants under consideration. In other words, the larger is the size of the surfactant, the weaker is the micellar solubilization and, consequently, the faster will be the observed migration. Therefore, it appears that under aforementioned conditions micellar partitioning does not seem to largely affect the migration behaviour of metal ion complexes of Hdapmp.

The micellar systems studied differred in their separation efficiency. In general, theoretical plate numbers were higher with micelles formed by the surfactants having the longer alkyl chain. For the test complexes, an average plate count goes from 8600 with DTAB to 21200 with DDTAB and then to 25200 and 24700 with TDTAB and CTAB, respectively. This fact can also be explained as a result of the diminishing effect of the partitioning processes. However, the micellar system based on CTAB was considered as less effective in separating the complexes since the migration times are

less reproducible and the background signal is higher (owing to increased light-scattering). Thus, TDTAB micellar phase yielded an overall separation performance that was the best among the varied alkyltrimethylammonium micellar phases.

Concentration of TDTAB

Fig. 5 presents the relationship between the effective mobility of metal complexes and TDTAB concentration in the electrolyte. The latter is usually the most important operational parameter in the micellar CE which determines the magnitude of the phase ratio of the micellar phase (i.e., ratio of the volume of micellar phase to that of the bulk aqueous phase). In the range of lower surfactant concentrations, effective mobilities decrease considerably up to ca. 25 mM TDTAB, followed by an increase in resolution as described above. This character of μ_{eff} versus surfactant concentration dependences is usually interpretated in terms of the solubilization of the solutes by the micelle [20]. Apparently until the hydrophobic phase ratio remains relatively low the electrostatic repulsion does not act strongly; once metal complexes and micelles are close enough together, hydrophobic attraction may provide the distribution of complexes into the hydrophobic core of the micelle.

At a surfactant concentration of about 25 mM, the effective mobility shows an inflection point and then increases gently up to 150 mM (the highest concentration studied). The packing density of the capillary with micelles grows at higher amounts of surfactant in the electrolyte, which

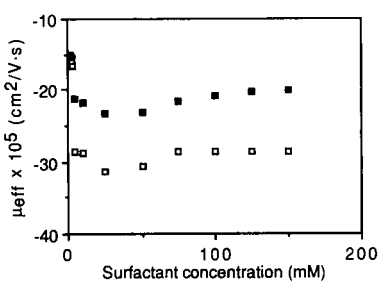

Fig. 5. Effect of TDTAB concentration on effective mobilities of H_2dapmp complexes of (■) iron and (□) cadmium. Electrolyte, 10 mM borate buffer (pH 9.0).

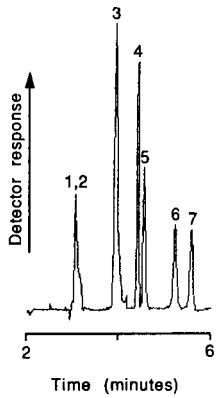

Fig. 6. Separation of metal complexes with the moderate micellar concentrations. Electrolyte, 10 mM borate buffer (pH 9.0), 50 mM TDTAB. Other conditions as in Fig. 3. Peaks: 1 = acetone; 2,3 = H_2dapmp; 4 = Fe; 5 = Zn; 6 = Cd; 7 = Cu.

would give rise to the electrostatic repulsion. This suggests that the migration behaviour in this region should be affected by the electrophoretic mobility in the bulk solution rather than by micellar partitioning. Although increasing the micellar concentration produces only a modest change in the effective mobility, the migration times of the complexes aptly increased with added TMTAB due to reduced EOF. Resolution is also improved with further increase in the content of surfactant owing to the enlarged elution range. As seen in Fig. 6, the complete separation of the test mixture was finally achieved only with 50 mM TDTAB (i.e., approximately 14 times the critical micellar concentration). The electropherograms depicted in Fig. 7 illustrate the effect of higher surfactant concentrations on the resolution of closely migrated complexes of Co(II) and Ni(II). In this instance, the complexes almost co-eluting at 100 mM TDTAB give well-resolved peaks on increasing the micellar concentration to 125 and 150 mM, respectively. However, optimization of the separation gained by addition of more surfactant in the running electrolyte is accompanying by consequent elongation of analysis time. Furthermore, these conditions produce relatively high currents that deteriorate the performance of the CE system (high and erratic baseline, poor peak shapes, less reproducible migration times). Therefore a micellar electrolyte composed of

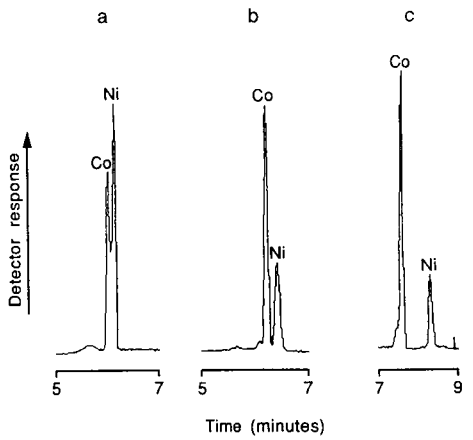

Fig. 7. Effect of TDTAB surfactant concentration on separation of cobalt and nickel complexes. TDTAB concentration, (a) 100; (b) 125; (c) 150 mM. Other conditions as in Fig. 3.

TDTAB at a moderate concentration of 75 mM was recommended for further experiments.

Ion-pairing studies

In an attempt to improve the separations, the influence of sodium salts of different counter anions was examined at a constant concentration of 10 mM. The positively charged quaternary ammonium groups in the dapmp ligand can attract anions to form ion pairs. Therefore the resolution of metal complexes is likely to be affected by the particular anion that is present.

Chloride and bromide as the counter ion did not afford a better separation. Neither could perchlorate be convenient for this purpose despite the fact that sodium perchlorate was reported to provide better separations of metal ion complexes of H_2dapmp in LC [14,15]. Anions of greater ion-pairing strength were believed to perform better. Indeed, a certain gain in resolution was only possible when a strong ion-pairing anion such as *n*-octanesulfonate was present (sodium dodecylsulphate, that was also tried, results in precipitation during the run). However, the effect of sodium *n*-octanesulfonate (SOS) on the resolving power has no connection with micellar partitioning processes. Regardless the nature of counterions under consideration, the effective mobilities presented in Table 1 were very little changed in these experiments. It therefore seems reasonable that paired complexes are also hardly incorporated in the cationic micelle. However, with SOS in the running electrolyte the peaks appeared narrower than those with other salts. Thus, the overall separation of metal complexes could be enhanced by the inclusion of SOS into the TDTAB micellar phase.

3.4. Application to the separation of metal–H_2dapmp complexes

Under micellar CE conditions studied above peaks were obtained for the following metal ion complexes: Al(III), Bi(V), Ca(II), Cd(II), Co(II), Cu(II), Fe(II), Fe(III), Hg(II), Mg(II), Mn(II), Mo(VI), Nb(V), Ni(II), Pb(II), Sc(III), Sn(IV), Ta(V), U(VI), V(IV), V(V), Y(III), Zn(II), Zr(IV) and rare earths. Fig. 8 shows that a fairly large number of these complexes can be simultaneously resolved. The majority of peaks is very narrow and well-shaped. All of those except the molybdenum complex migrated after the last migrating peak of the reagent. It should also be noted that by minimizing a ligand-to-metal ratio in the sample a decrease of the second peak of H_2dapmp ascribed to the chelating geometrical isomer, till its complete disappearance can be attained. Apart from metal complexes shown in Fig. 8, Pb and Mg co-migrate with Zn whereas V(IV, V), Al, Mn and Ca complexes migrate with close mobilities as a block of partially resolved peaks between those of Zr and Co. Some separation of V(IV) and V(V) is evident, but they are not well-resolved from the other co-migrating peaks of this

Table 1
Effective mobilities (in $cm^2/V \cdot s$) of metal complexes with various sodium salts in the electrophoretic buffer [a]

Complex	$-\mu_{eff} \times 10^5$			
	Chloride	Bromide	Perchlorate	Octanesulfonate
Cd(II)	28.5	29.2	30.0	28.2
Cu(II)	31.2	32.9	33.5	31.4
Fe(III)	21.6	22.0	22.1	21.3
Zn(II)	24.5	25.9	27.8	23.4

[a] Electrolyte conditions, 10 mM borate buffer (pH 9.0), 75 mM TDTAB and 10 mM sodium salt.

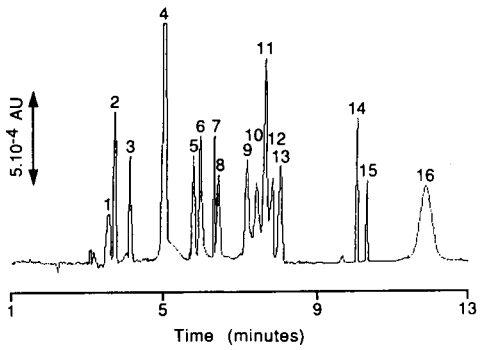

Fig. 8. Separation of 14 metal ions as H_2dapmp complexes. Electrolyte, 10 mM borate buffer (pH 9.0), 75 mM TDTAB and 10 mM SOS; power supply, negative; injection, 10 s. Peaks: 1 = acetone; 2,4 = H_2dapmp; 3 = Mo(VI)(1×10^{-4} M); 5 = Sc(III)(8×10^{-5} M); 6 = Fe(III)(4×10^{-5} M); 7 = Y(III)(8×10^{-5} M); 8 = Zn(II)(1×10^{-4} M); 9 = Cd(II)(1×10^{-4} M); 10 = Zr(IV)(8×10^{-5} M); 11 = Co(II)(1.5×10^{-4} M); 12 = U(VI)(1.7×10^{-4} M); 13 = Cu(II)(1.7×10^{-4} M); 14 = Sn(IV) (8×10^{-5} M); 15 = Ta(V)(8×10^{-5} M); 16 = Hg(II)(4×10^{-5} M).

block. Niobium produced a peak with the same migration time as the tantalum peak. Peaks due to both Fe(II) and Fe(III) complexes were also obtained with the same migration times (presumably because of the same composition). Migration characteristics of metal complexes are summarized in Table 2.

Table 2
Migration times (in min) and effective mobilities (in $cm^2/V\cdot s$) of metal complexes [a]

Complex	$-\mu_{eff}\times10^5$	t_M	Complex	$-\mu_{eff}\times10^5$	t_M
Al(III)	28.8	7.57	Pb(II)	33.9	6.43
Bi(III)	28.7	7.58	Sc(III)	37.0	5.89
Ca(II)	28.8	7.57	Sn(IV)	21.6	10.07
Cd(II)	30.8	7.07	Ta(V)	21.2	10.26
Co(II)	28.8	7.56	U(VI)	28.1	7.75
Cu(II)	27.4	7.95	V(IV)	29.7	7.33
Fe(III)	36.1	6.03	V(V)	28.8	7.56
Hg(II)	18.0	12.07	Y(III)	34.4	6.33
Mg(II)	33.9	6.42	Zn(II)	33.9	6.42
Mn(II)	28.8	7.57	Zr(IV)	29.7	7.33
Mo(VI)	53.4	4.08			
Nb(V)	21.2	10.26			
Ni(II)	28.8	7.56			

[a] CE conditions as in Fig. 8.

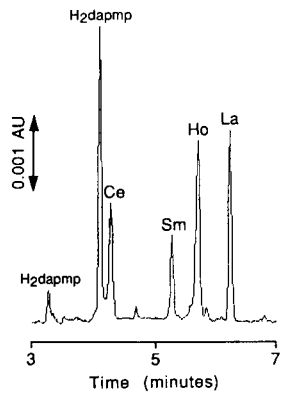

Fig. 9. Separation of rare earth complexes of H_2dapmp. TDTAB concentration, 150 mM. Other CE conditions as in Fig. 8. Concentrations, 3×10^{-4} M Ce; 9×10^{-5} M Ho; 9×10^{-5} M Sm; 1×10^{-4} M La.

Rare earth metal ions proved to be unresolvable at 75 mM TDTAB owing to the closely related migration of the H_2dapmp complexes. The use of higher surfactant concentrations enabled the separation of four rare earths to be achieved, as shown in Fig. 9. The same separating conditions give also a possibility to speciate different oxidation states of vanadium. Fig. 10 demonstrates an additional advantage of CE separation with completely complexed metal ions, that is, reduced problems from metal ions possessing a slow complexation kinetics.

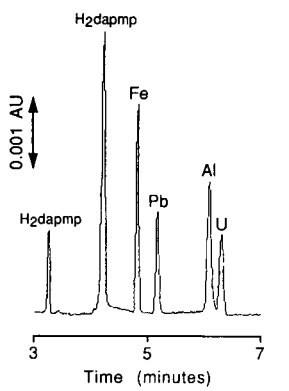

Fig. 10. Separation of metal ion complexes of H_2dapmp. TDTAB concentration, 100 mM. Other CE conditions as in Fig. 8. Concentrations, each 2×10^{-4} M, except Fe(III) (9×10^{-5} M).

Table 3
Detection parameters for metal H_2dapmp complexes [a]

Metal ion	Linear calibration range (M) [b]	Detection limit (M) [c]
Cd(II)	2×10^{-6}–3×10^{-4}	2×10^{-6}
Co(II)	1×10^{-6}–7×10^{-4}	2×10^{-6}
Cu(II)	1×10^{-6}–3×10^{-4}	2×10^{-6}
Fe(III)	3×10^{-7}–1×10^{-4}	1×10^{-6}
Hg(II)	4×10^{-6}–2×10^{-4}	8×10^{-6}
Mo(VI)	1×10^{-5}–7×10^{-4}	1.3×10^{-5}
Sc(III)	1×10^{-6}–3×10^{-4}	3×10^{-6}
V(V)	2×10^{-6}–1×10^{-4}	4.4×10^{-5}
U(VI)	5×10^{-6}–1×10^{-3}	1.0×10^{-5}
Y(III)	3×10^{-6}–7×10^{-4}	5×10^{-6}
Zn(II)	9×10^{-6}–7×10^{-4}	1.4×10^{-5}

[a] CE conditions as in Fig. 8.
[b] Injection time: 25 s; in all cases the upper limit corresponds to the maximum concentration studied.
[c] Injection time: 5 s.

3.5. Analytical performance parameters

Calibration graphs were prepared for a representative set of metal ions under optimized separating conditions. The linear working ranges are given in Table 3. All metals studied gave a linear dependence of the peak area on injected concentration over a range of at least two orders of magnitude. Possibly longer working ranges could be obtained since no peak broadening was observed at the higher concentration end. Also shown in Table 3 are the detection limits defined as three times the baseline noise. It is worth noting that limits of detection obtained with the standard injection time for our previous work (5 s) are substantially poorer than those attained in LC using the same chelating agent [14,15]. An electropherogram resulting from the introduction of a 25-s sample is presented in Fig. 11. These results indicated the comparable sensitivity of CE and LC methods. In Fig. 12 it can be seen that reproducibility of migration times (9 successive injections) ranged from 0.9 to 1.8%. Relative standard deviations of peak areas (seven to nine measurements) were also adequate for practical purposes, with the minor exception of Hg(II) which produced a relatively poor peak shape (see Fig. 8).

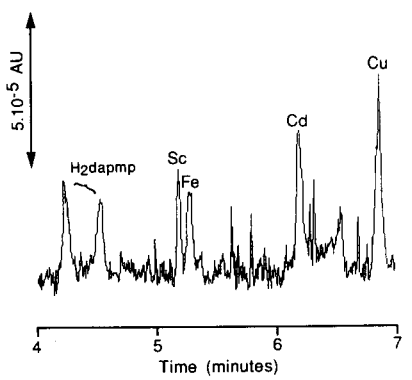

Fig. 11. Performance near detection limits. CE conditions as in Fig. 8. Concentrations, 5×10^{-7} M of each cation.

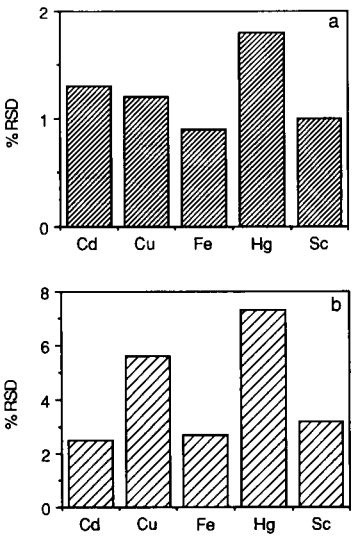

Fig. 12. Reproducibility of (a) migration times and (b) peak area. Concentrations, 2.2×10^{-5} M iron(III); 4.4×10^{-5} M mercury; 6.6×10^{-5} M cadmium, copper and scandium. Other conditions as in Fig. 8.

4. Conclusions

We have a continuing interest in the search for new approaches to metal ion CE separations which take advantage of complex-forming reactions. In CE it is now quite common to use the chelating reagent to complex metal ions before the separation and to obtain thereby the separation selectivity different to those of other CE

methods. This study has proved that analytical potentialities of this technique in terms of multi-element separations can be further expanded within acceptable analysis times by using non-traditional chelating reagents like polydentate bis(quaternary ammonium hydrazones) of 2,6-diacetylpyridine. LC had been used previously for the separation of several metal ions in form of H_2dapmp complexes [14,15]. However, we obtained even better separations by CE.

It was observed that "pure" CE is not very powerful for the separation of metal–H_2dapmp complexes since it requires a sufficient difference in the electrophoretic mobilities. On the other hand, micellar-mediated CE has a definite advantage over free-solution CE, and with cationic alkyltrimethylammonium surfactants added to the electrophoretic medium, it permits a substantially improved resolution. Along with electrophoresis in bulk carrier electrolyte, a differential solubilization by the cationic micelle governs the separation in a certain extent. It can be concluded that the gain in resolution is also due to the enhancing effect of surfactant on the migration range. However, it is speculative at this time to suggest a more probable separation mechanism.

Although surfactant addition makes the separating conditions more sophisticated and the migration behaviour more complex, this provides the widest selection in optimization. Therefore, the H_2dapmp-complexing system described here could present an advantage in the determination of various metal ions over the more conventional CE procedures and it is simple enough to be used on a routine basis.

Acknowledgments

We wish to thank the Austrian Ministry of Science and Research for financial support under grant No. 45.270/-46a/93. The assistance of R.C. Freeze, Ames Laboratory in synthesizing the chelating reagent is gratefully acknowledged. Ames Laboratory is operated for the US Department of Energy under Contract No. W-7405-Eng-82. This work was supported by the Director of Energy Research, Office of Basic Energy Sciences.

References

[1] F. Foret, S. Fanali, A. Nardi and P. Bocek, Electrophoresis, 11 (1990) 780.
[2] P. Jandik, W.R. Jones, A. Weston and P.R. Brown, LC·GC, 9 (1991) 634.
[3] A. Weston, P.R. Brown, P. Jandik, W.R. Jones and A.L. Heckenberg, J. Chromatogr., 593 (1992) 289.
[4] Y. Shi and J.S. Fritz, J. Chromatogr., 640 (1993) 473.
[5] W. Lu and R.M. Cassidy, Anal. Chem., 65 (1993) 1649.
[6] S. Motomizu, S. Nishimura, Y. Obata and H. Tanaka, Anal. Sci., 7 (1991) 253.
[7] A.R. Timerbaev, W. Buchberger, O.P. Semenova and G.K. Bonn, J. Chromatogr., 630 (1993) 379.
[8] M. Iki, H. Hoshino and T. Yotsuyanagi, Chem. Lett., (1993) 701.
[9] S. Motomizu, M. Oshima, S. Matsuda, Y. Obata and H. Tanaka, Anal. Sci., 8 (1992) 619.
[10] A.R. Timerbaev, W. Buchberger, O.P. Semenova and G.K. Bonn, in A. Dyer, M.J. Hudson and P.A. Williams (Eds.), Ion Exchange Processes: Advances and Applications, Royal Society of Chemistry, Cambridge, 1993, p. 111.
[11] W. Buchberger, O.P. Semenova and A.R. Timerbaev, J. High Resolut. Chromatogr., 16 (1993) 153.
[12] M. Aguilar, A. Farran and M. Martinez, J. Chromatogr., 635 (1993) 127.
[13] A.R. Timerbaev, O.P. Semenova, P. Jandik and G.K. Bonn, J. Chromatogr., 671 (1994) 419.
[14] M.V. Main and J.S. Fritz, Anal. Chem., 61 (1989) 1272.
[15] M.V. Main and J.S. Fritz, Anal. Chim. Acta, 229 (1990) 101.
[16] A.R. Timerbaev, O.P. Semenova and G.K. Bonn, Chromatographia, 37 (1993) 497.
[17] T. Saitoh, H. Hoshino and T. Yotsuyanagi, J. Chromatogr., 469 (1989) 175.
[18] D. Crosby and Z. El Rassi, J. Liquid Chromatogr., 16 (1993) 2161.
[19] T. Kaneta, S. Tanaka and M. Taga, J. Chromatogr., 653 (1993) 313.
[20] J. Vindevogel and P. Sandra, Introduction to Micellar Electrokinetic Chromatography, Hüthig, Heidelberg, 1992.

ELSEVIER

Analytica Chimica Acta 296 (1994) 129–140

ANALYTICA CHIMICA ACTA

Radial dispersion by computer-aided simulation with data from zone circulating flow-injection analysis

Yoshio Narusawa *, Yuichi Miyamae

Department of Chemistry, College of Science, Rikkyo (St. Paul's) University, 3-34-1, Nishi-Ikebukuro, Toshima-ku, Tokyo 171, Japan

Received 17 March 1994; revised manuscript received 29 April 1994

Abstract

By analysing damped response curves obtained by zone circulating flow-injection analysis (ZCFIA), correlations between FIA parameters and radial dispersion were obtained with the aid of computer simulation. This paper proposes definitions of axial and radial dispersion, and axial and radial diffusion. Quantitative correlations among residence time, flow rate, length and inner diameter of tube, sample volume and radial dispersion coefficient of dichromate ion were obtained by evaluating constants, K, and exponents, μ, for each qualitative formulation. Six qualitative expressions were obtained, and the three most important expressions are:

$D = K_1 L_r^{\mu_1} Q_c^{\mu_2} + 1$ $(0 < \mu_1 < 1, \mu_2 < 0)$

$K_1 = 0.349 \pm 0.000$, $\mu_1 = 0.558 \pm 0.003$, $\mu_2 = -0.222 \pm 0.008$

$D = K_2 Q_c^{\mu_2} t^{\mu_3} + 1$ $(0 < \mu_2, \mu_3 < 1)$

$K_2 = 0.449 \pm 0.002$, $\mu_2 = 0.339 \pm 0.013$, $\mu_3 = 0.564 \pm 0.006$

$D = K_3 L_r^{\mu_1} t^{\mu_3} + 1$ $(0 < \mu_1, \mu_3 < 1)$

$K_3 = 0.388 \pm 0.002$, $\mu_1 = 0.351 \pm 0.019$, $\mu_3 = 0.206 \pm 0.028$

Data obtained by computer simulation are fairly consistent with the prospective ranges and signs. This paper mainly describes the radial dispersion.

Keywords: Flow injection; Computer aided simulation; Diffusion; UBASIC program; Zone circulating FIA

1. Introduction

Yu [1] studied the dispersion of a small amount of a solute initially injected into a round tube in which steady-state laminar flow exists. Lisy and Turna [2] solved the diffusion of a solute in laminar flow through a circular tube. Vrentas and Vrentas [3] developed an asymptotic solution for the dispersion of a passive solute in a Newtonian fluid in fully developed, laminar flow through a straight, circular tube. Daskopoulos and Lenhoff

* Corresponding author.

SSDI 0003-2670(94)00210-D

[4] studied the axial dispersion coefficient in laminar flow in a tube and pointed out that the dispersion is generally smaller in a curved tube than in a straight tube, because of the enhancement of lateral transport by secondary flows. Mansour [5] solved an exact, closed-form solution of a mathematical model describing the transport of solution matter in a solvent inside a circular tube in terms of a confluent hypergeometric function and showed it to be in excellent agreement with published experimental and numerical works. Shankar and Lenhoff [6] pointed out that the axial dispersion of an impulse tracer injected into a fluid in a flow in a tube is caused by the interaction of radial diffusion and the nonuniform velocity profile. Mansour and Hussein [7] studied an analytical solution for diffusion with homogeneous, *n*th order nonlinear reaction in laminar flow of a Newtonian fluid in a tubular reactor. Betteridge [8] reported a dispersion profile on the basis of the convection–diffusion model.

Vanderslice et al. [9] derived expressions for the dispersion and the travel times of samples in single flow-injection analysis (FIA) systems. Reijn et al. [10] investigated dispersion phenomena playing a very important role in FIA. Painton and Mottola [11] studied the contribution of chemical kinetics on practical dispersion, D, in FIA on the oxidation of L-ascorbic acid by dichromate ion. Ramsing et al. [12] proposed a study of highly reproducible concentration gradients formed between an injected sample zone and the carrier stream in FIA for titration based on measuring the time span between points of identical gradient dispersion. Vanderslice et al. [13] discussed papers on FIA by Gerhardt and Adams (1982) and Alexander and Thalib (1983). Reijn et al. [14] reported the dispersion of an injected sample zone caused by transport phenomena in most FIA systems. Betteridge et al. [15] studied dispersion and chemical reactions in a single-channel flow-injection system modelled by a random walk method. Stone and Tyson [16,17] reported the effects of flow cell geometry and the nature of the solute on peak shape and the dispersion–flow rate relationship. Tyson [18] derived accurate equations for relating peak width to injected concentration for single-line and merging-stream manifolds.

Brooks et al. [19] reported on the dispersion coefficient. Israel and Barnes [20] derived a relationship to permit a comparison of the dispersion heights in normal and reverse FIA. Johnson et al. [21] studied the reduction of injection variance in FIA. Van Staden [22,23] investigated the response time phenomena of coated open-tubular solid-state silver halide selective electrodes and their influence on sample dispersion in FIA. Korenaga [24] studied solute dispersion of an injected sample plug. Wentzell et al. [25] investigated the evaluation of dispersion profiles by using random walk simulation in FIA. Ríos et al. [26] applied multidetection in unsegmented flow systems with a single detector to chemical reactions.

There are some reviews (Ruzicka and Hansen [27], Varcárcel and Luque de Castro [28] and Burguera [29]) on dispersion in FIA. In laminar flow, the concentration of a sample zone injected into the carrier flow decreases owing to the phenomenon of dispersion, and diffusion occurs accompanied by dispersion. However, the differentiation of these terms "dispersion" and "diffusion" is not clear; Ruzicka and Hansen [27] take the standpoint of dispersion and Valcárcel et al. [28] diffusion. This discrepancy may be attributed to the fact that the experimental conditions are not adequate for resolving the complicated problems involved. Kolev and van der Linden reported theoretical considerations of dispersion for parallel plate systems [30–33], mathematical modelling [34], and application of Laplace transforms [35].

Recently, Li and Narusawa proposed the term "zone circulating flow-injection analysis (ZCFIA)" in this journal [36]. By using this technique, they obtained a set of damped response curves. By analysing those curves in detail, the present authors obtained correlations between FIA parameters (flow rate, residence time, length and diameter of coil and sample volume) and radial dispersion, FIA parameters and axial dispersion, and radial dispersion and axial dispersion. In this paper computer-aided simulation results are described on whether the correlations

between FIA parameters and radial dispersion are correct or not. Another aim of the present paper is to discuss the correct understanding of axial and radial dispersion as well as axial and the radial diffusion.

2. Experimental

2.1. Preparation of sample and carrier solutions

All procedures were described in our previous paper [36].

Apparatus

Equipment for measuring damped response curves of ZCFIA was also described in a previous paper [36]. For the computer simulation, the UBASIC program [37] was used with minor alterations. A NEC PC-9801FA computer was used for the computational simulation.

2.2. Procedure for detecting damped curves with the ZCFIA method

ZCFIA is a technique for obtaining damped response curves which contain essential information on dispersion, diffusion and FIA parameters. However, the damped response curves obtained by ZCFIA cannot be obtained by regular FIA, because the latter is operated without sample zone circulation [36].

After ensuring that the instrument was operating stably, the reproducibility of the instrument was tested by analysing the sample eleven times (S_v = 100 μl). Water as a carrier was then pumped into the tubular reactor and, simultaneously, the sample solution was aspirated into a loop by the pump. After this procedure the pump was stopped. After connecting the inlet of the carrier to the outlet of the waste in the single line-manifold (no bubbles were allowed to enter), the valve was switched from the load to the injection position. The pump and the recorder were started at the same time, and the analysis of the injected sample was started. A set of damped response curves was obtained. A determination time of 12 min was required per sample. The initial peak is attributed to the result of the injected sample zone which travelled only for 100 cm. As the closed-flow system has a total length (L) of 200 cm, the peak of the damped curve will appear at every distance of 200 cm until it is completely homogenized. The number of peaks appearing for each curve coincides with the number of times that the zone passes through the detector. The sample zone diffuses as it travels forward, and the peak heights decrease with increasing residence time (T). Finally, when the zone is completely mixed by the carrier, the detector signal (absorbance, A, or height, H) reaches a steady state plateau. In order to obtain the dispersion coefficient (D), H^0 was measured by pumping the sample solution through the detector instead of the carrier stream. H^0 appeared to be 23.6 cm in this experiment.

The procedure was repeated using 10 sets of different revolution speeds of the pump and the overall results were presented as a three-dimensional diagram [38]. In this diagram, a large amount of information concerning flow injection dispersion and diffusion phenomena is available. By analysing these curves, it is possible to clarify correlations among Q, L, t, r, S_v, D, σ and H (detector signal) under various conditions in a flow injection system.

3. Dispersion and diffusion model

3.1. Dispersive transport model

Ideal flow model and equations for injected sample zone in a tubular reactor

The ideal flow model of the injected sample zone in a flow injection system in which no chemical reaction is involved was presented in our previous paper [36]. The following equations are derived when the model is analysed (symbols and definitions are shown in Table 1):

$$L_s = S_v/\pi r^2 \quad (1)$$

$$L_{m,f} = Q_m t/\pi r^2 \quad (2)$$

$$T = t + \sigma_{s,t} \quad (3)$$

Table 1
Symbols and definitions used in this text

C	Concentration
D	Radial dispersion
D_A	Axial dispersion
D	Dispersion according to Ruzicka's definition
F_c	Mean linear velocity of the carrier stream
F_m	Mean molecular diffusion velocity of the sample zone
H	Signal height on the chart, which corresponds to concentration
L	Length (cm) of the tubular reactor
L_r	Distance traveled (cm) by the injected sample plug making physical dispersion
L_s	Plug width (mm) of the injected sample at a split second
$L_{m,f}$	Diffusion distance in the forward and backward diffusion in the axial direction caused by the axial dispersion
Q	Total flux of the sample zone (cm^3/s)
Q_c	Volumetric flow rate (cm^3/s) of the carrier stream
Q_m	Volume of molecular diffusion per second (cm^3/s)
r	Radius of the reactor
S_v	Injected sample volume (μl)
t	Elapsed time
t_s	Elapsed time needed by sample zone without diffusion to pass through the detector
Δt_b	Elapsed time from baseline to baseline
T	Residence time of the sample zone
T_o	Overall residence time of the sample zone
T'	Return time from maximum value of the peak to baseline
$\sigma_{s,l}$	Length (mm) of the peak width on the chart
$\sigma_{s,t}$	Peak width expressed in terms of elapsed time of sample zone from injection to the detector: $\sigma_{s,l}$ (mm) = $a\sigma_{s,t}$ (s); a = constant
$\sigma_{t,f}$	Dispersion width expressed in terms of elapsed time of injected sample zone
$\sigma_{l,f}$	Dispersing width expressed in terms of length of injected sample zone
Θ	Width of the sample plug expressed as time

$$\sigma_{s,t} = \theta + \sigma_{t,f} \quad (4)$$

$$\theta = \pi r^2 L_s / Q_c \quad (5)$$

$$\sigma_{s,t} = \pi r^2 L_s / (Q_m + Q_c) \quad (6)$$

$$Q = Q_m + Q_c \quad (7)$$

$$t = \pi r^2 L_r / (Q_m + Q_c) \quad (8)$$

$$T = \pi r^2 (L - L_s) / (Q_m + Q_c) + \sigma_{s,t} \quad (9)$$

$$L = (T - \sigma_{s,t})(Q_m + Q_c) / \pi r^2 + L_s \quad (10)$$

3.2. Definition of dispersion

Ruzicka and Hansen [27], Valcárcel and Luque de Castro [28] and Burguera [29] published important books in which dispersion is considered. The descriptions of Ruzicka and Hansen (p. 99), Valcárcel and Luque de Castro (p. 59) and Burguera (editor) (p. 34) on dispersion are not necessarily adequate. The present authors classify dispersion as the axial dispersion and the radial dispersion. The direction of travel in a narrow conduit is axial, and the perpendicular direction to it is radial. The direction of travel with axial dispersion is straightforward, but the perpendicular direction is infinite in the xy-plane. In this paper, axes are taken as in Fig. 1. Of course, the dispersion directed to the z-axis is axial dispersion and that directed perpendicular to the z-axis is radial dispersion. Axial and radial dispersion are represented schematically in Fig. 2a and b, respectively.

Axial dispersion

The phenomenon of a sample zone injected into a laminar flow as forced flow in a narrow conduit is considered. If there is no dispersion, the sample zone flows as a plug flow. However, that is only the ideal case. In fact, the dispersive transport is the prevailing mode immediately after injection, as shown in Fig. 2a. The zone profile is typically parabolic. The recorded concentration signal would be a curve consisting of an initial vertical portion corresponding to the emer-

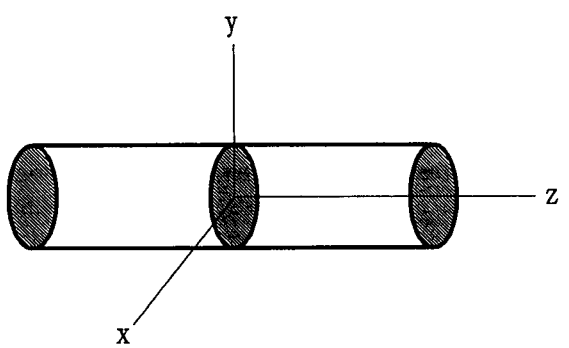

Fig. 1. Schematic representation of the coordinate for dispersion and diffusion. z-axis defines axial and xy-plane defines radial.

gence of the molecules at the "head" of the parabola and a "tail" corresponding to the retarded portion of the sample. As the parabola head travels at twice the mean velocity, the shape from the head to the tail gradually spreads with time, as is shown in Fig. 2a. The axial dispersion (D_A) is defined as the travelling time needed for the head and tail of an axially dispersing slug to cross the detector.

Radial dispersion

The radial dispersion is nearly equal to the dispersion defined by Ruzicka. Except for the plug flow, the radial dispersion is defined as the ratio of non-dispersive signal peak height to maximum peak height emerging during the travel time needed from the baseline to the baseline of the curve consisting of an initial vertical portion corresponding to the emergence of the molecules at the "head" of the parabola and a "tail" corresponding to the retarded portion of the sample, as shown in Fig. 2b.

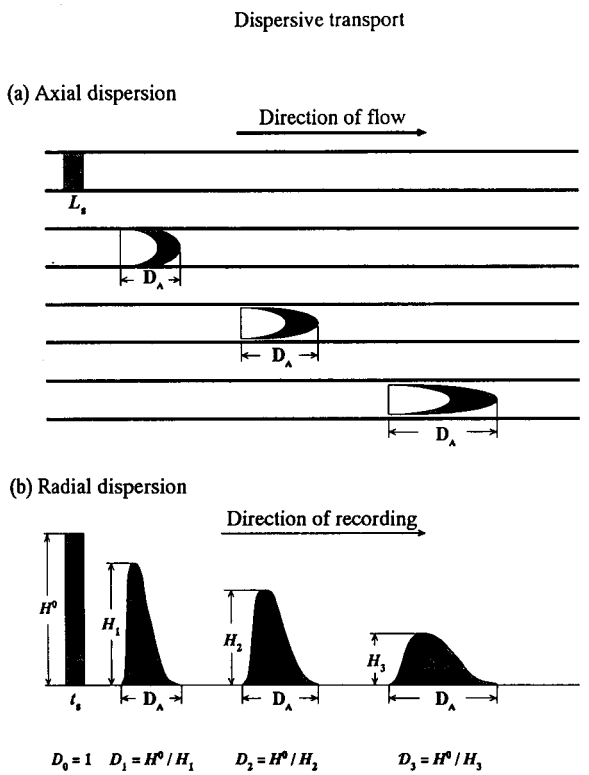

Fig. 2. Schematic representation of (a) axial dispersion and (b) radial dispersion.

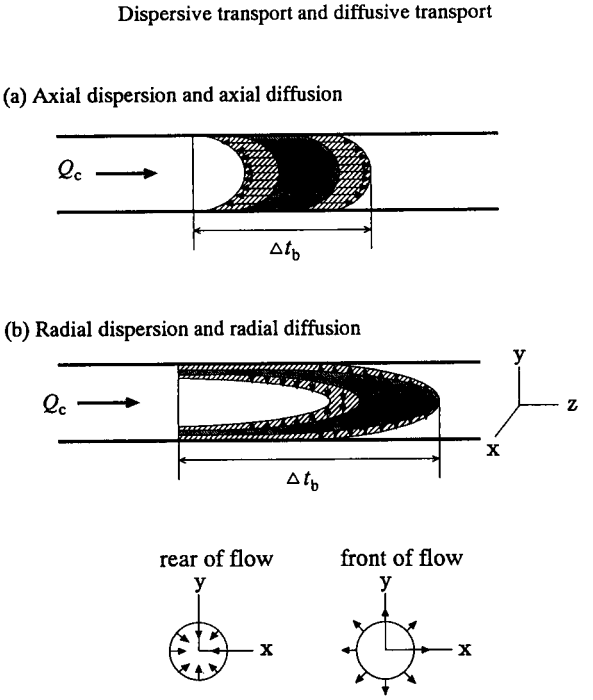

Fig. 3. Schematic representation of dispersion–diffusion model for (a) axial dispersion and axial diffusion and (b) radial dispersion and radial diffusion. Symbol D in (b) is the dispersion according to Ruzicka's definition except for eliminating the effect of radial diffusion (for details, see text).

3.3. Diffusive transport model

Definition of axial diffusion

The axial diffusion is defined as the molecular diffusion occurring along the axis where the sample flows (Fig. 3a). It is difficult to determine it precisely. As diffusion occurs by a concentration gradient, dispersion always occurs accompanying diffusion. On the other hand, the phenomenon of diffusion occurs alone without flow. Axial diffusion acts so as to increase the axial dispersion. Therefore, the observed dispersion becomes greater than the true axial dispersion. The discussion presented by Israel and Barnes [20] may be valid for the effect of radial diffusion with respect to radial dispersion, as they discussed the dispersion of Ruzicka's definition. The time elapsed

from baseline to baseline (Δt_b) involves the effect of axial diffusion (cf. Fig. 3). Therefore, the axial dispersion is not equal to Δt_b. To make sure, the axial dispersion does not involve any diffusional contribution.

Definition of radial diffusion

The radial diffusion is defined as the molecular diffusion in the plane perpendicular to the flow direction by the two types of diffusion as shown in Fig. 3b. This phenomenon is inherently accompanied by the dispersion according to Ruzicka's definition. To make sure again, the radial dispersion D in Fig. 3b does not involve any diffusional contribution. In this sense, the radial dispersion is not equal to the dispersion according to Ruzicka's definition. The radial diffusion is defined by the difference between the true radial dispersion and the dispersion according to Ruzicka's definition. However, it is difficult to distinguish the radial dispersion from the dispersion according to Ruzicka's definition on the basis of the usual FIA techniques. The present authors succeeded in distinguishing them by using computer-aided simulation and the procedure and the results are discussed later.

4. Results and discussion

Although the theory relating to the dispersion of a sample zone flowing in a narrow conduit has been studied by many investigators, all of these are partial. There are few fundamental studies in relation to the basic theory of FIA. The present paper deals with the analyses of the damped response curves obtained under the conditions of various pump speeds by computer-aided simulation. In FIA, as Reynolds number does not exceed 2000 [10], we discuss the flow as laminar flow. The phenomenon where the solute moves in laminar flow depends on dispersion and diffusion. Most investigators have dealt with the dispersion without distinctly differentiating it from the diffusion [8,9,12]. This makes the phenomenon of dispersion ambiguous. The present authors propose the classifications of the dispersion to be axial dispersion and radial dispersion, and the diffusion to be axial diffusion and radial diffusion. In the present step, although the analysis of diffusion was qualitative, the four physical phenomena were distinctly differentiated from each other [36,38].

4.1. Computer-aided simulation of data by ZCFIA

Many correlations between the dispersion coefficient according to Ruzicka's definition and FIA parameters (flow rate, residence time, length and inner diameter of tube, sample volume, etc.) were obtained by analysing the damped curves with ten different steps of pump speeds. By analysing these curves manually, Li and Narusawa [36] obtained six qualitative expressions. In order to evaluate the values of K and μ in these expressions, it was necessary to use the computer simulation. Moreover, it was necessary to eliminate the contribution of the diffusion from the dispersion according to Ruzicka's definition. In the present paper, we succeeded in obtaining the correlations between the radial dispersion and the above-mentioned FIA parameters with correction for the diffusion.

Optimization of data

It is necessary to optimize the data obtained by ZCFIA, because they involve some experimental errors and a substantial contribution of the effect of diffusion. The computer programs for the optimization were almost the same as those used previously [37]. In the present case, the optimization of data was obtained with repetition by trial and error. Although this procedure is time consuming, data were optimized steadily to the global minimum without falling in any local minimum.

Correlations between Q, L, T, R, S_v and D

The dispersion coefficient D is defined as the ratio of concentrations of sample material before and after the dispersion process has taken place. Using the height H (cm) of the peak of the output signal, D can be expressed as

$$D_i = H^0/H_i \, (i = 1,2,\cdots,n) \qquad (11)$$

The numerical values of D_i were obtained by substituting H_i for the peaks in Fig. 2b into Eq.

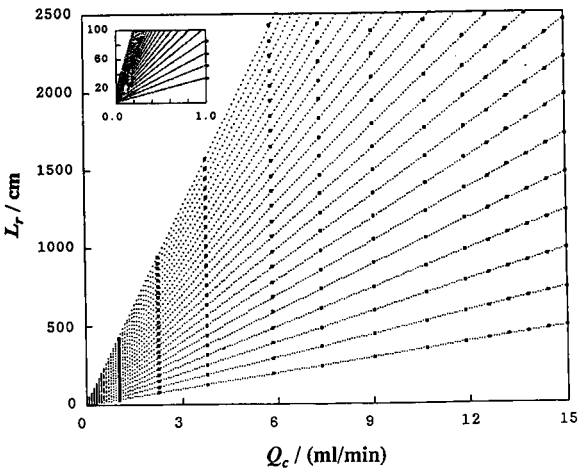

Fig. 4. Relationship between L_r and Q_c at each constant value of t. Values of t (s) are 20–250 s at 10-s intervals from bottom to top.

11. This is the dispersion according to Ruzicka's definition.

Computer-aided simulation

UBASIC is a language developed by Kida (Department of Mathematics, Rikkyo University) for long-digit calculation. The present authors developed the UBASIC program with the curve-fitting procedure to test the computational errors [37]. As a result, it was found to be safe for calculations up to the 50th dimension of the matrix (1000 figures or more). There were no problems with the software and the hardware. Using the UBASIC program, the following three relationships were obtained: t and L_r at constant Q_c (DIM 2), t and Q_c at constant L_r (DIM 10), and L_r and Q_c at constant t (DIM 2, Fig. 4).

Next, the following five relationships between the radial dispersion coefficient D and FIA parameters were obtained: D and L_r at constant Q_c (DIM 7), D and Q_c at constant L_r (DIM 7), D and Q_c at constant t (DIM 7), D and t at constant Q_c (DIM 7) and D and t at constant L_r (DIM 7). DIM means the dimension of the matrix in the curve-fitting program and DIM − 1 corresponds to the order of polynomials. Therefore, DIM = 2 means the relationship is the linear regression.

Evidence for the axial diffusion

A group of the plots of L_r against Q_c at each constant of residence time (t) was obtained as shown in Fig. 4. It is observed that even if the Q_c is zero, L_r is not zero and the intercept increases with increase in residence time (t). Analysing the phenomenon, it is considered that the intercept comprises the length of the injected sample plug (L_s) as shown in Fig. 2a and the diffusion distance ($L_{m,f}$) caused by the dispersion of the sample plug. On the other hand, according to the Eq. 10, if Q_c is decreased to zero, the following equation can be derived:

$$L = L_s + (T - \sigma_{s,t})(Q_m + Q_c)/\pi r^2$$

$$= L_s + Q_m t/\pi r^2 = L_s + L_{m,f}$$

where $L_{m,f}$ is positive and increases as the time t increases. Fig. 4 shows that the intercept at $Q_c = 0$ represents the value of $L_{m,f}$. That is, the theory predicts the same conclusion as the experimental result. By the definition (cf., *Definition of axial diffusion*), the radial diffusion is indifferent to the peak width, although it correlates with the signal height. $L_{m,f}$ is interpreted as being due not to the radial diffusion but to the axial diffusion, because this phenomenon is independent of the signal height. Therefore, $L_{m,f}$ directly correlates only with the axial diffusion.

Evidence for the radial diffusion

A group of plots of D against L_r at each constant flow rate Q_c was obtained by the computer-aided simulation so as to reproduce the result of the manual analysis [36] as shown in Fig. 5a, where DIM = 7 was applied. By comparing the result by the manual analysis (cf., Fig. 8 in Ref. [36]) with the present result, it was recognized that there were essentially no differences between these results. If the dispersion coefficient D is constant and an expression such as Eq. 12 holds for D, the plot of $\log(D - 1)$ vs. $\log L_r$ is predicted to give a straight line with a slope μ_1. However, plots of these curves gave convex curves, as shown in Fig. 5b. This phenomenon is interpreted as being due to the effect of the radial diffusion. The experimentally obtained dispersion

constant D is the dispersion based on Ruzicka's definition, and involves the contribution of the diffusion. By the definition (cf., *Definition of radial diffusion*), it is the radial diffusion that affects the signal height. On the other hand, the radial diffusion acts so as to increase the concentration (or the signal height) in the plane perpendicular to the flow axis (*cf.* Fig. 3b), which causes the dispersion to decrease. Therefore, the pure radial dispersion increases in the later portion of the curve in comparison with the dispersion according to Ruzicka's definition (the experimentally obtainable dispersion), because the effect of the radial diffusion becomes large in that portion. There is another positive evidence for this interpretation. By the computer-aided simulation, we obtained the relationship between D and L_r at each constant of Q_c (see above). Plotting log(D − 1) against log L_r gave straight lines, as shown in Fig. 6. This means that the radial diffusion contributes so as to decrease the radial dispersion. The axial diffusion is indifferent to this phenomenon, because the axial diffusion does not contribute to the signal height.

We succeeded in obtaining results for the relationship between D and L_r at each constant flow rate Q_c, where D does not involve any diffusional effects, by computer simulation. In this case, the plots of log(D − 1) vs. log L_r were linear (cf. Fig. 6). This means that we succeeded in distinguishing the radial dispersion from the dispersion according to Ruzicka's definition and that the effect of radial diffusion contributes in the opposite sense to the radial dispersion.

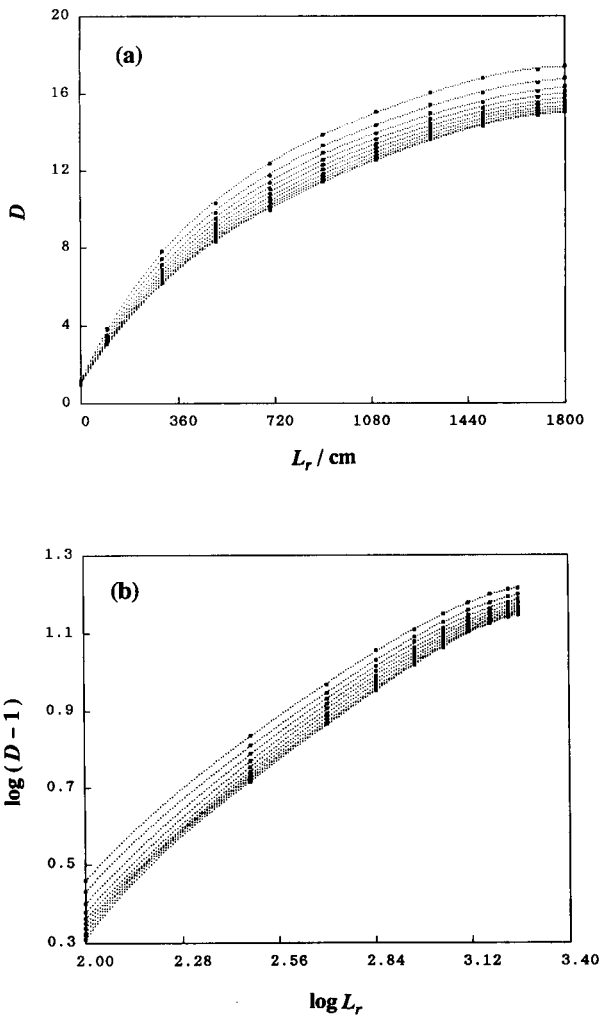

Fig. 5. Relationships between (a) D and L_r at each constant value of Q_c and (b) log$(D-1)$ and log L_r at each constant value of Q_c. Values of Q_c (ml/min) are 1.02, 2.25, 3.80, 5.84, 7.39, 9.03, 10.7, 11.9, 12.6 and 13.2 from top to bottom for both (a) and (b).

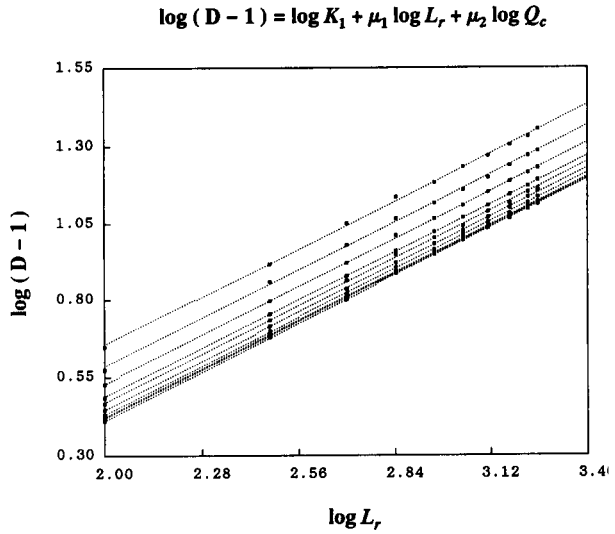

Fig. 6. Relationship between log(D − 1) and log L_r at each constant value of Q_c. Slope and intercept give μ_1 and a_1, respectively. Values of Q_c (ml/min) are 1.02, 2.25, 3.80, 5.84, 7.39, 9.03, 10.7, 11.9, 12.6 and 13.2 from top to bottom.

Analytical expressions of dispersion

Analysing those curves concerning Q_c, L_r and D, the following mathematical expressions were obtained [36].

$$D = K_1 L_r^{\mu_1} Q_c^{\mu_2} + 1 \quad (12)$$

$(0 < \mu_1 < 1,\ \mu_2 < 0)$

$$D = K_1 (L - L_s)^{\mu_1} Q_c^{\mu_2} + 1 \quad (12')$$

$(0 < \mu_1 < 1,\ \mu_2 < 0)$

where K_1 is a constant and μ_1 and μ_2 are also constants but their values will change with differences in the experimental conditions in some definite ranges.

Correlations between the dispersion coefficient of the sample zone and the volumetric flow rate of the carrier stream were obtained. Consequently, the following expressions similar to Eq. 12 were again obtained:

$$D = K_2 Q_c^{\mu_2} t^{\mu_3} + 1 \quad (13)$$

$(0 < \mu_2,\ \mu_3 < 1)$

$$D = K_2 Q_c^{\mu_2} (T - \sigma_{s,t})^{\mu_3} + 1 \quad (13')$$

$(0 < \mu_2,\ \mu_3 < 1)$

where K_2 is a constant and μ_3 is also a constant under limited conditions.

If the volumetric flow rate of the carrier stream, the length and inner diameter of the reaction coils, and the injected sample volume are not changed, data concerning correlations between the residence time and dispersion coefficients of the injected sample zone will be found. As a result, these data were obtained under various conditions of Q_c and t. By analysing these data, the following expressions were also obtained:

$$D = K_3 L_r^{\mu_1} t^{\mu_3} + 1 \quad (14)$$

$(0 < \mu_1,\ \mu_3 < 1)$

$$D = K_3 (L - L_s)^{\mu_1} (T - \sigma_{s,t})^{\mu_3} + 1 \quad (14')$$

$(0 < \mu_1,\ \mu_3 < 1)$

where K_3 is a constant.

In addition, if Eq. 1 is substituted into Eqs. 12 and 14, the following expressions will be further deduced:

$$D = K_1 \left(L - S_v/\pi r^2\right)^{\mu_1} Q_c^{\mu_2} + 1 \quad (15)$$

$(0 < \mu_1 < 1,\ \mu_2 < 0)$

$$D = K_3 \left(L - S_v/\pi r^2\right)^{\mu_1} t^{\mu_3} + 1 \quad (16)$$

$(0 < \mu_1,\ \mu_3 < 1)$

From Eqs. 8, 9, 10 and 14, the following expressions are also obtained:

$$D = K_3 L_r^{\mu_1 + \mu_3} \left(\pi r^2/Q\right)^{\mu_3} + 1 \quad (17)$$

$(0 < \mu_1,\ \mu_3 < 1)$

$$D = K_3 \left(Q/\pi r^2\right)^{\mu_1} t^{\mu_1 + \mu_3} + 1 \quad (17')$$

$(0 < \mu_1,\ \mu_3 < 1)$

4.2. Computer aided simulation for dispersion theory

Relationship between dispersion coefficient D *and length of tubular conduit* L_r and volumetric flow rate Q_c

By taking the logarithm of $D - 1$ in Eq. 12, we obtain the following equation:

$$\log(D - 1) = \log K_1 + \mu_1 \log L_r + \mu_2 \log Q_c \quad (18)$$

By plotting $\log(D - 1)$ against $\log L_r$ at each constant $\log Q_c$, linear relationships were obtained. The regression coefficients were 0.9996 to 0.9999. The results are shown in Fig. 6. The slopes of these curves give μ_1 and the intercept a_1 gives $\log K_1 + \mu_2 \log Q_c$. The mean value of μ_1 is 0.559 ± 0.002. By plotting a_1 against $\log Q_c$, μ_2 was obtained from the slope and $\log K_1$ was obtained from the intercept. Values of μ_2 and $\log K_1$ were obtained as -0.224 and -0.457, respectively. The regression coefficient $r = -0.9989$. The intercept a_1 showed a linear relationship vs. $\log Q_c$ with a negative slope. This is coincident with the prospect that μ_2 will be negative in Eq. 12.

Next, linear plots of $\log(D - 1)$ vs. $\log Q_c$ at each constant $\log L_r$ were obtained. The regression coefficients were -0.9987 to -0.9999. The results are shown in Fig. 7. The slopes of these curves give μ_2 and the intercept a_1' gives $\log K_1 + \mu_1 \log L_r$. The mean value of μ_2 is -0.219 ± 0.006. Plotting a_1' against $\log L_r$ gave μ_1 from the slope and $\log K_1$ from the intercept. The values of μ_1 and $\log K_1$ were 0.557 and -0.457, respectively. The regression coefficient $r = 0.9996$. The intercept a_1' showed a linear relation-

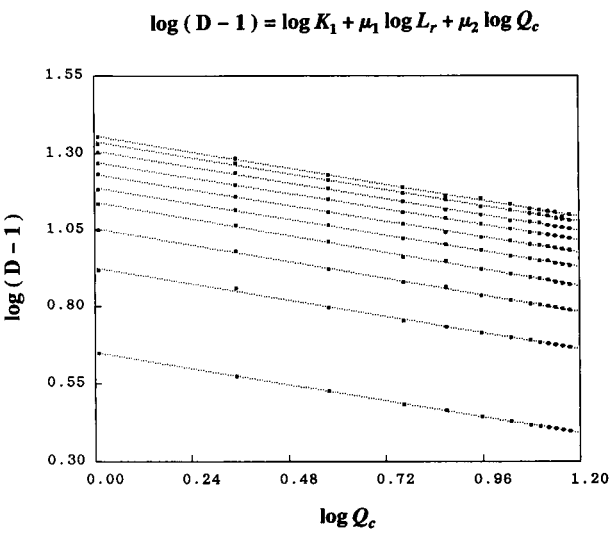

Fig. 7. Relationship between log(D − 1) and log Q_c at each constant value of L_r. Slope and intercept give μ_2 and a'_1, respectively. Values of L_r (cm) are 100, 300, 500, 700, 900, 1100, 1300, 1500, 1700 and 1800 from bottom to top.

ship with log L_r with a positive slope. The results are summarized in Table 2. Two sets of K_1, μ_1 and μ_2 coincided very well with each other.

Relationship between dispersion coefficient D *and the volumetric flow rate* Q_c *and the time t*

By taking the logarithm of D − 1 in Eq. 13, we obtain the following equation:

$$\log(D-1) = \log K_2 + \mu_2 \log Q_c + \mu_3 \log t \quad (19)$$

By plotting log(D − 1) against log Q_c at each constant log t, linear relationships were obtained. The regression coefficients were 0.9993–0.9999. The slopes give μ_2 and the intercept a_2 gives log $K_2 + \mu_3 \log t$. The intercept a_2 showed a linear relationship with log t with a positive slope. This is coincident with the prospect that μ_3 will be positive in Eq. 13.

Next, linear plots of log(D − 1) against log t at each constant log Q_c were obtained. The regression coefficients were 0.9995–0.9998. The slopes give μ_3 and the intercept a'_2 gives log $K_2 + \mu_2 \log Q_c$. The intercept a'_2 showed a linear relationship with log Q_c with a positive slope. The results are summarized in Table 2. Two sets of K_2, μ_2 and μ_3 coincided very well with each other.

Relationship between dispersion coefficient D *and the length of the tubular conduit* L_r *and the time t*

By taking the logarithm of D − 1 in Eq. 14, we obtain the following equation:

$$\log(D-1) = \log K_3 + \mu_1 \log L_r + \mu_3 \log t \quad (20)$$

By plotting log(D − 1) against log L_r at each constant log t, linear relationships were obtained. The regression coefficients were all larger than 0.9999. The slopes give μ_1 and the intercept a_3 gives log $K_3 + \mu_3 \log t$. The intercept a_3 showed a linear relationship with log t with a positive slope. This is coincident with the prospect that μ_3 will be positive in Eq. 14.

Table 2
Constants obtained by computer aided simulation

Analytical expression	Constants obtained by simulation		
	K_1	μ_1	μ_2
Eq. 12 or Eq. 18	0.349	0.559 ± 0.002	-0.219 ± 0.006
From a_1 or a'_1	0.349	0.557	-0.224
Average	0.349 ± 0.000	0.558 ± 0.003	-0.222 ± 0.008
	K_2	μ_2	μ_3
Eq. 13 or Eq. 19	0.447	0.335 ± 0.009	0.561 ± 0.003
From a_2 or a'_2	0.451	0.343	0.567
Average	0.449 ± 0.002	0.339 ± 0.013	0.564 ± 0.006
	K_3	μ_1	μ_3
Eq. 14 or Eq. 20	0.390	0.363 ± 0.006	0.225 ± 0.008
From a_3 or a'_3	0.386	0.338	0.186
Average	0.388 ± 0.002	0.351 ± 0.019	0.206 ± 0.028

Next, linear plots of log(D − 1) against log t at each constant log L_r were obtained. The regression coefficients were 0.997–0.999. The slopes give μ_3 and the intercept a'_3 gives log $K_3 + \mu_1 \log L_r$. The intercept a'_3 showed a linear relationship with log L_r with a positive slope. The results are summarized in Table 2. Two sets of K_3, μ_1 and μ_3 coincided fairly well with each other.

Correlation among three equations

Finally, quantitative conclusions for the analytical expressions were realized from Eq. 12 to Eq. 17′ by the computer aided simulation. The results are given in Table 2. If Q_m is neglected in comparison with Q_c, and $Q_c = Q$, Eq. 12 becomes equal to Eq. 17 except for constant K. In this case, μ_1 and μ_2 in Eq. 12 become equal to $\mu_1 + \mu_3$ and μ_3 in Eq. 17, respectively, except for the opposite sign in the latter. In comparison of Eq. 13 with Eq. 17′, μ_2 and μ_3 in Eq. 13 become equal to μ_1 and $\mu_1 + \mu_3$ in Eq. 17′, respectively. These relationships are valid within the ranges of errors. Based on these results, the present authors succeeded in simulating the zone circulating FIA data by using computer-aided simulation with the UBASIC program [37].

5. Conclusions

Definitions of the dispersion and the diffusion in FIA systems have been proposed, that is, the dispersion is classified as the axial dispersion and the radial dispersion and also the diffusion is classified as the axial diffusion and the radial diffusion. With computer-aided simulation, correlations among the radial dispersion and FIA parameters (L, Q, T, r and S_v) were obtained quantitatively. These expressions and constants K and exponents μ obtained in this work are as follows:

$$D = K_1 L_r^{\mu_1} Q_c^{\mu_2} + 1$$

$$(0 < \mu_1 < 1,\ \mu_2 < 0)$$

$$K_1 = 0.349 \pm 0.000,\ \mu_1 = 0.558 \pm 0.003,$$

$$\mu_2 = -0.222 \pm 0.008$$

$$D = K_2 Q_c^{\mu_2} t^{\mu_3} + 1$$

$$(0 < \mu_2,\ \mu_3 < 1)$$

$$K_2 = 0.449 \pm 0.002,\ \mu_2 = 0.339 \pm 0.013,$$

$$\mu_3 = 0.564 \pm 0.006$$

$$D = K_3 L_r^{\mu_1} t^{\mu_3} + 1$$

$$(0 < \mu_1,\ \mu_3 < 1)$$

$$K_3 = 0.388 \pm 0.002,\ \mu_1 = 0.351 \pm 0.019,$$

$$\mu_3 = 0.206 \pm 0.028$$

These expressions hold in both ordinary FIA and ZCFIA. These expressions are also valid in the tubular region of liquid chromatography, ion chromatography and other flow systems, although the values of the constants K and exponents μ may differ.

Acknowledgments

We gratefully thank Mr. S. Kitahama, Denki Kagaku Keiki, for supplying the multi-step peristaltic pump and Mr. Y.-S. Li and Mr. K. Takahashi, Rikkyo University, for their assistance with some parts of the experiments. Nomura Micro-Science Co. is also acknowledged for the supply of ultra-pure water.

References

[1] J.S. Yu, J. Appl. Mech., 48 (1981) 217.
[2] V. Lisy and L. Turna, Czech. J. Phys., B33 (1983) 480.
[3] J.S. Vrentas and C.M. Vrentas, AIChE J., 34 (1988) 1423.
[4] P. Daskopoulos and A.M. Lenhoff, AIChE J., 34 (1988) 2052.
[5] A.R. Mansour, Sep. Sci. Technol., 24 (1989) 1437.
[6] A. Shankar and A.M. Lenhoff, AIChE J., 35 (1989) 2048.
[7] A.R. Mansour and A.M. Hussein, Int. Commun. Heat Mass Transfer, 17 (1990) 823.
[8] D. Betteridge, Anal. Chem., 50 (1978) 832A.
[9] J.T. Vanderslice, K.K. Stewart, A.G. Rosenfeld and D.J. Higgs, Talanta, 28 (1981) 11.
[10] J.M. Reijn, W.E. van der Linden and H. Poppe, Anal. Chim. Acta, 126 (1981) 1.
[11] C.C. Painton and H.A. Mottola, Anal. Chem., 53 (1981) 1713.
[12] A.U. Ramsing, J. Ruzicka and E.H. Hansen, Anal. Chim. Acta, 129 (1981) 1.
[13] J.T. Vanderslice, G.R. Beecher and A.G. Rosenfeld, Anal. Chem., 56 (1984) 292.
[14] J.M. Reijn, H. Poppe and W.E. van der Linden, Anal. Chem., 56 (1984) 943.
[15] D. Betteridge, C.Z. Marczewski and A.P. Wade, Anal. Chim. Acta, 165 (1984) 227.

[16] D.C. Stone and J.F. Tyson, Anal. Proc. (London), 23 (1986) 23.
[17] D.C. Stone and J.F. Tyson, Anal. Chim. Acta, 179 (1986) 427.
[18] J.F. Tyson, Anal. Chim. Acta, 179 (1986) 131.
[19] S.H. Brooks, D.V. Leff, M.A. Hernandez Torres and J.G. Dorsey, Anal. Chem., 60 (1988) 2737.
[20] Y. Israel and R.M. Barnes, Mikrochim. Acta, 1 (1990) 17.
[21] B.F. Johnson, R.E. Malick and J.G. Dorsey, Talanta, 39 (1992) 35.
[22] J.F. van Staden, Analyst (London), 117 (1992) 51.
[23] J.F. van Staden, Anal. Chim. Acta, 261 (1992) 381.
[24] T. Korenaga, Anal. Chim. Acta, 261 (1992) 539.
[25] P.D. Wentzell, M.R. Bowdridge, E.L. Taylor and C. MacDonald, Anal. Chim. Acta, 278 (1993) 293.
[26] A. Ríos, M.D. Luque de Castro and M. Valcárcel, Anal. Chem., 57 (1985) 1803.
[27] J. Ruzicka and E.H. Hansen, Flow Injection Analysis, Wiley, New York, 2nd edn., 1988.
[28] M. Valcárcel and M.D. Luque de Castro, Flow-Injection Analysis – Principles and Applications, Ellis Horwood, Chichester, 1987.
[29] J.L. Burguera (Ed.), Flow Injection Atomic Spectroscopy, Marcel Dekker, New York, 1989.
[30] S.D. Kolev and W.E. van der Linden, Anal. Chim. Acta, 247 (1991) 51.
[31] S.D. Kolev and W.E. van der Linden, Anal. Chim. Acta, 256 (1992) 301.
[32] S.D. Kolev and W.E. van der Linden, Anal. Chim. Acta, 257 (1992) 317.
[33] S.D. Kolev and W.E. van der Linden, Anal. Chim. Acta, 257 (1992) 331.
[34] S.D. Kolev and W.E. van der Linden, Anal. Chim. Acta, 268 (1992) 7.
[35] S.D. Kolev and W.E. van der Linden, Int. J. Heat Mass Transfer, 36 (1993) 135.
[36] Y.-S. Li and Y. Narusawa, Anal. Chim. Acta, 289 (1994) 355.
[37] Y. Narusawa and Y. Miyamae, J. Chem. Software (in Japanese), 1 (1993) 99.
[38] Y.-S. Li and Y. Narusawa, J. Flow Inject. Anal. (in Japanese), 11 (1994) 68.

ELSEVIER

Analytica Chimica Acta 296 (1994) 141–154

ANALYTICA CHIMICA ACTA

Recognition of visual characteristics of infrared spectra by artificial neural networks and partial least squares regression

T. Visser [a,*], H.J. Luinge [b], J.H. van der Maas [b]

[a] *Laboratory for Organic-analytical Chemistry, National Institute for Public Health and Environmental Protection, PO Box 1, 3720 BA Bilthoven, Netherlands*

[b] *Analytical Molecular Spectrometry, Utrecht University, PO Box 80083, 3508 TB Utrecht, Netherlands*

Received 20 January 1994; revised manuscript received 27 April 1994

Abstract

The potentials of artificial neural networks and partial least squares regression for computerized interpretation of infrared spectra are studied. Experiments are carried out to establish the capabilities of these methods to recognize characteristic band shapes and spectral patterns, commonly used by experienced spectroscopists for interpretation. Classification is performed on (i) organic, inorganic and polyaromatic compounds using the entire spectral profiles, (ii) organophosphorus and non-organophosphorus compounds using specific absorption patterns of the O–P and P=S bands, and (iii) alcohols, carbamates and terminal alkynes using the shape of the individual O–H, N–H and ≡C–H bands. Results are compared with the information obtained from classification using frequency/intensity–structure correlation tables, and with interpretation as performed by experts. Classification by skilled interpreters is found to be superior in all cases. The multivariate methods give a significant improvement of the results compared to the predictions obtained from frequency/intensity data. Differences between artificial neural networks and partial least squares regression are small when full spectra or spectral regions are considered. Networks score better in recognising individual bands. The band width and the absorption frequency play an important role in the recognition process. The results prove to be practically insensitive to reduction of the number of spectral data points by a factor 16.

Keywords: Infrared spectrometry; Computerized interpretation; Multivariate methods

1. Introduction

Infrared (IR) spectroscopy is widely used for structural analysis and identification of compounds. The technique can be applied without elaborate preparations to a variety of samples irrespective the physical state. An IR spectrum contains a lot of structural information as all vibrations and rotations depend on atom types (including hybridization), geometrical orientations, bond strengths and molecular interactions. Therefore, IR spectra are well suited for the

* Corresponding author.

SSDI 0003-2670(94)00208-4

identification of samples by comparison with reference spectra. Automation of this process has been achieved by the development of library search procedures, which are very successful in case a matching library spectrum is available. If this is not the case the unknown spectrum has to be interpreted. IR spectra, however, can be very complex with a large number of absorption bands of various position, intensity and shape. This complexity largely hampers the translation of a spectrum into a molecular structure, making interpretation of IR spectra a difficult and time consuming task. It requires much patience and its success is strongly related to the experience of the interpreter. In order to shorten analysis time and to circumvent or reduce the dependence on expert knowledge, computerisation of the interpretation process has been subject of investigation for many years.

Several techniques have been applied to find correlations between IR spectral data and structural features [1]. Many of the relations obtained have been implemented into computer assisted interpretation systems. Early procedures were based on the straightforward use of frequency/intensity–structure correlation (FSC) tables, derived from literature or composed from available data bases [2–4]. In the late 1980's, these procedures were followed by more sophisticated knowledge based systems constructed with artificial intelligence software [5–12]. We too developed such an interpretation system, called EXSPEC, which was found to be a useful tool in the hands of unexperienced interpreters, particularly for rapid functional group classification [10]. However, the performance of these systems is still inferior to that of experienced spectroscopists, mainly because the procedures are based on frequency and intensity data only, whereas experts use the complete spectrum, including specific visual features (e.g., band shapes and patterns) and non-absorbing regions. Encoding the latter type of interpretation as carried out by experienced spectroscopists into a mathematic algorithm might be a way to improve computerised interpretation of IR spectra. Advanced pattern recognition techniques can be used for this purpose and many different approaches have been investigated (e.g., principal component analysis [13,14] and artificial neural networks [15–21]).

The chemometric and the human approach of interpreting IR spectra are quite different. Chemometric techniques process spectral data in a strictly mathematical and statistical way; all spectra are treated identically, e.g., as a set of floating point numbers in the mid IR range. Contrary, humans deal with spectra in many different ways depending on individual knowledge and experience. The correctness and certainty of the conclusions is person related therefore. Different from chemometric methods, men are able to derive essential structural information from visual elements such as the size, shape and symmetry of absorption bands in addition to frequency and intensity data. Besides, men show the peculiar talent of making assumptions and neglecting defects or distortions caused by noise or impurities. To our knowledge, these aspects have not been incorporated into IR interpretation systems so far. Modern advanced pattern recognition techniques may be useful to mimic parts of the human process and to improve present interpretation programs. Besides, the current fast and powerful dedicated and personal computers have brought such techniques into the reach of spectroscopists.

The goal of this study was to get more insight into the potentials of two multivariate techniques, viz., partial least squares regression (PLS) and artificial neural networks (ANN), in recognizing characteristic visual features as used by IR spectroscopists. PLS is commonly used for quantitative purposes but it is expected to have potentials for qualitative analysis as well. Besides, PLS has become a standard software package on most IR instruments. ANN are thought to match closely human pattern recognition abilities [22].

Training and validation of ANN and PLS models requires substantial computer time and facilities. Enhancement of the calculation speed by reducing the number of spectral data points is attractive but may result into worse classifications. Therefore, an additional aim of this study was to gain insight into the effect of data point reduction on the classification results of PLS and ANN.

2. Experimental

All spectra have been recorded on a Bruker IFS-85 FTIR spectrometer equipped with an Aspect 1000 data station. Solids were prepared as melts or as KBr pellets, liquids as a neat film between KBr windows. Scanning conditions were: region 4000–625 cm^{-1}, data point resolution 1 cm^{-1}, 32 scans co-added. Acquisition and processing software: Bruker ATS89B.

Spectra have been scaled to 100% T for the transmission maximum and 3.2% T (1.5 absorbance units) for the strongest peak in the spectrum. Peak tables of transmission minima have been obtained from the system software by the peak picking program using a sensitivity threshold of 70 arbitrary units. Band intensities have been related to the transmission maximum of the spectrum defined as 0 and the strongest band in the spectrum, defined as intensity 100.

Visual interpretation has been performed by two experienced interpreters. For all experiments the training set was shown twice (1 min per spectrum) on subsequent days. Classification of the training and validation set was carried out on the third day.

The neural network was a backward-error-propagation type with one hidden layer which consisted of 4 neurons (1 offset neuron) [26]. The number of input neurons varied between 44 and 844 depending on software restrictions, the desired data point resolution and the spectral region to be studied. One output neuron has been used for classification in all experiments. The learning rate was set to 0.5 and the momentum to 0.3. Training has been carried out with synchronous prediction of the validation set. The minimum in the root mean square error of prediction (RMSE) value of the validation set has been used to determine the optimum number of iterations. In case a minimum was not determined, the training has been stopped after 2000 iterations or after convergence in the training set (RMSE < 0.01). The network has been programmed in Think Pascal™.

PLS calibrations have been performed to a maximum of five factors. Cross validation has been applied to determine the optimum number of factors to be used in the PLS model. The program has been written in Think Pascal™.

Data point reduction has been applied for all ANN and PLS calculations. Reduction has been performed by a stepwise elimination of data points from the original spectra, i.e., leaving out every 2, 4, 8 etc. datapoints depending on the required reduction.

Frequency–structure correlations (FSC), i.e., selective spectral regions (no false negatives), have been acquired from the training data by the Prolog™ program ERGA as described earlier [27]. The intervals have been transformed into interpretation rules and incorporated into the knowledge based system EXSPEC [10]. Next, EXSPEC has been used to classify the spectra of the validation set.

Three levels of prediction regarding the structural class of interest were allowed for the interpretation by spectroscopists, i.e., present, absent and unknown, corresponding with numerical values of 1, 0 and 0.5 respectively. The values obtained for EXSPEC, PLS and ANN were scaled between 1 and 0 for comparison purposes. Furthermore, values > 0.6 were regarded as a "present" classification, values < 0.4 as "absent", and values in between as "unknown". Comparison with the true molecular structure thus allowed calculation of the number of false and correct positives and negatives for each method.

Alternatively, average correctness of prediction (ACP) values were calculated according to:

$$ACP = \frac{\sum_{i}^{n_+} p_{+,i} + \sum_{j}^{n_-} (1 - p_{-,j})}{n_+ + n_-}$$

Here, $p_{+,i}$ and $p_{-,j}$ stand for the predictions of samples i and j that do (+) or do not (−) belong to the class of interest, whereas n_+ and n_- stand for the number of samples in each class, respectively. When, for instance, all samples are predicted correctly, i.e., $p_{+,i}$ equals 1 and $p_{-,j}$ equals 0, ACP equals 1, whereas when all predictions are wrong ACP becomes 0. Next, ACP values were calculated for both classes separately, i.e., ACP_+ for the collection of spectra of the

compounds with the structural feature of interest and ACP_{-} for the set without it.

All calculations have been carried out on Apple Macintosh™ computer type SE/30 equipped with a Motorola 68030 processor.

3. Methods and materials

Insight into the interpretation process as carried out by men has been obtained from observing and interviewing several experienced spectroscopists and more than 40 students [23] during the interpretation of dozens of spectra. The students showed a uniform and rather systematic approach: they checked the absorption bands one by one with matching intervals of frequency/intensity–structure correlation tables. Little attention was paid to band intensities compared to skilled interpreters. Characteristic band-shapes and -patterns were recognized only rarely, despite they had been taught to take notice of visual features. Use of these features seems to increase with experience.

The experts virtually manifested a less systematic approach. Interpretation paths seemed arbitrary and sometimes even different when the same spectrum was shown a second time. In all cases FSC data formed the basis of the extracted information as it did for the students. Furthermore, essential conclusions were drawn from visual characteristics. Briefly spoken, three types of visual features were distinguished; (i) the entire spectral profile from 4000 to 625 cm^{-1}, (ii) groups or combinations of bands in a certain wavenumber region, and (iii) the shape and size of individual absorption bands. A characteristic example of each type is presented in Fig. 1. The skew baseline combined with the first derivative like bands of spectrum A is generally recognized by spectroscopists as originating from a crystalline (poly) aromatic sample. The band pattern of spectrum B is characteristic for the overtone pattern of *ortho*-substituted benzenes and the smooth band C is typical for an alcohol.

3.1. Full spectrum classification

Experts generally start interpreting with a general impression of the complete spectrum. At this stage, exact peak locations are not yet looked for. As a result, spectra are classified into rough chemical groups such as organics/inorganics, aliphatic/olefinic, etc. This information is kept in mind during further, more detailed, interpretation. For that reason we first studied the capability of ANN and PLS to classify spectra in a similar way, i.e., by using the complete spectral range 4000–625 cm^{-1}. To do so spectra of three compound classes with clearly different spectral images have been selected. The visual features of these classes are illustrated by the spectra in Fig. 2. The skew baseline and first derivative like bands of the spectra type A are classified by spectroscopists as originating from polyaromatic compounds while the smooth and simple spectra

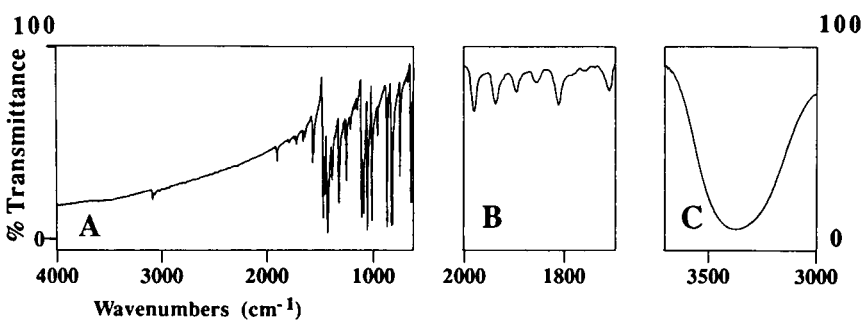

Fig. 1. Examples of different visual characteristics of infrared spectra: (A) the spectral profile of a polyaromatic hydrocarbon, (B) the overtone pattern of an *ortho*-substituted benzene, and (C) the characteristic OH-stretching band of an alcohol.

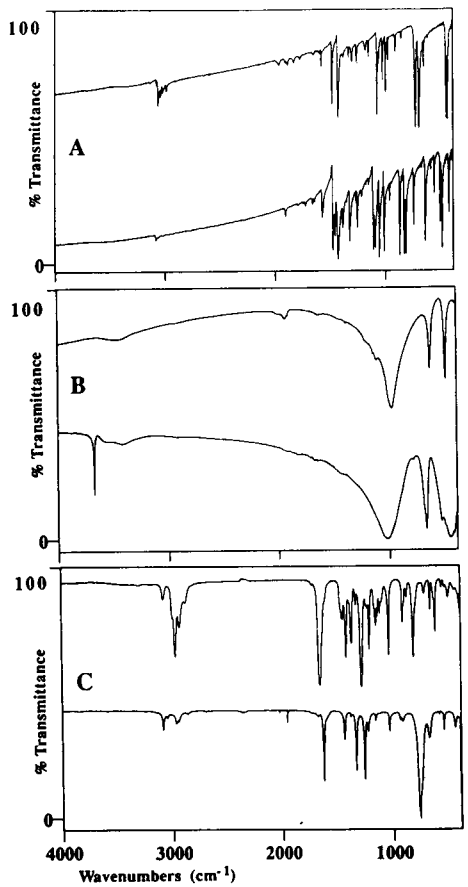

Fig. 2. Characteristic IR spectra of (A) polyaromatic, (B) inorganic and (C) ordinary organic compounds.

type B are assigned to inorganic molecules. Spectra with a straight baseline, like in C are recognized as ordinary organic samples.

Classification of these spectra was carried out on a set of 55 spectra of 3 different classes, i.e., polyaromatic, inorganic and general organic compounds. Ten spectra of each group were randomly chosen in a subset for training and the remaining 25 (9 polyaromatics, 6 inorganics and 10 organics) were used for validation. Original transmission spectra were used for expert classification. The number of input neurons for the training of the ANN was reduced from 3376 spectral data points to 422 owing to RAM limitations and to speed up calculation time. The same data were used for PLS calculations.

3.2. Band pattern classification

Structural information is frequently derived from spectral patterns in limited wavenumber regions. Well known examples are the irregularly shaped O–H stretching bands of carboxylic acids around 3000 cm^{-1} and the earlier mentioned overtone patterns of substituted benzenes in the interval 2000–1700 cm^{-1}. Less commonly known is the complex though characteristic band pattern of the structural fragment O–P=S. This structural element is present in a large variety of

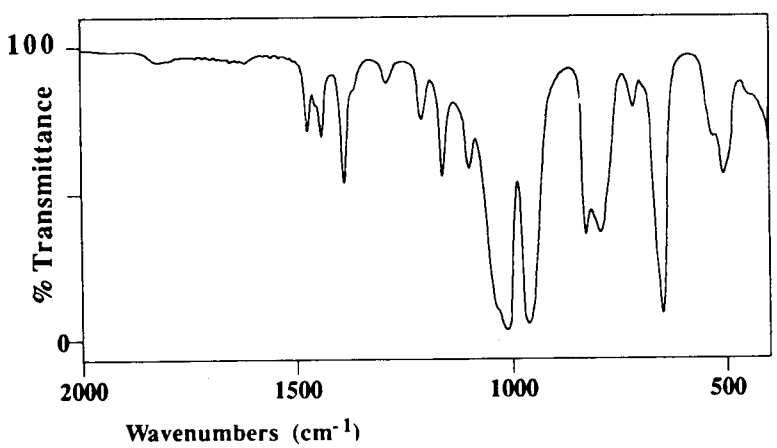

Fig. 3. Spectrum of the organophosphorus pesticide Ethion. The broad bands around 1020 and 820 cm^{-1} are characteristic for the presence of the O–P=S group.

organophosphorus pesticides. According to the literature [24,25], its presence is difficult to detect from the spectrum. In our lab however, the presence is often determined from two bands around 1020 and 820 cm^{-1} by considering the specific broad band pattern in addition to the absorption frequencies. The band pattern in the region 1200–625 cm^{-1} in the spectrum of the pesticide Ethion in Fig. 3 illustrates the absorption characteristics of the O–P=S group.

This structural element and the corresponding spectral region were chosen to establish the classifying capabilities of ANN and PLS when only a limited spectral region is examined. Both the spectral region 1200–625 cm^{-1} and the full spectra from 4000–625 cm^{-1} were investigated to establish differences between reduced spectral window interpretation and classification based on full spectra. A set of 98 pesticide spectra was used for this experiment. This set consisted of 55 compounds with and 43 without the O–P=S group,. A principal component analysis was applied on the total set and the scores describing 75% of the variation in the data were used in a cluster analysis to obtain a representative subset for training. This set contained 20 spectra of each class. The remaining 58 spectra (35 O–P=S and 23 non O–P=S) were used for validation. Visual classification and calculations of frequency/intensity–structure correlations were performed on the original data (data point resolution 1 cm^{-1}). ANN and PLS calculations were carried out after reduction of the number of data points to 844, 422, 211 and 105 (data point resolution 4, 8, 16 and 32 cm^{-1}, respectively) for the full spectra and 288, 144, 72 and 36 data points (data point resolution 2, 4, 8 and 16 cm^{-1}, respectively) for the region 1200–625 cm^{-1}.

3.3. Single bandshape classification

Valuable structural information can be obtained from individual bandshapes. Characteristic features like bandwidth and asymmetry are often used by spectroscopists to differentiate between structural elements particularly in case of overlapping absorption regions. An example is shown in Fig. 4. The smooth and broad absorption band (A) is characteristic for an O–H stretching band of an alcohol. It is easily distinguished from the smaller bands (B) and (C) originating from the N–H stretching vibration of a carbamate and the ≡C–H stretching vibration of a terminal alkyne, respectively.

In order to establish the recognizing potentials of ANN and PLS in this respect a set of 60 O–H, N–H and ≡C–H bands in the region 3700–3000 cm^{-1} was composed. A subset of 10 O–H, 10 N–H and 4 ≡C–H bands was visually selected for training and the remaining 36 bands (16 O–H, 16 N–H and 4 ≡C–H) were used for validation. Two classifications were carried out on these data. One was performed on the original bands thus including frequency and intensity variation. The other one was executed after scaling and centring of the bands in order to get insight into the

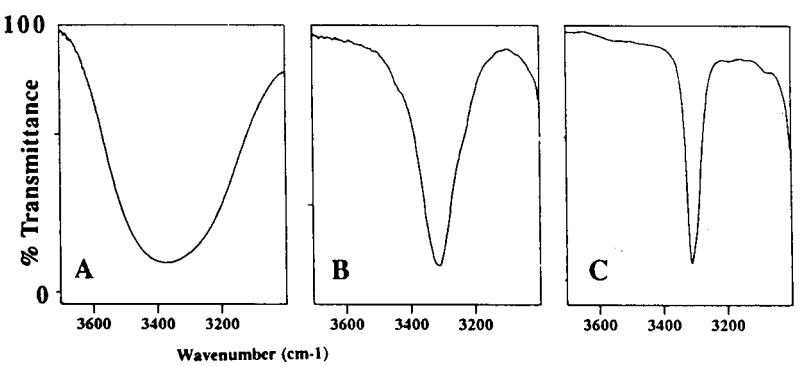

Fig. 4. Characteristic band shapes of (A) ν_{OH} of an aliphatic alcohol, (B) ν_{NH} of a carbamate, and (C) $\nu_{\equiv CH}$ of an alkyne.

Table 1
Results of ANN classification of aromatic, inorganic and average organic compounds based on full IR spectrum analysis

	Training set			Validation set		
	Aromatics	Inorganics	Organics	Aromatics	Inorganics	Organics
Correct positive	10	10	10	4	5	9
Correct negative	20	20	20	14	17	12
False positive	0	0	0	1	2	1
False negative	0	0	0	5	1	0
Unknown	0	0	0	1	0	3
ACP_+	1.00	0.99	0.99	0.48	0.82	0.94
ACP_-	1.00	0.99	0.99	0.89	0.89	0.83
ACP	1.00	0.99	0.99	0.69	0.87	0.91

potentials to recognize real band shapes. For this experiment all bands were centred around the bandmaximum ν_{max} resulting in spectra ranging from $\nu_{max} + 350$ cm^{-1} to $\nu_{max} - 350$ cm^{-1}. The absorption maximum was scaled to 3.2% transmission (1.5 absorbance units).

Classification by experts and generation of frequency/intensity–structure correlations were carried out on the original data (data point resolution 1 cm^{-1}). The data point resolution for ANN and PLS calculations was reduced to 2, 4, 8 and 16 cm^{-1} (350, 175, 88 and 44 data points, respectively).

4. Results and discussion

Repeated training of a neural network for the same set of spectra revealed variation in the number of iterations for optimal prediction of the spectra in the validation set. This phenomenon is well known and it is due to the random values assigned to the weight vectors at the start of the training. For that reason we have chosen to train three networks for each training set and to use the network with the lowest root mean square error (RMSE) in the validation set for classification.

4.1. Full spectrum classification

Cross validation of the obtained PLS models revealed a minimum for a 3-factor model in all cases. The number of iterations of the selected networks were 756, 120 and 467 for respectively the aromatic, inorganic and organic spectra. The ACP values and the classification results of the spectra of the training and validation sets as obtained from ANN and PLS are presented in Tables 1 and 2. The ANN predictions of the training set are perfect for all 3 classes (Table 1). The results of the validation set are fairly satisfactory for the inorganic and organic spectra but 5 out of 9 aromatic compounds are misclassified

Table 2
Results of PLS classification of aromatic, inorganic and average organic compounds based on full IR spectrum analysis

	Training set			Validation set		
	Aromatics	Inorganics	Organics	Aromatics	Inorganics	Organics
Correct positive	8	10	10	2	4	9
Correct negative	18	20	19	13	15	12
False positive	1	0	0	0	1	1
False negative	0	0	0	5	2	0
Unknown	3	0	1	5	3	3
ACP_+	0.66	0.88	0.90	0.48	0.56	0.93
ACP_-	0.90	0.94	0.95	0.96	0.84	0.83
ACP	0.78	0.91	0.92	0.72	0.77	0.87

($ACP_+ = 0.48$). The PLS results (Table 2) are worse for both subsets. Only the organics are predicted well ($ACP_+ = 0.93$). The spectroscopists classified all spectra correct (all *ACP*'s = 1.00).

4.2. Band pattern classification

Referring to the literature [24,25], at least two IR absorption bands are related to the O–P=S group: the P–O stretching in the region 1088–922 cm^{-1} and the P=S stretching in the interval 730–535 cm^{-1}. Both bands may be split in an in-phase and an out-of-phase component due to mechanical coupling of vibrations. The selective absorption intervals (no false negatives) as generated from the full spectra by the ERGA program are presented in Table 3. As appears, three intervals match well with the literature data. The number of spectra with interfering bands in the different intervals is large but can be reduced to zero by using the four intervals in a cumulative combination. The interval 2934–2839 cm^{-1} is not directly correlated to the O–P or P=S vibrations. It originates from the C–H stretching bands of alkyl groups attached to the organophosphorus oxygen atom(s) in most of these pesticides. It follows that using the region 1200–625 cm^{-1} produces worse

Table 3
Selective spectral windows generated by ERGA for the structural element O–P=S. Data obtained from the training set. Spectral region 4000–625 cm^{-1}

Selective window (cm^{-1})	Intensity window (relative units)	Interferences per interval	Interferences cumulative
1038–1001	100–89	7	7
2934–2839	55–10	10	3
835– 808	97–58	13	2
1018– 933	100–70	12	0

Table 4
Classification results for organophosporus pesticides obtained from ANN, PLS and EXSPEC models and expert interpretation. Spectral region 4000–625 cm^{-1}. Datapoint resolution 4 cm^{-1}

	Training set				Validation set			
	ANN	PLS	EXSPEC	EXPERT	ANN	PLS	EXSPEC	EXPERT
Correct positive	20	18	20	19	33	34	26	33
Correct negative	20	20	20	20	17	15	17	18
False positive	0	0	0	0	7	3	1	3
False negative	0	0	0	0	0	0	14	0
Unknown	0	2	0	1	1	6	0	4
ACP_+	1.00	0.91	1.00	0.97	0.98	0.99	0.74	0.98
ACP_-	1.00	0.92	1.00	0.99	0.73	0.70	0.74	0.81
ACP	1.00	0.91	1.00	0.98	0.88	0.87	0.74	0.91

Table 5
Classification results for organophosporus pesticides obtained from ANN, PLS and EXSPEC models and expert interpretation Spectral region 1200–625 cm^{-1}. Datapoint resolution 4 cm^{-1}

	Training set				Validation set			
	ANN	PLS	EXSPEC	EXPERT	ANN	PLS	EXSPEC	EXPERT
Correct positive	20	17	20	19	33	31	20	33
Correct negative	20	18	17	20	12	15	17	18
False positive	0	0	3	0	7	2	6	3
False negative	0	0	0	0	0	1	15	0
Unknown	0	5	0	1	6	9	0	4
ACP_+	0.99	0.86	0.88	0.97	0.97	0.92	0.57	0.98
ACP_-	1.00	0.87	0.85	0.99	0.66	0.65	0.74	0.81
ACP	0.99	0.86	0.87	0.98	0.85	0.81	0.64	0.91

Table 6
The effect of the datapoint resolution on the *ACP* values of ANN and PLS classification for organophosporous pesticides. Spectral region 4000–625 cm^{-1}

	Training set				Validation set			
Resolution:	4/cm	8/cm	16/cm	32/cm	4/cm	8/cm	16/cm	32/cm
ANN								
ACP_+	1.00	0.99	1.00	1.00	0.98	1.00	0.99	0.99
ACP_-	1.00	0.99	1.00	0.99	0.73	0.65	0.61	0.72
ACP	1.00	0.99	1.00	0.99	0.88	0.86	0.84	0.88
PLS								
ACP_+	0.91	0.92	0.91	0.92	0.99	0.99	0.87	0.99
ACP_-	0.92	0.92	0.92	0.92	0.70	0.69	0.61	0.69
ACP	0.91	0.92	0.91	0.92	0.87	0.87	0.77	0.87

results compared to the full spectrum. This is confirmed by the results obtained from EXSPEC, ANN, PLS and the experienced interpreters as summarised in Table 4 and Table 5. Implementation of the cumulative combination of the four best intervals generated by ERGA, as interpretation rules into EXSPEC yield considerably higher scores for the full spectra than for the limited spectral regions. For the latter, spectra are even predicted false positive when using a combination of five intervals.

Subsequent neural network training of the sub-sets of the full spectra and of the 1200–625 cm^{-1} region revealed a minimum in the RMSE of the validation set after 800 and 120 iterations, respectively. Optimal PLS models contained two factors in both cases. The results of ANN and PLS are similar but significantly better than the scores obtained from EXSPEC. ANN, PLS and EXSPEC classifications obtained from the full spectra, are slightly better than when using the reduced region. Apparently all methods extract information from spectral area's which seem not directly correlated with O–P or P=S vibrations.

Expert classification is not affected by the wavenumber interval. Again, experts produce the highest scores with average prediction factors of 0.98 (O–P=S), 0.81 (non O–P=S) and 0.91 (total).

The effect of the data point resolution on the classification results of ANN and PLS is shown in Table 6 and Table 7. The number of iterations for the networks was kept the same (800 and 120, respectively) and the PLS predictions were obtained from two factor models. The *ACP* values are virtually unaffected by the applied spectral resolution. It follows that, at least for certain

Table 7
The effect of the datapoint resolution on the *ACP* values of ANN and PLS classification for organophosporous pesticides. Spectral region 1200–625 cm^{-1}

	Training set				Validation set			
Resolution:	4/cm	8/cm	16/cm	32/cm	4/cm	8/cm	16/cm	32/cm
ANN								
ACP_+	0.99	0.99	0.99	0.99	0.97	0.97	0.94	0.93
ACP_-	1.00	0.99	0.99	0.99	0.66	0.60	0.63	0.61
ACP	0.99	0.99	0.99	0.99	0.85	0.82	0.81	0.80
PLS								
ACP_+	0.86	0.86	0.86	0.85	0.92	0.92	0.89	0.89
ACP_-	0.87	0.88	0.87	0.85	0.65	0.64	0.61	0.63
ACP	0.86	0.87	0.86	0.85	0.81	0.81	0.78	0.79

Table 8
Absorption frequency window and intensity interval with number of interfering compounds of the O–H, N–H and ≡C–H stretching vibration of respectively alcohols, carbamates and terminal alkynes as generated by ERGA

Vibration	Selective interval (cm^{-1})	Intensity interval (%T)	Interferences training set	Interferences validation set
ν_{OH}	3421–3217	80–100	10	6
ν_{NH}	3377–3275	55–100	7	10
$\nu_{\equiv CH}$	3314–3296	45– 80	2	5

applications of ANN and PLS, data point reduction can be applied.

4.3. Band shape classification

The FSC data produced by ERGA from the original bands are presented in Table 8. The intervals overlap, leading to a large number of interferences in the training and the validation set. PLS cross validation revealed maximum correlation for a 2-factor model for the O–H and N–H bands and a 3-factor model for the ≡C–H bands. Training of the ANN revealed considerable variation in the optimal number of iterations. Therefore networks obtained from 120 iterations were chosen for all classifications.

The results obtained from EXSPEC, PLS, ANN and the experts are presented in the Tables 9–11. The ACP_+ value of the original O–H bands as obtained from EXSPEC (Table 9) is high (0.94) as all absorption maxima of the validation set except one, fall within the selective interval of Table 8. The ACP_- is small (0.65) because of 6 false positives in the validation set. The ANN and PLS classifications are on average slightly better although the ACP_+ values are smaller than expected. A closer examination of the false

Table 9
Classification results of the O–H stretching band of alcohols. ANN, PLS, EXSPEC and expert results obtained from the original bands. ANN(C) and PLS(C) acquired from the centred and scaled data

	Training set						Validation set					
	ANN	PLS	EXSPEC	EXPERT	ANN(C)	PLS(C)	ANN	PLS	EXSPEC	EXPERT	ANN(C)	PLS(C)
Correct positive	10	10	10	10	10	10	12	11	15	16	11	11
Correct negative	14	14	4	12	14	14	17	15	13	19	18	16
False positive	0	0	10	0	0	0	1	0	6	0	2	0
False negative	0	0	0	0	0	0	4	4	1	0	5	3
Unknown	0	0	0	2	0	0	2	6	0	1	1	6
ACP_+	1.00	0.97	1.00	0.97	1.00	0.97	0.73	0.74	0.94	1.00	0.71	0.71
ACP_-	1.00	0.99	0.28	0.99	1.00	0.99	0.89	0.83	0.65	0.95	0.90	0.86
ACP	1.00	0.99	0.58	0.96	1.00	0.98	0.82	0.79	0.78	0.97	0.82	0.79

Table 10
Classification results of the N–H stretching band of carbamates. ANN, PLS, EXSPEC and expert results obtained from the original bands. ANN(C) and PLS(C) acquired from the centred and scaled data

	Training set						Validation set					
	ANN	PLS	EXSPEC	EXPERT	ANN(C)	PLS(C)	ANN	PLS	EXSPEC	EXPERT	ANN(C)	PLS(C)
Correct positive	10	10	10	9	10	9	13	11	14	14	13	8
Correct negative	14	10	7	14	14	14	17	13	10	18	15	16
False positive	0	4	7	0	0	0	3	6	10	0	4	2
False negative	0	0	0	0	0	0	2	0	2	0	3	4
Unknown	0	0	0	1	0	1	1	6	0	4	1	6
ACP_+	1.00	0.88	1.00	0.90	1.00	0.83	0.83	0.73	0.87	0.94	0.74	0.61
ACP_-	1.00	0.75	0.50	1.00	1.00	0.88	0.81	0.60	0.50	0.95	0.74	0.77
ACP	1.00	0.81	0.71	0.95	1.00	0.85	0.82	0.69	0.66	0.94	0.74	0.69

Table 11
Classification results of the ≡C–H stretching band of terminal alkynes. ANN, PLS, EXSPEC and expert results obtained from the original bands. ANN(C) and PLS(C) acquired from the centered and scaled data

	Training set						Validation set					
	ANN	PLS	EXSPEC	EXPERT	ANN(C)	PLS(C)	ANN	PLS	EXSPEC	EXPERT	ANN(C)	PLS(C)
Correct positive	4	2	4	3	4	3	4	2	2	4	2	2
Correct negative	20	19	18	20	20	20	30	30	27	29	28	25
False positive	0	0	2	0	0	0	1	0	5	0	4	4
False negative	0	0	0	0	0	0	0	0	2	0	1	0
Unknown	0	3	0	1	0	1	1	4	0	3	1	5
ACP_+	1.00	0.58	1.00	1.00	1.00	0.66	0.90	0.58	0.50	1.00	0.66	0.55
ACP_-	1.00	0.92	0.90	1.00	1.00	0.91	0.96	0.93	0.84	0.95	0.89	0.84
ACP	1.00	0.85	0.92	0.98	1.00	0.87	0.94	0.90	0.80	0.96	0.89	0.84

negatives revealed that this is due to bands of O – H groups that are shielded from intermolecular interactions. The corresponding half-bandwidths are considerably smaller than of the ordinary O–H bands as chosen in the training set. It follows that both ANN and PLS can be used to distinguish between small and broad bands. ACP_+ values of 0.99 were obtained by ANN and PLS after the small O–H bands were removed from the validation set. Differences between the classifications of the validation sets of the original and the centred O–H bands are found to be negligible.

The original N–H bands are recognized quite well by the network and the experts whereas the PLS and EXSPEC results are worse (Table 10). The number of false positives is larger and the number of correct negatives smaller. The centred bands are predicted less good (smaller *ACP* values) by both ANN as well as PLS.

Similar results (Table 11) are obtained for the ≡C–H bands despite the fact that only four bands were present in the training sets. The four ethynyl compounds in the validation set of the original bands are distinguished correctly by the ANN and the experts, whereas PLS and EXSPEC scored smaller *ACP* values. A decreased performance is also seen for the centred bands. These results are consistent with the N–H band classifications.

Two conclusions can be drawn from these results. First, ANN seem to be better in recognizing specific bandshapes than PLS. This is particularly true for the classification of the relatively narrow

Table 12
The effect of the datapoint resolution on the ANN classification of the original O–H, N–H and ≡C–H stretching bands of alcohols, carbamates and terminal alkynes

	Training set				Validation set			
Resolution:	2/cm	4/cm	8/cm	16/cm	2/cm	4/cm	8/cm	16/cm
O–H Original band								
ACP_+	1.00	1.00	1.00	1.00	0.73	0.74	0.74	0.74
ACP_-	1.00	1.00	1.00	1.00	0.89	0.87	0.87	0.90
ACP	1.00	1.00	1.00	1.00	0.82	0.81	0.81	0.83
N–H Original band								
ACP_+	1.00	1.00	1.00	1.00	0.81	0.77	0.80	0.77
ACP_-	1.00	1.00	1.00	1.00	0.83	0.87	0.86	0.87
ACP	1.00	1.00	1.00	1.00	0.82	0.82	0.83	0.82
C–H Original band								
ACP_+	1.00	0.97	1.00	1.00	0.90	0.90	0.99	0.99
ACP_-	1.00	0.98	1.00	1.00	0.96	0.96	0.88	0.87
ACP	1.00	0.97	1.00	1.00	0.95	0.95	0.89	0.88

Table 13
The effect of the datapoint resolution on the PLS classification of the original O–H, N–H and ≡C–H stretching bands of alcohols, carbamates and terminal alkynes

	Training set				Validation set			
Resolution:	2/cm	4/cm	8/cm	16/cm	2/cm	4/cm	8/cm	16/cm
O–H Original band								
ACP_+	0.97	0.97	0.98	0.97	0.74	0.73	0.70	0.73
ACP_-	0.99	0.99	0.99	0.99	0.83	0.83	0.86	0.87
ACP	0.98	0.98	0.98	0.98	0.79	0.79	0.79	0.81
N–H Original band								
ACP_+	0.88	0.73	0.78	0.88	0.75	0.66	0.66	0.75
ACP_-	0.75	0.85	0.84	0.75	0.57	0.67	0.66	0.60
ACP	0.81	0.80	0.81	0.81	0.65	0.67	0.66	0.67
C–H Original band								
ACP_+	0.58	0.58	0.58	0.58	0.58	0.58	0.58	0.57
ACP_-	0.92	0.91	0.94	0.95	0.93	0.95	0.94	0.93
ACP	0.75	0.74	0.76	0.76	0.89	0.91	0.90	0.89

Table 14
The effect of the datapoint resolution on the ANN classification of the centred O–H, N–H and ≡C–H stretching bands of alcohols, carbamates and terminal alkynes

	Training set				Validation set			
Resolution:	2/cm	4/cm	8/cm	16/cm	2/cm	4/cm	8/cm	16/cm
O–H Original band								
ACP_+	1.00	1.00	1.00	1.00	0.71	0.71	0.74	0.74
ACP_-	1.00	1.00	1.00	1.00	0.90	0.89	0.88	0.87
ACP	1.00	1.00	1.00	1.00	0.82	0.81	0.82	0.82
N–H Original band								
ACP_+	1.00	1.00	1.00	1.00	0.74	0.75	0.74	0.74
ACP_-	1.00	1.00	1.00	1.00	0.74	0.71	0.69	0.69
ACP	1.00	1.00	1.00	1.00	0.74	0.73	0.71	0.71
C–H Original band								
ACP_+	1.00	0.97	1.00	1.00	0.66	0.67	0.65	0.69
ACP_-	1.00	0.98	1.00	1.00	0.89	0.90	0.90	0.85
ACP	1.00	0.97	1.00	1.00	0.86	0.87	0.87	0.83

Table 15
The effect of the datapoint resolution on the PLS classification of the centred O–H, N–H and ≡C–H stretching bands of alcohols, carbamates and terminal alkynes

	Training set				Validation set			
Resolution:	2/cm	4/cm	8/cm	16/cm	2/cm	4/cm	8/cm	16/cm
O–H Centered band								
ACP_+	0.97	0.97	0.97	0.97	0.80	0.79	0.80	0.80
ACP_-	0.98	0.96	0.98	0.98	0.86	0.91	0.86	0.86
ACP	0.97	0.96	0.97	0.97	0.83	0.86	0.83	0.83
N–H Centered band								
ACP_+	0.83	0.83	0.83	0.82	0.74	0.74	0.74	0.75
ACP_-	0.88	0.89	0.88	0.83	0.83	0.86	0.85	0.87
ACP	0.85	0.86	0.85	0.82	0.83	0.86	0.85	0.87
C–H Centered band								
ACP_+	0.66	0.65	0.65	0.63	0.55	0.55	0.54	0.56
ACP_-	0.91	0.93	0.87	0.93	0.84	0.79	0.82	0.71
ACP	0.78	0.79	0.76	0.78	0.82	0.76	0.79	0.69

N–H and ≡C–H bands. It indicates that the bandwidth is involved in the recognition process. Secondly, the smaller *ACP* values obtained from the experiments with the centred N–H and ≡C–H bands confirm that classification by ANN and PLS is also related to the absorption frequencies.

The effect of the data point resolution on the *ACP* values of ANN and PLS classification of the original and the centered O–H, N–H and ≡C–H stretching bands is presented in the Tables 12–15. The *ACP* values of each series of experiments appears to be practically unaffected by the resolution. This is in agreement with the results of the same experiments on the band pattern of the organophosphorus compounds. Similar conclusions have recently been reported [28]. It follows that for classification purposes by means of ANN and PLS considerably lower data point resolutions suffice.

5. Conclusions

Characteristic band shapes and patterns of infrared spectra are better recognized by experienced spectroscopists than by backpropagation ANN and PLS models. Differences in scores between experts and multivariate methods tend to increase with the complexity of the spectral pattern. It endorses the specific human talent to recognize complicated images. However, ANN and PLS prove to be useful techniques to improve computerised interpretation based on FSC data only. Incorporation of ANN or PLS modules into an interpretation system is to be recommended therefore. The excellent prediction of all spectra in the training sets indicates that further enhancement can be achieved when extended, well composed, training sets are used

ANN and PLS perform comparably for both full spectra and limited spectral regions. Networks are better in recognizing individual bandshapes. The use of limited spectral regions instead of full spectra leads to a small decrease of the information yield. The results are virtually unaffected by the datapoint resolution.

The experiments with the centred bands prove that the classifying potentials of PLS and ANN are related to the position and the intensity of the absorption band. It emphasises the importance of absorption frequency information in the interpretation process. The band width appears to be a relevant parameter too. The role of (a)symmetry of bands is not yet clear and requires further study.

A disadvantage of ANN is the dependence of the weights in a trained network on the starting values. Consequently, the number of iterations for optimal configuration can differ considerably and several training sessions are necessary to establish the optimum number. This is of particular importance as the training of a neural network is time-consuming.

References

[1] H.J. Luinge, Vib. Spectrosc., 1 (1990) 3.
[2] H.B. Woodruff and G.M. Smith, Anal. Chem., 52 (1980) 2321.
[3] T. Visser and J.H. van der Maas, Anal. Chim. Acta, 133 (1981) 451.
[4] R. Tsao and W.L. Switzer, Anal. Chim. Acta, 136 (1982) 3.
[5] Z. Hippe, Trends Anal. Chem., 2 (1983) 240.
[6] T. Blaffert, Anal. Chim. Acta, 191 (1986) 161.
[7] B. Curry, ACS Symp. Ser., 306 (1986) 350.
[8] S. Moldeveau and C.A. Rapson, Anal. Chem., 59 (1987) 1207.
[9] H.J. Luinge, Thesis, Universiteit Utrecht, 1989.
[10] H.J. Luinge, Trends Anal. Chem., 9 (1990) 66.
[11] M. Cadisch and E. Pretsch, Fresenius' J. Anal. Chem., 344 (1992) 173.
[12] M. Cadisch, M. Farkas, J.-T. Clerc and E. Pretsch, J. Chem. Inf. Comput. Sci., 32 (1992) 286.
[13] J.C.W.G. Bink and H.A. van't Klooster, Anal. Chim. Acta, 150 (1983) 53.
[14] E.J. Hasenoehrl, J.H. Perkins and P.R. Griffiths, Anal. Chem., 63 (1991) 1738.
[15] J.E. Dayhof, Neural Network Architectures, Van Nostrand Reinhold, New York, 1990.
[16] E.W. Grob and M.E. Munk, Mikrochim. Acta, I (1990) 131.
[17] B.J. Wythoff, S.P. Levine and S.A. Tomellini, Anal. Chem., 62 (1990) 2702.
[18] H.J. Luinge, J.H. van der Maas and T. Visser, SPIE, Vol. 1575 (1991) 499.
[19] A. Reinders, T. Visser, D. Roos, P.F.J. de Vink and H.J. Luinge, RIVM-report No. 421504001 (1991).
[20] U.M. Weigel and R. Herges, J. Chem. Inf. Comput. Sci., 32 (1992) 723.

[21] M. Meyer and T. Weigelt, Anal. Chim. Acta, 265 (1992) 183.
[22] J.R.M. Smits, P. Schoenmakers, A. Stehmann, F. Sijstermans and G. Kateman, Chemom. Intell. Lab. Syst., 18 (1993) 27.
[23] Annual International Course on Infrared Spectroscopy, Utrecht University, August 16–20, 1993.
[24] L.J. Bellamy, The Infrared Spectra of Complex Molecules, Wiley, Chichester, 1975.
[25] D. Lin-Vien, N.B. Colthup, W.G. Fateley and J.G. Grasselli, Infrared and Raman Characteristic Frequencies of Organic Molecules, Academic Press, New York, 1991.
[26] D.E. Rummelhart and J.L. McClelland, Parallel Distributed Processing: Explorations in the microstructure of Cognition, MIT Press, Cambridge, MA, 1988.
[27] H.J. Luinge, G.J. Kleywegt, H.A. van't Klooster and J.H. van der Maas, J. Chem. Inf. Comput. Sci., 27 (1987) 95.
[28] P.R. Griffiths, 9th Int. Conf. on Fourier Transform Spectroscopy, Calgary, August 23, 1993.

ELSEVIER

Analytica Chimica Acta 296 (1994) 155–161

ANALYTICA CHIMICA ACTA

Stopped-flow near-infrared spectrometric determination of ethanol and maltose in beers

Máximo Gallignani, Salvador Garrigues, Miguel de la Guardia *

Department of Analytical Chemistry, University of Valencia, 50 Dr. Moliner St., 46100 Burjassot, Valencia, Spain

Received 1 February 1994; revised manuscript received 20 April 1994

Abstract

A near-infrared spectrometric procedure has been developed for the determination of ethanol in beer samples, based on the measurement of the ethanol absorbance maximum at 1693 nm above a base-line established between 1657 and 1720 nm, employing an 1 cm pathlength cell, and using a 4.5% (w/v) aqueous solution of maltose as a reference. For the analysis of real samples the method only requires a previous degassing of the samples, by filtration, and aqueous solutions of ethanol can be employed as standards. All types of beers, from regular beers containing about 5% (v/v) ethanol to low-alcohol beers with less than 1% (v/v) can be analyzed by using the same procedure. The method has a limit of detection of 0.07% (v/v) and a relative standard deviation of 0.2% for regular beer samples, and less than 2% for low-alcohol beer analysis. The use of the stopped-flow strategy provides a fast filling and cleaning of the measurement cells and a sample frequency of 120 injections per hour. Maltose can also be determined by additional measurement at ca. 1410 nm.

Keywords: Flow system; Infrared spectrometry; Ethanol; Beer analysis; Stopped-flow near-infrared spectrometric determination

1. Introduction

The determination of ethanol in beers can be carried out by official methods, based on the measurement of sample gravity or refractive index after a previous distillation [1,2]. These methods are very tedious and time consuming, however, and chemical procedures based on the oxidation of ethanol to acetic acid and titrimetric determination of the excess of the reagent employed can therefore be preferable [3]. At present, instrumental methods based on the use of gas chromatography [4,5], liquid chromatography [6,7], potentiometry [8] and differential-pulse polarography [9] offer good alternatives for the fast and accurate determination of ethanol. For the determination of ethanol in alcohol-free and low-alcohol samples, enzymatic methods provide very sensitive and accurate procedures [10,11] which can be applied in flow systems [12,13].

Fourier transform infrared (FT-IR) spectrometry in the medium range has been applied for the determination of ethanol in alcoholic beverages [14–17], but in general the methods developed

* Corresponding author.

SSDI 0003-2670(94)00205-Z

provide poor sensitivity. In a recent paper, however, we have proposed a new derivative FT-IR procedure for the direct determination of ethanol in all types of alcoholic beverages [18]. It can be applied for the direct analysis of beer samples with a limit of detection of 0.025% (v/v) and a typical relative standard deviation of 0.8% and 1% for 5 independent analysis of real samples containing 5% (v/v) and 1% (v/v) of ethanol, respectively [19].

Near-infrared (NIR) spectrometry has been applied for the direct determination of ethanol in beers [20,21] and wines [22], by reflectance analysis, and also transmission NIR spectrometry has been employed for the analysis of beers [23] and molasses [24]. However, previously developed methods need the use of multiple linear regression analysis or other complex mathematical treatment of data and provide poor sensitivity.

We have proposed a new NIR-derivative spectrometric procedure for the direct determination of ethanol in all types of alcoholic beverages, which provides a limit of detection of 0.1% (v/v), and can be applied for the determination of ethanol in regular beer samples [25]. The aim of the present paper is to improve the previously developed procedure in order to enhance the limit of detection and to make this kind of measurements suitable for the analysis of real beer samples, from regular ones to low-alcohol samples. Stopped-flow methodology has been incorporated to improve the sample throughput rate.

2. Experimental

2.1. Apparatus and reagents

A Perkin-Elmer Lambda 9 double beam UV–visible–NIR spectrometer, equipped with a tungsten halogen lamp source and a PbS detector, was used to carry out the absorbance measurements in the NIR region. The spectrometer covers a wavelength range from 185 to 3200 nm and is equipped with a monochromator with a grating of 260 lines per mm to enable it to operate in the NIR. Glass cells with 1 cm and 1 mm pathlengths and a quartz flow cell of 1 cm, were employed to carry out the direct determination of ethanol in beer samples, both in a batch and stopped-flow mode.

For carrying out measurements in the stopped-flow mode, a two-independent-channels system controlled by a Gilson Minipuls 2 peristaltic pump was employed. This system provides a means for suitable filling and cleaning of both the reference cell and the measurement cell, in order to provide the measurement of the absorbance of samples against a maltose solution as reference and that of aqueous standards against water.

An Anton Parr FPR 09 Model automatic beer analyzer, from German Weber (Austria), was employed to obtain reference values on the concentration of ethanol in a series of real samples.

Analytical reagent grade ethanol (99.5%) and maltose were obtained from Panreac (Barcelona) and all different standard solutions were prepared with high quality deionized water with a measured resistivity of 18 MΩ cm.

2.2. General procedure

NIR spectrometric determination of maltose and ethanol in beers

Beer samples were degassed by filtration through a Whatman No. 40 filter paper and their absorbance was measured between 1300 and 1800 nm, using a glass cell with a pathlength of 1 mm. Next the absorbance between the maximum at 1693 nm and the base-line established between 1657 and 1720 nm was measured using the 1 cm glass cell. In both cases water is used as a reference. From the experimental values obtained this way and from the parameters of the calibration graphs of ethanol and maltose, measured in both conditions, a system of two equations with two unknowns was established and, from the mathematical resolution of this system, the concentration of ethanol and maltose in beers was determined.

Stopped-flow NIR spectrometric determination of ethanol in beers

As an alternative to the above procedure a fast analytical procedure has been developed. Samples were degassed by filtration and injected into

a flow system. The absorbance difference between 1693 nm and the base-line established between 1657 and 1720 nm was measured in a flow cell of 1 cm pathlength and employing a 4.5% (w/v) maltose solution as a reference. The system was calibrated with aqueous ethanolic standards, measured against a water reference.

Reference procedure

25 ml of previously filtered beer samples were directly analyzed using an Anton Parr FPR 09 instrument, employing a characterized sample as a reference. These analyses were carried out in the laboratory of Cervezas El Águila S.A.

3. Results and discussion

3.1. NIR spectrum of ethanol and beer

Absolute ethanol provides, in the wavelength range from 1300 to 1800 nm, absorbance values which are, in general, lower than those obtained for water, which makes the NIR analysis of aqueous ethanolic solutions difficult. However, between 1670 and 1740 nm three absorption bands can be identified in the pure ethanol spectrum, at 1693, 1705 and 1735 nm, with a shoulder at 1718 nm, using CCl_4 as a reference. These bands can be used for the direct determination of ethanol in alcoholic beverages because their absorbance values are higher than those found of water. Thus, using water as a reference, the spectra indicated in Fig. 1 can be obtained for aqueous ethanolic solutions.

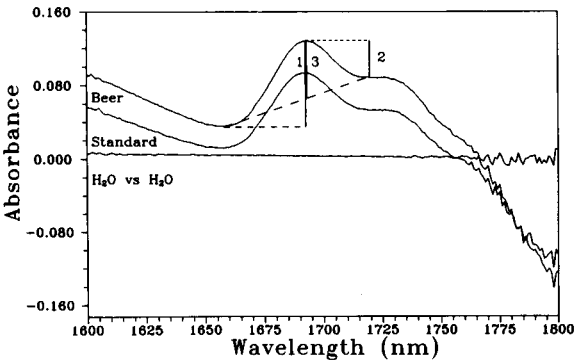

Fig. 1. NIR spectrum of ethanol and beer. Spectra correspond to a 5% (v/v) aqueous standard and a real beer sample containing a declarated value of 5.1% (v/v) of ethanol. Reference: water. The different criteria employed to determine the base-line are shown. In all cases a pathlength of 1 cm was employed.

The spectra of standards and beer samples have a maximum at 1693 nm and a shoulder at 1735 nm, which are appropriate for the direct determination of ethanol. However, on comparing the two spectra in Fig. 1 it can be seen that the sample spectrum provides higher absorbance values than correspond to the ethanol concentration and therefore it is necessary to select an

Table 1
Analytical features of the direct NIR determination of ethanol

Parameter		Measurement criteria [a]		
		1	2	3
Dynamic range (up to) (%, v/v)		10	15	12
LOD% (v/v)		0.05	0.1_2	0.07
Calibration equation [b]		$A = 0.0008 + 0.01720C$	$A = -0.0006 + 0.0078C$	$A = 0.0001 + 0.01250C$
Calibration equation [c]		$A = 0.001 + 0.01739C$	$A = 0.0007 + 0.0082C$	$A = 0.0008 + 0.01239C$
Typical absorbance signal $\pm s$				
[Ethanol]:	5% (v/v)	0.0860 ± 0.0003	0.0386 ± 0.0004	0.0623 ± 0.0003
	1% (v/v)	0.0173 ± 0.0002	0.0079 ± 0.0004	$0.0125 \pm 0.0001_4$

[a] Criteria: (1) between 1693 nm and a base-line at 1657 nm; (2) between 1693 nm and a base-line at 1720 nm; (3) between 1693 nm and a base-line established between 1657 and 1720 nm. LOD = Limit of detection. A = Absorbance. s = Standard deviation for 5 independent measurements. All measurements were carried out using a 1 cm cell.

[b] Calibration line obtained for the full dynamic range.

[c] Calibration line obtained between zero and 2% (v/v).

appropriate base-line. The different criteria employed for measuring the ethanol absorbance are summarized in Fig. 1. The first criterion is based on the difference in absorbance between the peak maximum at 1693 nm and the base-line absorbance at 1657 nm. The second is similar except the base-line is measured at 1720 nm. The third type uses the peak height at 1693 nm and a base-line absorbance at the same wavelength established by linear extrapolation from the base-line absorbance at 1657 and 1720 nm.

3.2. Analytical parameters of the direct NIR determination of ethanol

Using the above three measurement criteria, the analytical figures of merit of the direct absorbance measurement of ethanol in aqueous solutions, have been established for a series of aqueous ethanol standards. Table 1 summarizes all the data obtained.

The calibration lines have been determined for the full dynamic range and also from zero to 2% (v/v), in order to define an appropriate calibration for the analysis of low-alcohol content beer samples. As can be seen, both lines are very similar.

The limit of detection has been established from the repeatability of ten absorbance measurements of a blank solution and taking into account the sensitivity of the procedure (the slope of the calibration line) for a probability level of 99.86%. Typical absorbances found for standards containing 5% or 1% (v/v) of ethanol are also shown in Table 1. The standard deviations are very acceptable. All the analytical features seem to be satisfactory for the determination of ethanol. However, it must be indicated that values measured by use of criterion three have a better intra- and interday reproducibility.

3.3. Stopped-flow determination of ethanol in beers

The instrumentation employed to carry out this study is a dispersive spectrometer with a moving diffraction grating. Because of that, in order to carry out on-line absorbance signal and base-line measurements, it is necessary to stop the flow and scan over the appropriate wavelength range.

Table 2
Effect of the scan speed on the absorbance of ethanol at 1693 nm

Scan speed (nm min^{-1})	Absorbance $\pm$ s [a]	Sample frequency (h^{-1})
15	0.0628 ± 0.0002	7
30	0.0630 ± 0.0001	13
60	0.0630 ± 0.0001	25
120	0.0625 ± 0.0002	45
240	0.0627 ± 0.0002	72
480	0.0629 ± 0.0003	100
960	0.0633 ± 0.0003	120

[a] Absorbance values found for five independent measurements of an ethanol concentration of 5% (v/v) ± their standard deviation, based on criterion 3.

To evaluate the sample throughput rate of the method, different scan speeds were used and the relative standard deviations of the absorbance values determined. Table 2 summarizes the data found. As can be seen, increasing the scan speed has no significant effect on the sensitivity or repeatability of the NIR absorbance measurements, but of course it dramatically enhances the sample throughput rate. For the maximum scan speed of 960 nm min^{-1}, over the wavelength range 1640 to 1760 nm an absorbance value of 0.0633 is obtained for an ethanol concentration of 5% (v/v), with a relative standard deviation of 0.4%, which is very appropriate for the analysis of beers and provides an injection frequency of 120 h^{-1}.

The stopped-flow analysis of beers also diminishes the amount of sample used for an analysis and provides a continuous system for filling and cleaning the measurement cells.

3.4. Effect of the beer matrix

The matrix of beer samples has a NIR spectrum, which basically corresponds to that provided by a maltose solution, as can be seen in Fig. 2 which compares the spectrum of an alcohol-free beer and those of maltose solutions.

Fig. 2 shows that the presence of maltose gives a minimum at 1414 nm, the depth of which in-

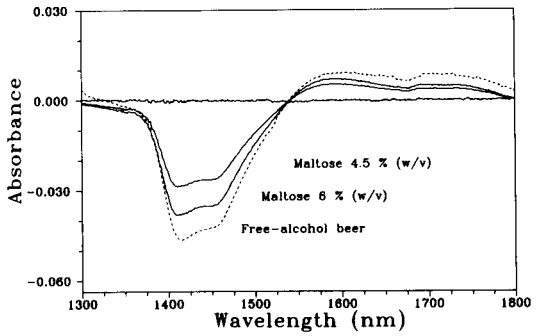

Fig. 2. NIR spectrum of an alcohol-free beer matrix and different aqueous solutions of maltose (spectra were obtained using a 1 mm pathlength cell with water as a reference).

creases on increasing maltose concentration. However, beer samples containing ethanol, and a standard ethanol solution also give a minimum at 1414 nm (see Fig. 3). Thus a regression line can be calculated which relates the absolute value of the minimum absorbance between 1414 and 1580 nm to both the ethanol and maltose concentrations.

Using a pathlength of 1 mm the following equations were obtained

$$A = 0.0000_6 + 0.01253C_{eth} \quad (1)$$

for ethanol, C_{eth} being the ethanol concentration in % (v/v) and

$$A = 0.0000_3 + 0.00822C_{malt} \quad (2)$$

for maltose (C_{malt} being the maltose concentration in g per 100 ml. From these equations it follows that

$$A = 0.01253C_{eth} + 0.00822C_{malt} \quad (3)$$

In contrast, in the range between 1640 and 1760 nm, the presence of maltose does not have a significant absorbance and the equation for the absorbance based on criterion three is

$$A = 0.01250C_{eth} + 0.00038C_{malt} \quad (4)$$

for a 1 cm pathlength cell. Therefore from measurements carried out using a 1 mm and a 1 cm cell, and using Eqs. 3 and 4 the concentration of both ethanol and maltose in the same sample can be determined.

Additional experiments studying the effect of increasing concentrations of maltose on the absorbance of ethanol standards, containing different ethanol concentrations, provided the following regression equations:

$$A = 0.0625 + 0.00038C_{malt} \quad (5)$$

$$A = 0.01250 + 0.00036C_{malt} \quad (6)$$

for the effect of maltose on the absorbance of a 5% (5), and 1% (v/v) (6) ethanol solution, respectively. As can be seen, the slope of these equations does not depend on the ethanol concentration of the samples, thus indicating that the absorbance of ethanol, measured according to criterion three, and the residual absorbance of maltose in this wavelength range are additive.

3.5. Analysis of real samples

The direct analysis of a real sample, with a declared value of 5% (v/v) and for which an actual value of 4.95% had been obtained by measurements in the range 1657–1720 nm, gave an ethanol concentration of 5.20% thus indicating that the effect of maltose must be taken into account in order to obtain accurate results.

When samples are analyzed by the systems involving Eqs. 3 and 4, values of 3.85 ± 0.03 g per 100 ml of maltose and 4.94 ± 0.01% of ethanol were found. However, this procedure involves two independent measurements on the same sample, using cells of different pathlengths. Therefore we have tried to simplify this method.

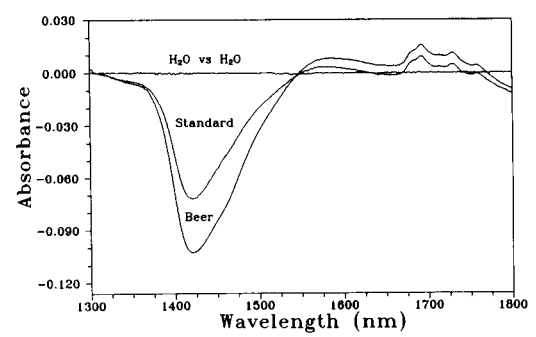

Fig. 3. NIR spectra of a beer sample and an ethanol standard, obtained by using a 1 mm pathlength cell. The concentration of ethanol was 5.0% for the standard solution and 5.1% (v/v) for the beer sample. Water was employed as a reference.

A systematic study of the influence of maltose on the ethanol calibration, measured with 1 cm cells, showed that maltose only affects the intercept, and that it is possible to correct the maltose effect by preparing the standard solutions in an alcohol-free beer matrix or to use the ethanol-free sample or an aqueous maltose solution as a reference. By using this simplified procedure an ethanol concentration of $4.92 \pm 0.01\%$ was obtained for the sample containing 4.95%.

For the analysis of low-alcohol content beer samples the above mentioned strategies could be also employed and, as for example, a sample containing less than 1% (v/v) of ethanol, with an actual concentration of 0.96%, when it is directly analyzed by NIR spectrometry gives a 1.13%, but gives $0.95 \pm 0.01\%$ by using the system of two equations and $0.96 \pm 0.01\%$ (v/v) by employing the above simplified procedure.

A series of 22 real samples of beer was analyzed by both the reference method and the recommended NIR simplified procedure and data found are summarized in Table 3. As can be seen, the developed procedure is very accurate and provides good repeatability at all the different concentrations of alcohol which can be found in real samples.

The regression between values found by the two-equation NIR method (Y) and those obtained by the reference procedure (X) provided a regression equation of $Y = -0.003 + 0.9998X$ ($n = 22$) which means that the NIR method is accurate, it does not require any blank correction (the intercept is almost zero) and does not present constant relative errors (the slope is very close to 1).

In addition, the use of the two-equation system provides a good estimation of the maltose concentrations in beer samples and, as can be seen in Table 4, all the samples analyzed had between 3.1 and 6.9 g of maltose in 100 ml of beer.

3.6. Evaluation of the performance of the developed procedure

The stopped-flow NIR spectrometric determination of ethanol in beers is a fast procedure (sampling frequency of 120 h^{-1}) which not requires any chemical pretreatment of samples and provides an adequate sensitivity and accuracy.

Table 3
Determination of ethanol in beer samples

Sample	Declared value (%, v/v)	Reference (%, v/v)	NIR (%, v/v) [a]
1	5.0	5.27	5.29 ± 0.02
2	5.5	6.26	6.22 ± 0.02
3	5.0	4.95	4.92 ± 0.01
4	5.1	5.10	5.14 ± 0.02
5	7.2	7.33	7.29 ± 0.02
6	5.4	5.72	5.70 ± 0.02
7	5.0	5.09	5.04 ± 0.03
8	5.0	5.00	5.01 ± 0.02
9	5.4	5.50	5.60 ± 0.02
10	5.0	5.06	5.01 ± 0.02
11	5.0	4.94	4.98 ± 0.03
12	0.5	0.56	0.53 ± 0.01
13	< 1	0.96	0.96 ± 0.01
14	< 1	0.93	0.95 ± 0.02
15	< 1	1.03	1.01 ± 0.01
16	< 1	1.04	1.02 ± 0.02
17	< 1	0.80	0.82 ± 0.01
18	< 1	0.71	0.74 ± 0.02
19	< 1	1.13	1.03 ± 0.02
20	0.0	0.00	0.03 ± 0.02
21	< 1	0.94	0.96 ± 0.02
22	0.5	0.50	0.48 ± 0.01

[a] Mean ± standard deviation ($n = 5$).

As compared with other procedures published in the literature, the method is faster than the current official methods based on physical measurements, carried out after a previous distillation of the sample [1,2] and requires less reagents than chemical procedures based on the oxidation of ethanol to acetic acid with potassium dichromate [3] and other procedures involving enzymatic determination [10–13].

Compared with other infrared spectrometric procedures, the method does not require the use of complex mathematical treatment of data [20,21] and provides a limit of detection comparable to that obtained by NIR derivative spectrometry [25] but with a better precision for the analysis of beer samples. A relative standard deviation of 0.2% can be achieved by stopped-flow NIR spectrometry for samples containing approximately 5% of ethanol, instead of the 2% relative standard deviation found by NIR derivative spectrometry [25].

Table 4
Maltose concentrations in beers determined by NIR using two cells with pathlengths of 1 mm and 1 cm

Sample	[Maltose] (g per 100 ml) [a]
1	4.10 ± 0.03
2	4.60 ± 0.04
3	3.85 ± 0.03
4	3.90 ± 0.04
5	6.90 ± 0.07
6	4.40 ± 0.03
7	3.95 ± 0.04
8	3.80 ± 0.04
9	5.9 ± 0.04
10	3.95 ± 0.05
11	4.60 ± 0.04
12	5.15 ± 0.04
13	5.8 ± 0.04
14	3.90 ± 0.03
15	4.60 ± 0.05
16	5.6 ± 0.04
17	3.10 ± 0.03
18	5.10 ± 0.03
19	6.70 ± 0.05
20	6.20 ± 0.04
21	4.50 ± 0.03
22	4.40 ± 0.03

[a] Mean ± standard deviation ($n = 5$).

The method developed is less expensive and faster than many other instrumental procedures for ethanol determination.

Acknowledgments

Máximo Gallignani acknowledges the grant of the Agencia Española de Cooperación Internacional to carry out PhD studies in Spain and the financial support of Los Andes University and CONICIT (Venezuela). Salvador Garrigues acknowledges the grant of the Conselleria de Cultura, Educació i Ciència de la Generalitat Valenciana to carry out PhD studies. The authors also acknowledge financial support from the Spanish DGICYT project PB-92-0870 and that of the Conselleria de Cultura, Educació i Ciència de la Generalitat Valenciana project GV 121/93.

References

[1] Official Methods of Analysis of the Association of Official Analytical Chemists, AOAC, Washington, DC, 1990.
[2] E. Kreneger and S. Weber, Monatsschr. Brau., 34 (1981) 70.
[3] G.J. Pilone, J. Assoc. Off. Anal. Chem., 68 (1985) 188.
[4] A.J. Caputi and D.P. Mooney, J. Assoc. Off. Anal. Chem., 66 (1983) 1152.
[5] A. Cutaia, J. Assoc. Off. Anal. Chem., 67 (1984) 192.
[6] T. Iwachido, K. Ishimaruk and K. Toei, Anal. Sci., 2 (1986) 495.
[7] J. Morawski, A.K. Dincer and K. Ivie, Food Technol., 37 (1983) 57.
[8] G.J. Kakabadse, Lab. Pract., 39 (1990) 51.
[9] W.H. Chan, A.W.M. Lee and P.X. Cai, Analyst, 117 (1992) 1509.
[10] G.K. Buckee and C.D. Baker, Brau. Rundsch., 97 (1986) 202.
[11] American Society of Brewing Chemists, J. Am. Soc. Brew. Chem., 48 (1990) 156.
[12] F. Lazaro, M.D. Luque de Castro and M. Valcarcel, Anal. Chim. Acta., 185 (1986) 57.
[13] F. Lazaro, M.D. Luque de Castro and M. Valcarcel, Anal. Chem., 59 (1987) 1859.
[14] P. López-Mahia, J. Simal Gándara and P. Paseiro Losada, Vib. Spectrosc., 3 (1992) 133.
[15] A.L. Glenn, J. Pharm. Pharmacol., 15 Suppl. (1963) 123T.
[16] J.V. Agwu and A.L. Glenn, J. Pharm. Pharmacol., 19 (1967) 76s.
[17] O. Heisz, Labor Praxis, 13 (1989) 402.
[18] M. Gallignani, S. Garrigues and M. de la Guardia, Anal. Chim. Acta., 287 (1994) 275.
[19] M. Gallignani, S. Garrigues and M. de la Guardia, Analyst, in press.
[20] S.A. Hasley, J. Inst. Brew., 91 (1985) 306.
[21] S.A. Hasley, Anal. Proc., 23 (1986) 126.
[22] A. Requejo-Gómez, Tec. Lab., 8 (1983) 911.
[23] A.G. Coventry and M.J. Hunston, Cereal Food World, 29 (1984) 715.
[24] E.D. Dumoulin, B.P. Azain and J.T. Guerain, J. Food Sci., 52 (1987) 626.
[25] M. Gallignani, S. Garrigues and M. de la Guardia, Analyst, 118 (1993), 1167.

ELSEVIER

Analytica Chimica Acta 296 (1994) 163–170

ANALYTICA CHIMICA ACTA

An alternative microbiosensor for hydrogen peroxide based on an enzyme field effect transistor with a fast response

Alexandre A. Shul'ga [a,*], Timothy D. Gibson [b]

[a] *Sector of Bioelectronics, Kiev University, P.O. Box 152, Kiev 252001, Ukraine*

[b] *Enzyme Biotechnology Group, Department of Biochemistry and Molecular Biology, University of Leeds, Leeds LS2 9JT, UK*

Received 28th January 1994; revised 13th April 1994

Abstract

The biosensor for hydrogen peroxide discussed in this article comprises horseradish peroxidase (EC 1.11.1.7) immobilised onto the gate area of a probe-type pH-sensitive field effect transistor (ISFET) by cross-linking in glutaraldehyde vapour. The measurements are performed in a buffer solution containing potassium iodide or potassium hexacyanoferrate(II) as reducing substrates. The recycling of the redox state of the active centre of peroxidase by successive action of hydrogen peroxide and the reducing substrate results in a depletion of H^+ ions inside the enzymatic layer that is detected by the ISFET. The biosensor response time is less than 2 s and the detection limit is 0.5 and 5 μM H_2O_2 in 1 and 10 mM sodium phosphate buffer at pH 6.0, respectively. The upper limit of the biosensor dynamic range may be extended up to several mM hydrogen peroxide by the increase of the reducing substrate concentration. At acidic pH the biosensor has higher sensitivity and wider dynamic range, while at pH > 6 the enzyme is subjected to a strong reversible inactivation. However, in the case of KI as a reducing substrate at pH < 5 stability of the immobilised enzyme is severely impaired resulting in a fast irreversible inactivation of peroxidase. The operational stability of the biosensor at pH 6 to 7 allows to make more than 1000 measurement cycles with less then 10% final attenuation of the response. The shelf-life of the biosensor constitutes at least several weeks when it is preserved in a dry state at +4°C.

Keywords: Biosensors; Enzymatic methods; ENFET; Horseradish peroxidase; Hydrogen peroxide; Mediators; Electrochemical sensors

1. Introduction

The development of potentiometric enzyme biosensors based on pH-sensitive field effect transistors (ENFET) dates back to the late 70s. The major targeted analytes for the ENFETs developed since then were primarily glucose, urea and penicillin. The slope of enzymatically catalysed reactions that could be used for the ENFETs construction has been limited to the reactions affecting the acid–base equilibrium of the medium by producing or consuming a product or a substrate, which is a base or an acid. This fundamental drawback resulted in many less ana-

* Corresponding author. Institut für Chemo- und Biosensorik Münster, Mendelstrasse 11, D-48149 Münster, Germany.

SSDI 0003-2670(94)00176-M

lytes being detected by ENFETs in comparison with those detected by amperometric enzyme electrodes. The application of glucose oxidase in ENFETs was based on the fact that the primary product of the enzymatic oxidation of glucose, gluconolactone, undergoes spontaneous hydrolysis giving gluconic acid ($pK_a \sim 3.8$). However, most of the reactions catalysed by other redox enzymes do not affect the acid–base equilibrium of the medium unless a suitable electron donor or acceptor other than dissolved oxygen is present, therefore the use of ENFETs has been limited.

Recently [1] we have proposed to use a soluble electron donor or acceptor added to the buffer solution that causes production or depletion of H^+ ions during recycling of the active centre of the enzyme incorporated into an ENFET. The case of a glucose-sensitive ENFET using potassium hexacyanoferrate(III) as an oxidising substrate was thoroughly investigated. This detection scheme is the subject of a patent application [2] and its use allows a significant extension of the range of analytes that can be detected by ENFETs because now practically any redox enzyme, e.g., flavo- and quinoproteins, dehydrogenases, etc., may be employed for the biosensor construction provided a judicious choice of an electron donor (acceptor) recycling the enzyme active centre has been made.

In this paper we present the results concerning the development of a horseradish peroxidase-based ENFET for the detection of hydrogen peroxide using potassium hexacyanoferrate(II) and potassium iodide as reducing substrates.

The detection of hydrogen peroxide or alternatively the use of such a detector for the monitoring of horseradish peroxidase activity are important from several points of view:

(i) In biotechnology and food industries hydrogen peroxide is frequently used as a sterilising and cleaning agent and may be present in great quantities in final products, e.g., in processed juices.

(ii) In bioanalytical chemistry oxidase enzymes coupled with an amperometric detection of hydrogen peroxide have been used extensively to construct both biosensors and automated analysers [3].

(iii) Horseradish peroxidase (HRP) is widely used as an immunoenzyme marker.

A number of electrochemical (bio)sensors for determination of hydrogen peroxide in complex media were recently reported. The detection principles employed include in particular:

(a) Direct electrochemical oxidation of hydrogen peroxide on a Pt or a carbon electrode. Suppression of background interferences was achieved by covering the electrode surface with a size exclusion membrane, e.g., an cellulose acetate membrane [4] or a thin film of an electrochemically produced ferric hydroxide [5].

(b) Amperometric monitoring of HRP catalysed reduction of hydrogen peroxide. Thereby the oxidised form of HRP is formed, which is then reduced by a suitable mediator. The oxidised form of the mediator is subsequently detected by a metal or a carbon electrode [6]. HRP may be in solution [7], covalently attached to [8] or immobilised by cross-linking on [9] the electrode surface, incorporated in a carbon paste electrode [10]. These biosensors were employed in a flow-through detection system with the mediator (ferrocene [7,8], hexacyanoferrate(II) [8,9], *o*-phenylenediamine [10]) present in the solution.

(c) The use of direct electron transfer between HRP adsorbed or covalently bound to the electrode surface and the electrode (see [11] and refs. cited therein).

(d) Gas-sensing amperometric probes for hydrogen peroxide based on electrochemical [12] and bioelectrochemical [13] detection.

(e) The application of potentiometric iodide or fluoride sensitive electrodes was proposed [14,15] making use of the HRP catalysed reactions:

$$H_2O_2 + 2I^- + 2H^+ \xrightarrow{HRP} I_2 + 2H_2O$$

$$H_2O_2 + 4 - \text{fluorophenol} \xrightarrow{HRP} H_2O + F^- + \text{polymeric product}$$

In general, the application of HRP in analytical devices is based on the monitoring of HRP catalysed reaction of hydrogen peroxide reduction.

In simplified terms, the normal HRP cycle [16,17] consists of a single two electron oxidation

of the enzyme by hydrogen peroxide which is followed by two single electron reductions. The first stage, when the oxidised form of HRP, usually denoted as compound-I, is formed, is practically irreversible with an equilibrium constant of $\sim 10^{-14}$ M. The product of the one-electron reduction of compound-I is called compound-II. Virtually any reducing agent is capable of donating electrons to compound-I and compound-II. There is a net uptake of one proton by the enzyme when hexacyanoferrate(II) is reducing compound-I as well as compound-II. Similar two step reduction is the case for most of the reducing substrates. However, for iodide the reduction of compound-I occurs by way of a single two electron transfer and a net uptake of two H^+ ions by the enzyme without formation of compound-II [16,17]. In the case of hexacyanoferrate(II) as well as iodide as a reducing substrate the necessary H^+ ions are taken from the surrounding medium. Examples of other commonly used reducing agents in this context are: phenols, *o*- and *p*-hydroquinones, pyrogallol, 2,2′-azino-di-[3-ethylbenzothiazoline-6-sulfonic acid] (ABTS), 3-methyl-3*H*-2-benzothiazolonhydrazone (MBTH), 4-methoxy-α-naphthol, 4-aminoantypyrine, guaiacol, *N*,*N*-alkylanilines, *o*- and *p*-phenylenediamines, ferrocenes (in a reduced form), etc. (see [16,17] and refs. cited therein). These reagents are used both in spectrophotometric and electrochemical detection systems to follow HRP catalysed reactions.

2. Experimental

2.1. Materials

The reagents used were peroxidase (HRP-4) from horse radish (EC 1.11.1.7) having activity 257 U/mg (guaiacol as a reducing substrate) from Biozyme; glutaraldehyde (25% aqueous solution, EM grade) from Agar Scientific; hydrogen peroxide (30% H_2O_2 w/v solution, AnalaR grade) and glycerol (GPR grade) from BDH; bovine serum albumin (BSA), fraction V, from Sigma; potassium hexacyanoferrate(II) trihydrate and potassium iodide (ACS reagents) from Aldrich. All other reagents were of AnalaR grade.

2.2. Sensor design

The probe-type ion-selective field effect transistors (ISFET) used were supplied by Emokon (Kiev). Each sensor chip (3 mm × 10 mm) contained two identical ISFETs. These were n-channel depletion mode pH-sensitive Si_3N_4-ISFETs fabricated on p-Si of orientation (100) and resistivity 7.5 Ohm cm. In our experiments ISFETs with a threshold voltage about −4 V were employed. Their pH-sensitivity in a pH range 2–10 was 52–54 mV/pH. The design and mode of operation made the sensors insensitive to light and allowed them to be used when the silicon substrate was in direct contact with the test solution.

2.3. Enzyme immobilisation

All solutions were prepared in a 5 mM sodium phosphate buffer pH 7.0. On the measuring ISFET one drop of a solution containing: (a) 5% w/v HRP; (b) 0.5% w/v HRP, 9.5% w/v BSA, 10% v/v glycerol and (c) 2.5% w/v HRP, 5% w/v BSA, 10% v/v glycerol, was deposited. For the reference ISFET a solution containing 10% albumin and 10% glycerol was used. The sensor chip was then exposed to a saturated glutaraldehyde vapour for 20 to 45 min and subsequently dried at room temperature for an hour.

2.4. Measurements

The biosensor was immersed in a measurement cell filled with ~ 1.5 ml of vigorously stirred buffer solution and a steady-state differential output between the measuring and the reference ISFETs was recorded. The ISFETs were operated at a constant source current and a constant drain-source voltage ($I_s = 300$ μA, $V_{ds} = 2$ V) using a differential ISFET-amplifier from Emokon (Kiev). The bare substrate of the sensor chip was used as a quasi-reference electrode. The concentration of hydrogen peroxide was varied by addition of aliquots of 500 to 10^5 times diluted solutions of hydrogen peroxide freshly prepared from the 30% solution. The experiments were carried out at room temperature.

3. Results and discussion

The diffusion reaction processes taking place in the layer of immobilised HRP deposited on top of the gate insulator of an ISFET are shown schematically in Fig. 1. It comprises diffusion of substrates and products of the enzymatic reaction, as well as mobile buffer species, in and out of the enzymatic layer. The steady state pH value at the enzymatic layer–ISFET interface is a result of the balance between the rate of proton consumption due to the cyclic reduction of compound-I and compound-II by a reducing substrate (hexacyanoferrate(II) in this case) inside the film and the influx of H^+ ions into the membrane via a carrier mediated transport mechanism, with buffer species playing the role of a carrier. ENFETs poor performance in highly buffered media is a direct consequence of the adverse effect of the latter mechanism.

The calibration curves of ENFETs with HRP immobilised under different conditions were

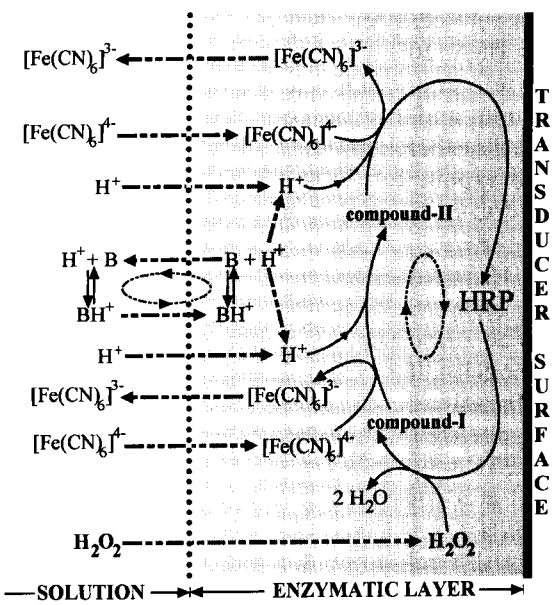

Fig. 1. Schematic representation of the reaction-diffusion processes within the layer of immobilised HRP in the case when both peroxide and hexacyanoferrate(II) are present in a buffer containing bathing solution. **B**, stands for the buffer residue, dashed arrows correspond to diffusional processes, solid lines to chemical reactions. Growing intensity of the grey colour corresponds to the increase of the solution pH.

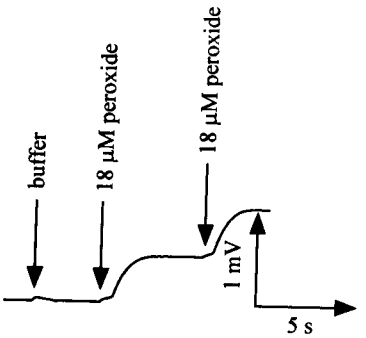

Fig. 2. Time-resolved response of the peroxide sensitive ENFET measured in a 10 mM phosphate buffer at pH 6.0 in the presence of 40 mM potassium hexacyanoferrate(II). Arrows show when peroxide or equivalent volume of buffer solution were added to the measurement cell.

measured in a 10 mM phosphate buffer at pH 6.0 in the presence of a reducing substrate. While the sensitivity and dynamic range were generally similar for all the ENFETs studied the steady-state response time (the time necessary to reach 95% of a full response) of the biosensors obtained by cross-linking HRP alone differed strikingly from those for HRP cross-linked with BSA, being 2 s and from 30 to 90 s respectively. The cross-linking time in the tested range did not substantially affect the biosensors performance, apart from the fact that longer cross-linking times correlated with slower biosensor responses. The latter is an indirect indication that an increase in the extent of cross-linking results in a denser membrane. In further investigation only the biosensors with the fastest response, i.e., those obtained by cross-linking HRP alone, were used. Typical time-resolved response curves for these ENFETs in a 10 mM buffer at low substrate concentrations are shown in Fig. 2. In this case the biosensor had a detection limit of ~ 5 μM for H_2O_2 that was chiefly determined by the rate of the background signal drift as well as a slight non-specific reaction of the biosensor on the sample addition to the measurement cell.

The ENFET performance depended strongly on the type and the concentration of the reducing substrate used. Generally the sensitivity of the ENFET with KI as a reducing substrate was from three to five times higher than for hexacyanofer-

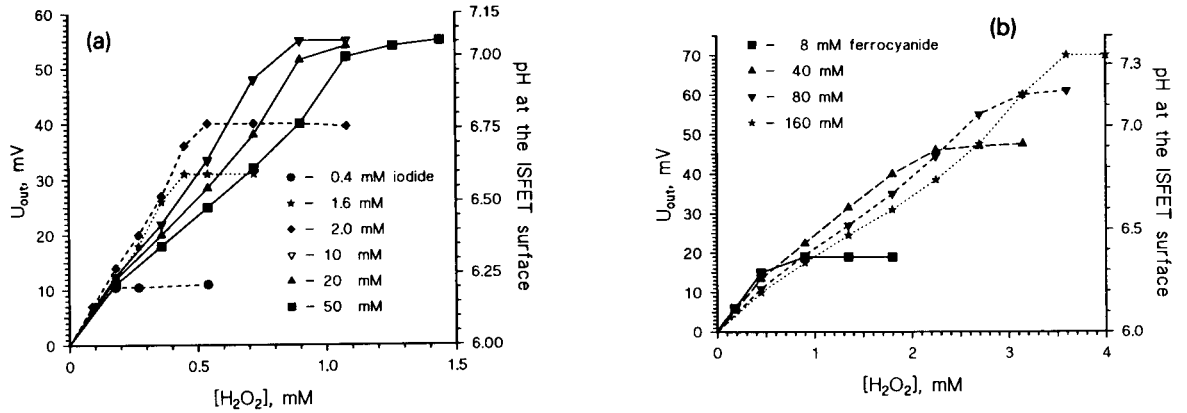

Fig. 3. Calibration curves of the ENFET measured at different concentrations of (a) potassium iodide and (b) potassium hexacyanoferrate(II) in a 10 mM phosphate buffer at pH 6.0.

rate(II). As one can see from the curves presented in Fig. 3, the increase of the reducing substrate concentration leads to an extension of its dynamic range in all cases but, at the same time, causes a slight attenuation of the biosensor sensitivity. Also, it is seen that after the magnitude of the biosensor response exceeds a certain value in the range from 30 to 40 mV, the curves assume a slightly sigmoidal form. A possible reason for this phenomenon may be the fact that for a sensor response of ~ 40 mV, corresponding to pH ~ 6.8 at the ISFET surface, the phosphate buffer solution inside the membrane passes through the maximum of its buffer capacity and any further increase of the intramembrane pH results effectively in the decrease of the solution buffer capacity, thus decreasing its adverse effect on the biosensor response. As is usually the case for ENFETs the decrease of the buffer capacity of the measurement solution allows the achievement of a higher sensitivity and a higher detection limit. So in a 1 mM sodium phosphate buffer at pH 6.0 the biosensor detection limit was ~ 0.5 μM. The respective calibration curve is presented in Fig. 4, its sigmoidal form in this case is quite distinct.

To elucidate the factors affecting the performance of the developed biosensor, the pH dependence of its response in a pH range of 3.5 to 8.9 was investigated. The measurements were performed in a multicomponent buffer (the buffer composition was 10 mM Tris, 10 mM NaH_2PO_4, 10 mM citric acid, 10 mM sodium tetraborate) with a practically constant buffer capacity for pH 3 to 9 [18]. The use of this buffer has allowed the influence of pH dependent variations of the buffer capacity on the ENFET response to be avoided. Under such conditions the dependence of the latter on pH is mainly due to the variation of the kinetics of immobilised HRP. In the case of hexacyanoferrate(II), the results obtained correlate well with those for the pH dependence of the current of a HRP-based amperometric electrode

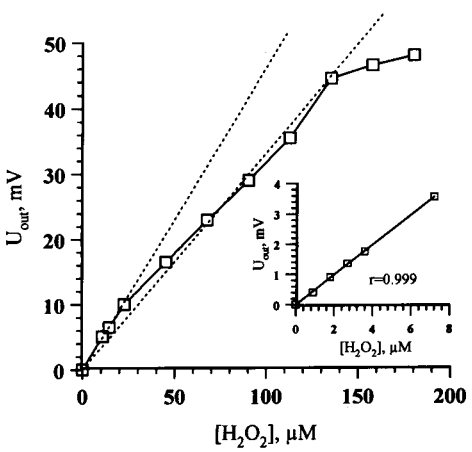

Fig. 4. The dependence of the biosensor response on the peroxide concentration in a 1 mM phosphate buffer pH 6.0 containing 10 mM KI. The inset shows the initial part of the calibration curve.

for the detection of hydrogen peroxide using hexacyanoferrate(II) as a mediator [9].

As one can see in Fig. 5, for both reducing substrates used, the ENFET response drops at pH > 6, though this decrease is much steeper in the case of KI compared to that of hexacyanoferrate(II). This reversible inactivation of immobilised HRP at pH > 6 is, apparently, responsible for the fact that, in the presence of sufficiently high concentrations of either hexacyanoferrate(II) or iodide, the ENFET calibration curves finally saturate at about the same maximum values of the response (see Fig. 3). Again, in accordance with a lower degree of inactivation in the case of hexacyanoferrate(II) the respective maximum response values are higher.

For hexacyanoferrate(II) the pH dependence has a bell shape with a rather broad maximum between pH 4.2 and 6, while for iodide the pH dependence has a plateau at pH 3.5 to 6. For both hexacyanoferrate(II) and iodide the ENFET dynamic range grows steadily with decreasing pH. The corresponding set of calibration curves measured at different pH in a 40 mM hexacyanoferrate(II) solution is shown in Fig. 6. Disappearance of a sigmoidal form of the curves measured at pH 5 to 8.3 favours the explanation given above for the origin of such a form observed earlier, when the measurements were performed in phosphate buffer at pH 6.0. On the other hand, a sigmoidal shape of the calibration curves obtained at pH 3.5 and 4.2 may be understood taking into account the pH dependence of the biosensor response at low pH. In this case the increase of pH inside the membrane associated with the consumption of H^+ ions leads to a higher HRP activity and, accordingly, to a higher slope of the calibration curve. As has to be expected this effect is more pronounced for the curve measured at pH 3.5.

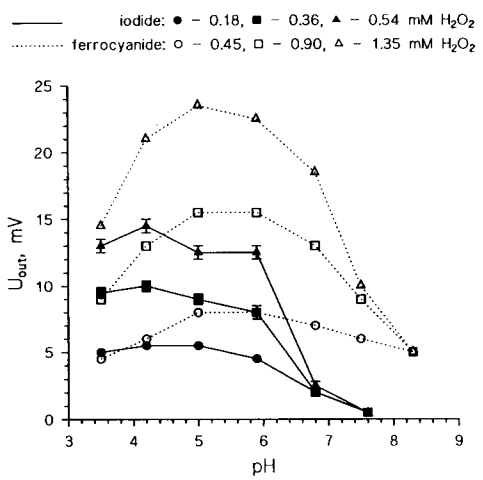

Fig. 5. The dependence of the ENFET response on pH with 40 mM hexacyanoferrate(II) or 10 mM iodide as a reducing substrate. The measurements were performed in a multicomponent buffer having nearly constant buffer capacity at pH 3 to 9 (see the text).

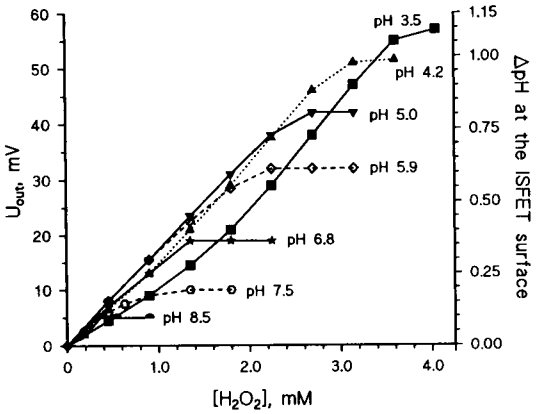

Fig. 6. The effect of solution pH on the ENFET calibration curves. The curves were measured in a multicomponent buffer (see the text) containing 40 mM hexacyanoferrate(II).

Though the peroxide sensitive ENFET is generally more sensitive when iodide is used as a reducing substrate, a rapid irreversible inactivation of the immobilised HRP at pH < 5 was observed in this case. This inactivation primarily affects the biosensor dynamic range and has a minor effect on the initial part of the calibration curves that is illustrated in Fig. 7, where the calibration curves corresponding to repeated measurements at pH 3.5 are shown (one curve was measured, then the sensor was rinsed with a fresh buffer and the measurements were immediately repeated). No similar effects were observed in the case of hexacyanoferrate(II).

As far as the response of the peroxide sensitive ENFET at high concentrations of peroxide is controlled by the kinetics of immobilised HRP, it

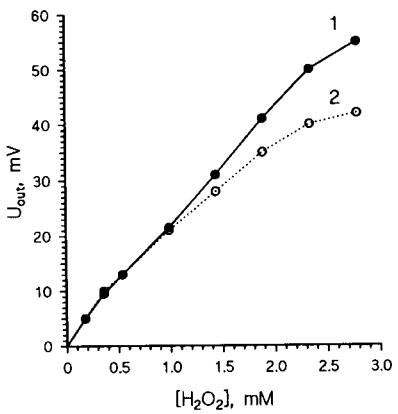

Fig. 7. The influence of the HRP inactivation at pH 3.5 in the presence of 10 mM KI on the ENFET calibration curves measured (1 = first measurement, 2 = repeated measurement) in a multicomponent buffer (see the text).

should be expected that the enzyme inactivation has a substantial effect on the biosensor response. However, HRP inactivation primarily affects the dynamic range of the biosensor, having only a slight effect on the slope of the calibration curve. In our case the attenuation of the biosensor response was less than 10% after more than 1000 measurement cycles during one working day. This attenuation was solely due to the inactivation of the immobilised enzyme. The biosensor also had a shelf life of at least several weeks when it was stored in a dry state at +4°C.

4. Conclusions

A peroxidase-based ENFET for the detection of hydrogen peroxide in the concentration range from several μM to several mM was developed. A pH-sensitive ion-selective field effect transistor is used to detect local changes of pH occurring inside the layer of immobilised enzyme in the presence of the analyte. The peroxidase catalysed reduction of hydrogen peroxide alone does not change the pH of the medium, the latter results from the recycling of the redox state of the enzyme active centre (ferroprotoporphyrin IX) by a soluble electron donor (hexacyanoferrate(II) or iodide in our case) with concomitant consumption of one proton per one-electron transfer step. The performance of the developed biosensor is generally better when hexacyanoferrate(II) is used as a reducing substrate, though at the cost of a higher sensitivity achievable with KI. To the best of our knowledge the ENFET described has the fastest response time reported for ENFETs so far. The detection limit and the dynamic range achieved are comparable to those reported for other hydrogen peroxide biosensors.

Acknowledgments

The support of this research by the AFRC, enabling Dr. A.A. Shul'ga in the framework of the International Scientific Interchange Scheme to visit and work in the Enzyme Biotechnology Group at the Department of Biochemistry and Molecular Biology of the University of Leeds, UK, is gratefully acknowledged.

References

[1] A.A. Shul'ga, M. Koudelka-Hep, N.F. de Rooij and L.I. Netchiporouk, Anal. Chem., 66 (1994) 205.
[2] A.A. Shul'ga, M. Koudelka-Hep and N.F. de Rooij, UK Pat. Appl., 9400201.1, 7 january 1994.
[3] A.P.F. Turner, I. Karube and G.S. Wilson (Eds.), Biosensors. Fundamentals and applications, Oxford University Press, New York, 1987.
[4] G. Sittampalam and G.S. Wilson, Anal. Chem., 55 (1983) 1608.
[5] Y.L. Huang, S.B. Khoo and M.G.S. Yap, Anal. Chim. Acta, 283 (1993) 763.
[6] P.N. Bartlett, P. Tebbutt and R.G. Whitaker, Prog. React. Kinet., 16 (1991) 55.
[7] M.J. Green and H.A.O. Hill, J. Chem. Soc., Faraday Trans. 1, 82 (1986) 1237.
[8] T. Tatsuma, Y. Okawa and T. Watanabe, Anal. Chem., 61 (1989) 2352.
[9] T. Yao, M. Sato, Y. Kobayashi and T. Wasa, Anal. Chim. Acta, 165 (1984) 291.
[10] J. Wang and M.S. Lin, Electroanalysis, 1 (1989) 43.
[11] L. Gorton, G. Jönsson-Pettersson, E. Csöregi, K. Johansson, E. Dominguez and G. Marko-Varga, Analyst, 117 (1992) 1235.
[12] G. Palleschi, M.H. Faridnia, G.J. Lubrano and G.G. Guilbault, Appl. Biochem. Biotechnol., 31 (1991) 21.

[13] S. Pan and M.A. Arnold, Anal. Chim. Acta, 283 (1993) 663.
[14] G. Nagy, L.H. von Storp and G.G. Guilbault, Anal. Chim. Acta, 66 (1973) 443.
[15] M.H. Wo and T.G. Wu, ISA Trans., 24 (1985) 61.
[16] H.B. Dunford, in J. Everse, K.E. Everse and M.B. Grisom (Eds.), Peroxidases in Chemistry and Biology, Vol. II, CRC Press, Boston, MA, 1990, Chap. 1.
[17] I. Yamazaki, M. Tamura and R. Nakajima, Mol. Cell. Biochem., 40 (1981) 143.
[18] D.D. Perrin and B. Dempsey, in Buffers for pH and Metal ion Control, Kodansha, Tokyo, 1981, pp. 24–49.

ELSEVIER

Analytica Chimica Acta 296 (1994) 171–180

ANALYTICA CHIMICA ACTA

Amperometric detection of catecholamines with liquid chromatography at a polypyrrole–phosphomolybdic anion-modified electrode

Anhua Liu, Erkang Wang *

Laboratory of Electroanalytical Chemistry, Changchun Institute of Applied Chemistry, Chinese Academy of Sciences, Changchun, Jilin 130022, China

Received 10 December 1993; revised manuscript received 25 April 1994

Abstract

A conducting polypyrrole film immobilized with $PMo_{12}O_{40}^{3-}$ anion on a glassy carbon electrode was prepared by an electrochemical method. This kind of chemically modified electrode (CME) was prepared successfully by doping the polypyrrole film electrode with heteropolyacid under a cycling potential between −0.2 and +0.6 V in 0.5 mol l^{-1} H_2SO_4 containing $Na_3PMO_{12}O_{40}$ dopant. The experimental results show that an electrode modified with a heterophosphomolybdic acid–polypyrrole film has a catalytic effect on the oxidation–reduction of catecholamines. When employed with a dual-electrode arrangement in liquid chromatography with electrochemical detection using the PPy–$PMo_{12}O_{40}^{3-}$ electrodes as generating and collecting detectors, high effective collection efficiencies for catecholamines were achieved with a linear response range over three orders of magnitude and a detection limit of 5.0×10^{-9} mol l^{-1} for norepinephrine. The amperometric response showed very good sensitivity and stability for catecholamine detection.

Keywords: Amperometry; Liquid chromatography; Catecholamines; Phosphomolybdic acid; Polypyrrole

1. Introduction

The use of polymer coating-modified electrodes has developed a new area in electrochemistry and has provided new materials for catalysis and electrocatalysis, electroanalysis, photoelectrochemistry and electronics [1,2]. A range of chemical processes including ion exchange, complication, precipitation and even enzyme reactions can be carried out on polymer surfaces. More recently, the electrical and electrochemical properties of polymers have also been investigated and are well documented [3,4]. In addition, polymeric materials have been well characterized and the chemistry of interactions on such surfaces has been described, especially in the area of chromatography [5,6]. Perhaps the most unique

* Corresponding author.

SSDI 0003-2670(94)00202-W

feature of some conductive electroactive polymers is the incorporation of a counter ion (C^-) during the polymerization step. This provides a convenient means of generating chemically active polymers. The entrapped functional groups present an excellent basis for further analytical applications. With respect to the range of counter ions that can be incorporated, polypyrrole far outperforms other polymers such as polythiophene and polyaniline. This is because the pyrrole polymer is readily synthesized from a range of solvent media.

The possibility of functionalizing an electrode surface by incorporation of oxometallates in an electronically conducting and non-conducting polymeric matrix, while maintaining and enhancing their beneficial properties, has been explored. Heteropolyacids have extensive applications in biochemistry, analysis, catalysis, photochemistry etc. These heteropolyanions have been studied extensively with respect not only to their crystal structures and physical properties in the solid state, but also to their chemical nature in solution where the heteropolyanion centre has redox properties. Recently, heteropolyacid-modified electrodes have been attracting much interest because of their good electrocatalytic properties [7]. Such chemically modified electrodes (CMEs) could be directly prepared by electrochemical deposition [8], anion exchange [9] and immobilization of heteropolyanions as a dopant in a conducting polymer matrix [10,11].

The stability and the electrochemical behaviour of the modified electrode by simple adsorption and by electrodeposition were affected by the sweep-potential range. More cathodic and anodic switching potentials led to destruction of the film, especially when using such CMEs in flow systems, resulting in the electroactive species leaving the electrode surface into the mobile solution. However, by using a conducting polymer to immobilize oxometallates, these problems can be overcome. The heteropolyacid-modified polymer film electrode, in particularly, may not only maintain the amount of the heteropolyanions in the polymer film, but also markedly increase the stability of the oxidation–reduction catalyst. Keita and Nadjo [12] first demonstrated that a poly(4-vinyl)pyridine (PVP) film appropriately incorporated anionic oxometallates, and entrapping $SiW_{12}O_{40}^{3-}$ in PVP was strongly beneficial to the catalytic electroreduction of oxygen. Recently, to enhance catalysis and electrocatalysis, the redox catalysis properties of this new type of modified electrode have attracted increasing interest, especially in the electrocatalysis of the evolution of hydrogen, reduction of oxygen and reduction of chlorate and bromate [13–15].

Liquid chromatography with electrochemical detection (LC–EC) has continued to grow in popularity for the sensitive determination of trace compounds and is best known for its application in neurochemistry. Catecholamines have been the primary compounds among the major neurotransmitter groups penetrated by LC–amperometric detection procedures. Amperometric dual-electrode detectors have recently become popular in LC–EC monitoring of catecholamine-related species. The dual-electrode detector has substantial advantages in selectivity compared with a single-electrode detector. Dual-electrode amperometric detectors usually have a configuration with two electrodes positioned in series in flowing streams. The downstream electrode of the dual electrode is used to collect the product generated at the upstream electrode. The collection efficiency, the ratio of the current response at the collector electrode to that at the generator electrode, in a glassy carbon electrode is usually smaller than 0.4, although a collection efficiency as high as 0.6 would be obtained theoretically with a horseshoe cell configuration [16]. The high performance collection of catecholamines (N_e of 0.5–0.6) with LC amperometric detection has recently been achieved with an interdigitated microarray electrode (IDAE) [17]. Zhou and Wang [18] developed a novel Prussian Blue chemically modified electrode for the amperometric detection of catecholamines. When arranged in a series configuration, using the modified electrodes as generating and collecting detectors, extremely high effective collection efficiencies ($N_e = 0.91$ for norepinephrine) were obtained.

Our recent efforts have been directed toward entrapping heteropolyanions in a polypyrrole matrix. The preparation of a PPy–$PMo_{12}O_{40}^{3-}$ film-

modified glassy carbon electrode and its electrochemical properties, with good catalytic activity for catecholamines detection, were investigated. This new type of heteropolyacid-modified electrode was constructed and characterized for liquid chromatography with electrochemical detection of catecholamines, and a number of unique features were obtained compared with conventional LC–EC procedures. The high collection efficiencies (0.53–0.67) could be obtained with a series dual-electrode configuration, according to the superior reversible redox mode of catecholamine on PPy–$PMo_{12}O_{40}^{3-}$ detector.

2. Experimental

2.1. Reagents

Pyrrole (Fluka) was distilled before use, Epinephrin (E) was obtained from Serva, norepinephrine (NE), dopamine (DA) and 3,4-dihydroxyphenylacetic acid (DOPAC) from Fluka and $Na_3PMo_{12}O_{40}$ from Beijing Chemical. Other chemicals were of analytical-reagent grade. Doubly distilled water was used for the preparation of all solutions. Catecholamine stock solutions (1 mg/ml) were prepared with 0.1 M perchloric acid, stored at 4°C in the dark. The mobile phase was 0.1 M phosphate buffer (pH 3.0) containing 1 mM EDTA + 5% methanol delivered at 1 ml min^{-1}, unless stated otherwise.

2.2. Apparatus

The CV and LC–EC instrumentation used were the same as in the previous report [18]. The electrode detector was a TL-5A thin-layer cell (BAS). The auxiliary electrode was located across the thin-layer channel from the working electrodes. All potentials were measured versus a saturated calomel electrode (SCE), unless stated otherwise.

2.3. Sample preparation

A urine sample from a healthy subject was immediately filtered through a G-4 glass-filter (pore size 2–5 μm) and kept at 4°C in the dark. Working standard solutions for 0.5–150 $\mu g\ ml^{-1}$ dopamine were obtained by serial dilution of the stock solution with urine. Aliquots (20 μl) of these solutions were chromatographed.

2.4. Working electrode

First, attempts were made to electrodeposit the $PMo_{12}O_{40}^{3-}$ sites on the glassy carbon electrode surface by cyclic voltammetry. The bare electrode was scanned in a solution containing 0.5 M H_2SO_4 for 5 min and then was continuously scanned in a solution containing 0.1 mol l^{-1} $Na_3PMo_{12}O_{40}$ and 0.5 mol l^{-1} H_2SO_4. It was found that a dark-blue material separated from the electrode surface when the electrode was removed from the cell. After rinsing with water, when the electrode was scanned again in a solution of 0.5 mol l^{-1} H_2SO_4 a peak current did not appear, indicating that the heteropolyanions did not immobilize the electrode surface. Hence the polymer matrix could be used.

Prior to modification, the glassy carbon electrode was polished with a 0.5-μm alumina suspension on a smooth cloth, then thoroughly ultrasonicated in a water-bath and rinsed with water. In an aqueous solution of 0.1 mol l^{-1} pyrrole containing 0.5 mol l^{-1} H_2SO_4 as a supporting electrolyte, a polypyrrole film was obtained on the glassy carbon electrode after continuously scanning in the potential range −0.2 to +0.8 V for ten cycles. After rinsing in water, the polypyrrole film electrode was scanned in a solution containing 0.5 mol l^{-1} H_2SO_4 and 0.01 mol l^{-1} $Na_3PMo_{12}O_{40}$ in the potential range −0.2 to +0.6 V for ten cycles, then the PPy–$PMo_{12}O_{40}^{3-}$ CME was prepared.

3. Results and discussion

3.1. Electrochemical behaviour of PPy–$PMo_{12}O_{40}^{3-}$ CME

In an aqueous solution of 0.1 mol l^{-1} pyrrole containing 0.5 mol l^{-1} H_2SO_4 as a supporting electrolyte, a polypyrrole film was obtained on

the glassy carbon electrode after continuously scanning in the potential range −0.2 to +0.6 V for ten cycles. After washing with water, the cyclic voltammogram of the film electrode in 0.5 mol l^{-1} H_2SO_4 is shown at Fig. 1A. In an aqueous solution containing 0.5 mol l^{-1} H_2SO_4 and 0.01 mol l^{-1} $Na_3PMo_{12}O_{40}$, the modified electrode was obtained by continuously scanning in the potential range −0.2 to +0.6 V; three pairs of redox peaks appeared with a gradually rise of the peak currents [Fig. 1B]. After rinsing in water, the CME was scanned in an aqueous solution of 0.5 mol l^{-1} phosphate buffer (pH 3.0); there was no change in the voltammogram [Fig. 1C]. After scanning many times, their peak potentials were very close to those of $PMo_{12}O_{40}^{3-}$ in H_2SO_4 solution, the peak current decreasing only negligibly. This indicates that the modified electrode is very stable with the chosen electrolyte.

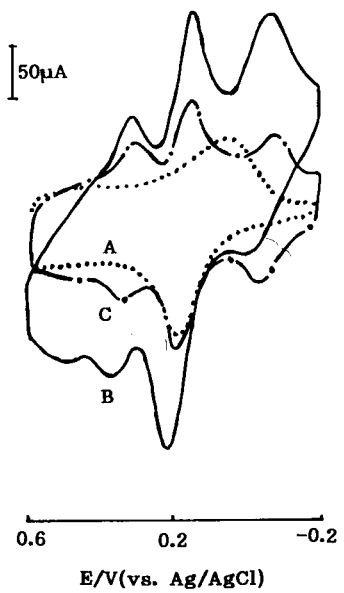

Fig. 1. (A) Cyclic voltammogram of polypyrrole film electrode in aqueous solution of 0.5 mol l^{-1} H_2SO_4. (B) Cyclic voltammogram of polypyrrole film electrode in aqueous solution containing 0.5 mol l^{-1} H_2SO_4 and 0.1 mol l^{-1} $Na_3PMo_{12}O_{40}$. (C) Cyclic voltammogram of PPy–$PMo_{12}O_{40}^{3-}$-modified electrode in aqueous solution of 0.5 mol l^{-1} phosphate buffer (pH 3.0).

It was indicated from the cyclic voltammogram of the PPy–$PMo_{12}O_{40}^{3-}$ CME in an aqueous solution of 0.5 mol l^{-1} H_2SO_4 with different scan rates that the peak current–scan rate dependence is linear in the range of scan rates studied. This result supports the assumption of surface-confined electroactive species. Moreover, the peak potential differences between each pair of anodic and cathodic peaks were approximately equal to 30 mV; anodic and cathodic peaks were symmetrical, and these results show that each peak corresponds a two-electron transfer process.

In the aqueous solution of H_2SO_4 at different pH values (from 0 to 3) with the same ionic strength, the half-wave potential of each pair of peaks decreased by about 60 mV per increment of 1 pH unit. This result shows that each two-electron reduction reaction involves the addition of two protons to the reduced form of each redox couple and vice versa. Therefore, the electrochemical reactions of the modified electrode in the aqueous solution of H_2SO_4 may be expressed as follows [8]:

$$[PMo_{12}O_{40}]^{3-} + 2nH^+ + 2ne \rightarrow$$

$$[H_{2n}PMo_{12}O_{40}]^{3-} \quad (n = 1, 2, 3, 4)$$

Fig. 2 shows the effect on the cyclic voltammograms (CVs) obtained at the PPy–$PMo_{12}O_{40}^{3-}$ CME with 0.5 mol l^{-1} phosphate buffer (pH 3.0) of the addition of dopamine to the blank supporting electrolyte. In the presence of dopamine, a pair of redox waves (with E_{pa} and E_{pc} = 0.54 and 0.45 V (vs. Ag/AgCl) at 100 mV s^{-1}, respectively) appeared, corresponding to the dopamine redox. Compared with CVs of dopamine at the bare glassy carbon electrode, the peak potential separation ΔEp was significantly reduced (from 600 mV at the bare to 90 mV at the CME at 100 mV s^{-1}), and the peak currents increased, indicating a great improvement in the reversibility of the dopamine electrode process. From the comparison of the CVs of dopamine at a PPy film electrode it was found that the peak currents clearly increased at the heteropolyanion–polymer electrode. These phenomena show the $PMo_{12}O_{40}^{3-}$ electrocatalytic behaviour for dopamine. The

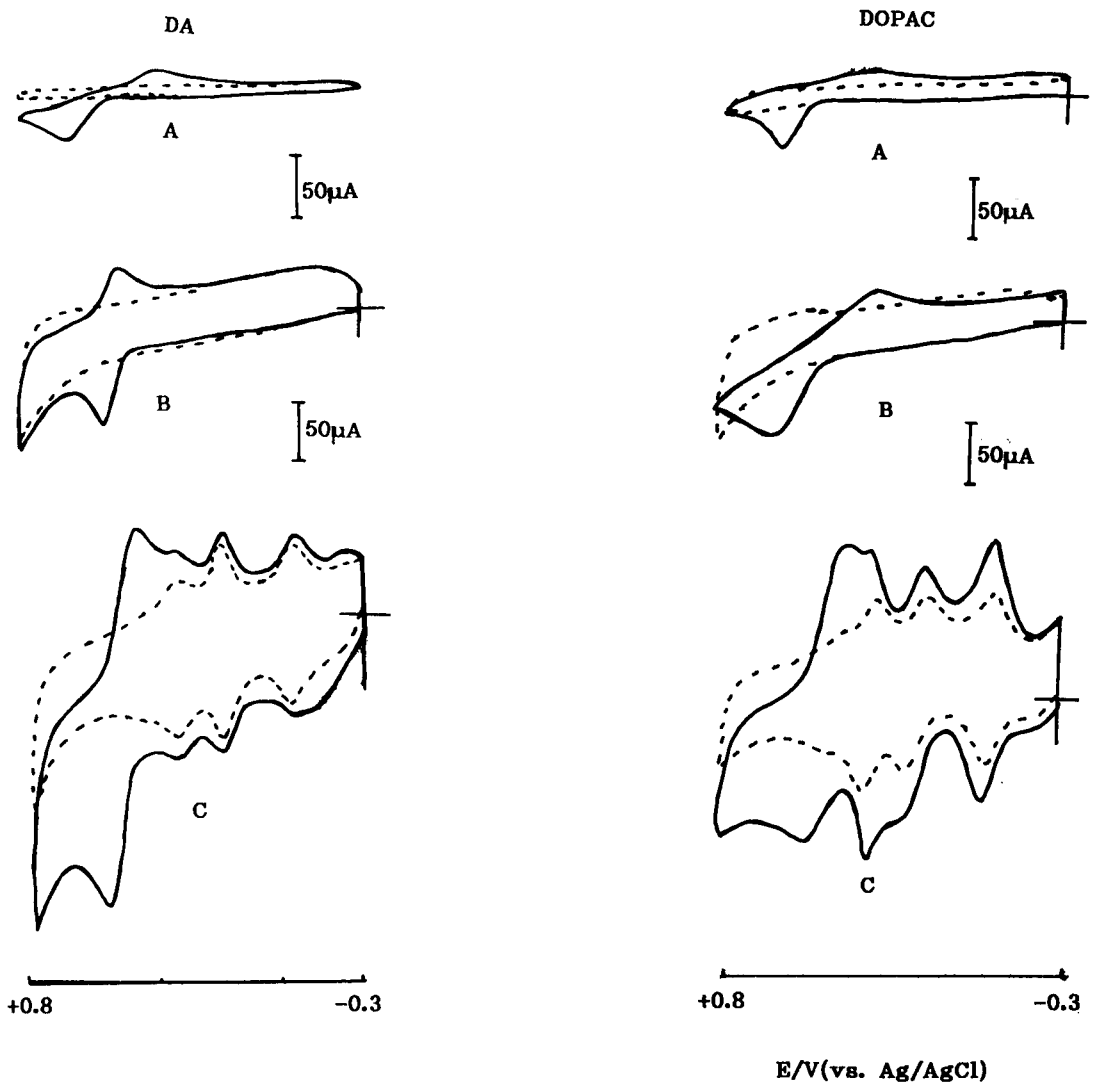

Fig. 2. Cyclic voltammograms of dopamine and DOPAC at (A) the bare glassy carbon electrode, (B) the PPy CME and (C) the PPy–$PMo_{12}O_{40}^{3-}$ CME. Scan rate, 100 mV s^{-1}; base electrolyte, 0.01 mol l^{-1} phosphate buffer (pH 3.0); DA and DOPAC concentrations, 1.0×10^{-3} mol l^{-1}.

electrocatalytic mechanism may be expressed as follows [19]:

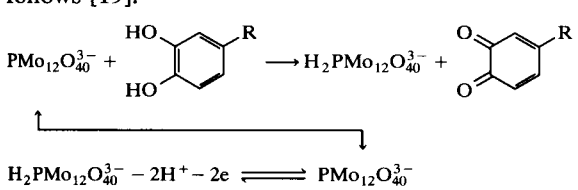

R: (1) $-(CH)_2-NH_2$ (DA)

(2) $-CHCH_2NH_2$ (NE)
OH

(3) $-CHCH_2NHCH_3$(E)
OH

(4) $-CH_2COOH$ (DOPAC)

Fig. 2 shows the cyclic voltammograms of DOPAC on glassy carbon, PPy film and PPy–$PMo_{12}O_{40}^{3-}$ CME. The CV behaviour was similar to that of dopamine.

3.2. Flow-through amperometric detection

Fig. 3A shows the hydrodynamic voltammograms (HDVs) for catecholamines at the single PPy–heteropolyanion-modified CME, with 0.1 mol l^{-1} phosphate buffer (pH 3.0) containing 0.1 mmol l^{-1} EDTA and 5% (v/v) methanol as mobile phase. In the anodic potential region, a plateau response level was achieved at +0.55 V (vs. SCE) and beyond. Fig. 3B shows the hydrodynamic voltammograms of catecholamines at the downstream CME at a series dual-electrode potential of 0.6 V (vs. SCE). It is clearly seen that the anodic plateau response levels were lower than those at the upstream CME (compared with Fig. 3A), indicating that a significant portion of the analyte was depleted in the diffusion layer before the mobile phase arrived at the downstream detector. However, the cathodic current level, from Fig. 3B, increased dramatically at the downstream CME in this series configuration, reaching a plateau level at a potential of 0.0 V. The enhancement of the current response could be due to the reduction of the oxidation products from upstream.

The effects of the pH of the mobile phase on peak current with LC–EC of catecholamine at the bare glassy carbon electrode and the CME are shown in Figs. 4 and 5, respectively. With the

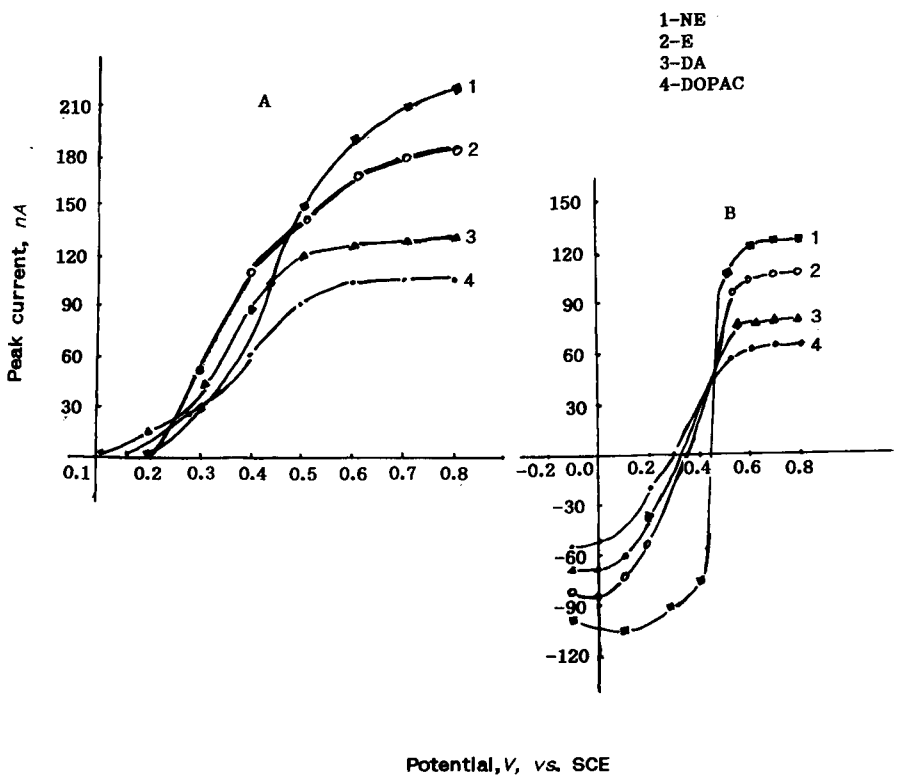

Fig. 3. Hydrodynamic voltammograms of 2 mg l^{-1} each of catecholamines at (A) a single CME and (B) downstream CME in series with the upstream CME monitored at 0.6 V (vs. SCE). Column, Nucleosil C_{18} (7 μm, 200 × 4.0 mm i.d.); mobile phase, 0.1 mol l^{-1} phosphate buffer (pH 3.0) + 5% (v/v) CH_3OH + 0.1 mmol l^{-1} EDTA; flow-rate, 1 ml min^{-1}; injection volume, 20 μl. 1 = NE; 2 = E; 3 = DA; 4 = DOPAC.

bare glassy carbon electrode, the current response of epinephrine at high pH (> 6.0) was nearly double that at low pH (2.5). Increasing pH had less effect on the current response for norepinephrine and a negligible effect for dopamine. This phenomenon is due to the electrode mechanism involving an electrochemical process of catecholamine on glassy carbon [20]. A higher pH is favourable for the indoline form of the epinephrine molecule, which has a high rate of nucleophilic addition, resulting in a net four-electron transfer and thereby the detector response may double [20]. DOPAC exhibited a maximum current response at pH 5.0. A lower pH is unfavourable for DOPAC oxidation owing to a more positive half-wave potential [18].

With the PPy–$PMo_{12}O_{40}^{3-}$ CME, however, the results are different: the NE response decreased with increasing pH up to 5.0, then increased, owing to indoline formation. Catecholamines (except for NE), however, showed a decreasing behaviour with increasing pH. This unique pH dependence involved an electrocatalytic mechanism

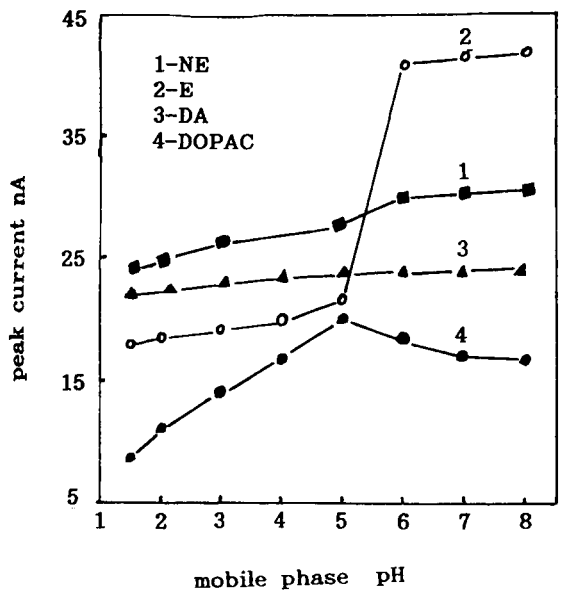

Fig. 4. Effect of mobile phase pH on the peak current in LC–EC of catecholamines at the bare glassy carbon electrode. Potential, 0.6 V (vs. SCE); analyte concentration, 1 mg l^{-1} for NE and E, 1.5 mg l^{-1} for DA and 2 mg l^{-1} for DOPAC; other conditions and lines as in Fig. 3.

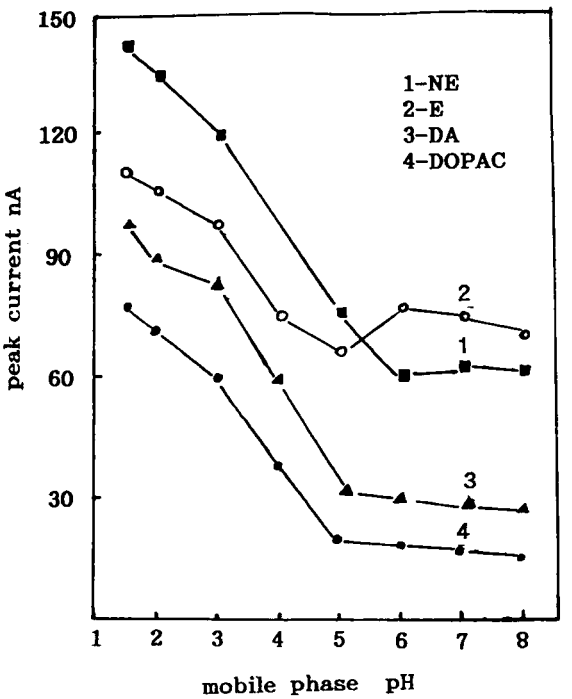

Fig. 5. Effect of mobile phase pH on LC–EC of 2 mg l^{-1} each of catecholamines at the CME. Potential, 0.6 V (vs. SCE); flow conditions and lines as in Fig. 3.

and stability of the catalytic sites ($PMo_{12}O_{40}^{3-}$). The acidity of the electrolyte solution had a marked effect on the electrochemical behaviour and stability of the PPy–$PMo_{12}O_{40}^{3-}$ film-modified electrode. As stated above [14], all the redox waves moved to more negative potentials as the pH increased in the low range between 0 and 5; the potential–pH dependence was about 60 mV pH^{-1}. At pH > 6, the wave shapes became ill-defined, because the heteropolyanions undergo a series of disproportionation–decomposition reactions [18]. Meanwhile, the stability of the film decreases with increasing pH. At pH ca. 9, the film is destroyed completely. Hence a lower pH is favourable for enhancing the current response, but it is unfavourable for the separation effect using a reversed phase (C_{18}) column. We therefore chose pH 3.0 as a suitable acidic condition.

Fig. 6 shows the dual-electrode chromatograms of catecholamines with a parallel–adjacent arrangement, using a bare glassy carbon elec-

trode and a CME as indicator detectors. A distinct peak current and a comparable sensitivity were observed with the CME at an applied potential of 0.8 V for the glassy carbon electrode and 0.5 V for the CME. With the comparable sensitivity, the applied potential of the CME changed negatively by 300 mV, which is consistent with CV experiment.

Fig. 7 shows dual-electrode chromatograms of catecholamines in the generation (oxidation)–collection (reduction) mode, using a bare glassy carbon electrode and PPy–$PMo_{12}O_{40}^{3-}$-modified CMEs. The current signals on the CME, both anodic and cathodic, were much higher than those

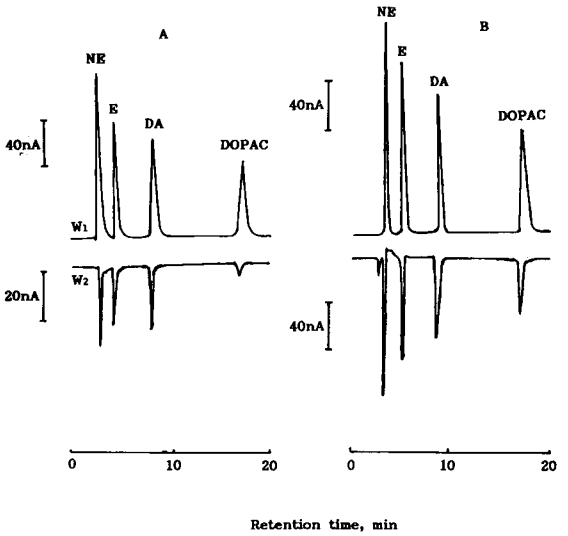

Fig. 7. Series dual-electrode chromatograms of 2 mg l^{-1} each of catecholamines with (A) bare glassy carbon electrode and (B) CME as working electrodes. Potential, +0.7 V for upstream W_1, (A) −0.2 V and (B) 0.0 V for downstream W_2; other conditions as in Fig. 3.

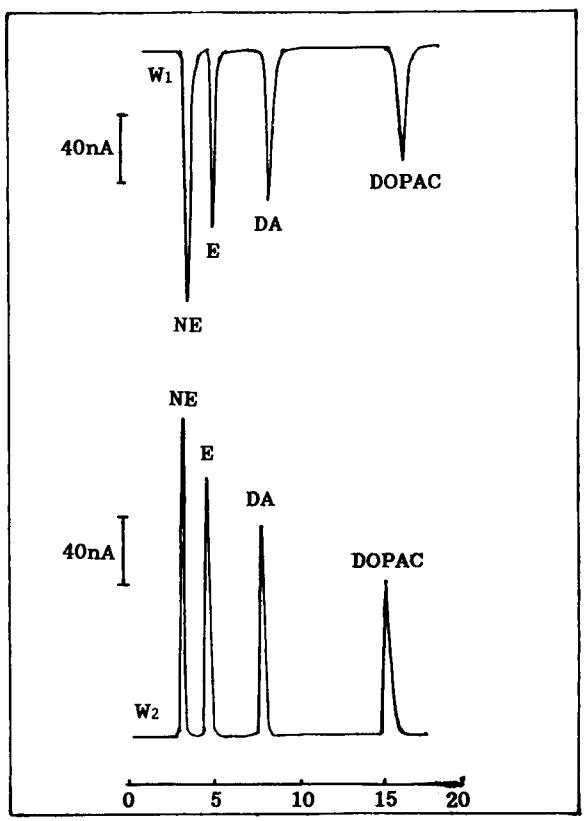

Fig. 6. Parallel-adjacent dual-electrode chromatograms of catecholamines at a bare glassy carbon (W_1) and the CME (W_2). Potential, 0.8 V for W_1 and 0.5 V for W_2. Flow parameters as in Fig. 3.

obtained at the bare glassy carbon electrode. The enhanced collection efficiencies (N_e) for catecholamines were > 0.5, and were greatly increased at the CME owing to the improvement of the reversibility of catecholamines in the electrode process. The collection efficiencies for the species used in this experiment are summarized in Table 1. The collection efficiencies for catecholamines are 0.53–0.67.

3.3. Detection of urinary dopamine

The analysis was performed using the described procedure using reductive detection at a modest positive potential applied to the down-

Table 1
Collection efficiencies (N_e) for glassy carbon electrode and CME (upstream W_1, downstream W_2)

Electrode	NE	E	DA	DOPAC
GC [a]	0.266	0.242	0.276	0.105
CME [b]	0.674	0.622	0.595	0.536

[a] Potential 0.6 V for W_1 and −0.2 V for W_2 vs. SCE.
[b] Potential 0.6 V for W_1 and 0.0 V for W_2 vs. SCE.

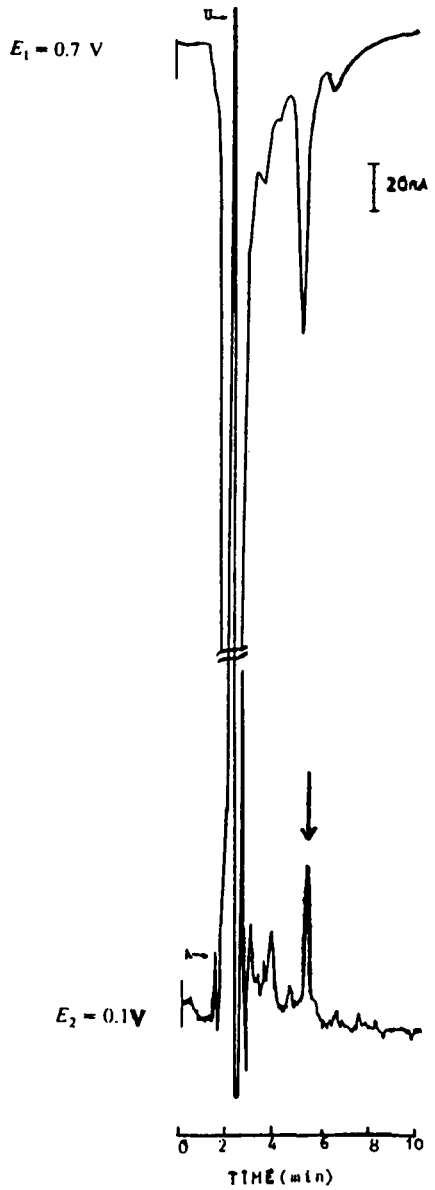

Fig. 8. Series dual-electrode chromatograms of a urine sample with 0.5 μg ml^{-1} DA added. The arrow indicates the DA peak. Other conditions as in Fig. 3.

stream electrode. Fig. 8 shows the dual PPy–PMo_{12}-modified electrode LC–EC of a urine sample doped with 0.5 μg ml^{-1} dopamine, demonstrating the applicability of the method to the accurate determination of dopamine in urine at low concentrations. The recovery of dopamine from urine samples was determined using the standard additions method and the results are given in Table 2. In the concentration range 0.5–300 μg ml^{-1}, the mean overall recovery was 97.7 ± 2.8%, which is acceptable.

3.4. Calibration, detection limit and reproducibility

Using the PPy–$PMo_{12}O_{40}^{3-}$-modified electrode as generating and indicating detectors in dual-electrode detection, the anodic peak currents for catecholamines increased linearly with increasing concentration over the range 3.0×10^{-8}–1.0×10^{-5} mol l^{-1}. The detection limits (signal-to-noise ratio = 2) were 5.0×10^{-9} mol l^{-1} for NE and 1.0×10^{-8} mol l^{-1} for DOPAC. Eight replicate injections of a stock solution containing 1.0×10^{-7} mol l^{-1} NE, 2.0×10^{-7} mol l^{-1} E, 5.0×10^{-7} mol l^{-1} DA and 1.0×10^{-6} mol l^{-1} DOPAC were carried out to determine the precision. The relative standard deviations of the peak height were 1.5% for NE, 2.5% for E, 4.8% for DA and 6.1% for DOPAC. Further, this method is satisfactory with respect to reproducibility. The PPy–PMo_{12} CME could be used for CV and LC–EC experiments for a periods of 1 week or longer with no evidence of chemical or mechanical deterioration. When used in LC–EC analysis, the peak current of catecholamines retained more than 95% of its initial level after 2 days of continuous service, indicating excellent stability and reproducibility. The detailed LC–EC conditions for

Table 2
Recovery of dopamine added to a urine sample

Amount added (ng)	Amount found [a] (ng)	Recovery [a] (%)
5	4.75 ± 0.45	95.0 ± 9.0
15	14.8 ± 1.2	98.6 ± 8.0
50	48.6 ± 0.6	97.2 ± 1.2
150	148.0 ± 1.4	98.6 ± 0.9
500	494.0 ± 5.4	98.8 ± 1.0
1500	1470 ± 16.0	98.0 ± 1.1
3000	2940 ± 5.5	98.0 ± 0.2
Blank	N.D. [b]	
Mean		97.7 ± 2.8

[a] Mean ± standard deviation (n = 3).
[b] Not detectable.

Table 3
LC–EC conditions for catecholamine determination at PPy–PMo_{12} CME

Separation column	Nucleosil C_{18} (7 μm) (200 mm × 4.0 mm i.d.)
Flow rate	1.0 ml min^{-1}
Column temperature	Room temperature
Sample loop	20 μl
Mobile phase	0.1 mol l^{-1} NaH_2PO_4–Na_2HPO_4 + 5% (v/v) CH_3OH + 0.1 mmol l^{-1} EDTA (pH 3.0)
Detector	TL-5A thin-layer amperometric detector (PPy–PMo_{12} CME)
Applied voltage	Oxidation 600 mV vs. SCE.
Complex matrix	NE, E, DA, DOPAC
Concentration	$C_{CA} = 1.0 \times 10^{-8}$ mol l^{-1}
Frequency of analysis	50 per day

catecholamine determination are summarized in Table 3.

4. Conclusion

This paper has reported a successful combination of a conventional reversed-phase liquid chromatographic system with an amperometric monitoring approach for application to catecholamines, based on the use of a novel heteropolyacid–polymer film-modified electrode (PPy–PMo_{12} CME). The PPy–PMo_{12} CME had a high catalytic effect on the oxidation–reduction of catecholamines. When employed with a series dual-electrode arrangement in LC–EC, high effective collection efficiencies of 0.67 for NE and 0.53 for DOPAC were achieved, greatly favouring the chromatographic speciation of the analyte in a complex matrix. Direct assay of urinary dopamine was performed to demonstrate the applicability of the PPy–PMo_{12} CME as catecholamine detector in the established LC–EC mode.

Acknowledgement

The support of the National Natural Science Foundation of China is gratefully appreciated.

References

[1] S. Dong, Anal. Chem. (Chin.), 16 (1988) 951.
[2] A.R. Hillman, in R.G. Linford (Ed.), Electrochemical Science and Technology of Polymers, Elsevier Applied Science, Barking, 1987 p. 241.
[3] T.A. Skotheim, Handbook of Conducting Polymers, Vol. 1, Dekker, New York, 1986.
[4] P.J. Riley and G.G. Wallace, Electroanalysis, 3 (1991) 191.
[5] C. Grob-Rhode, H.G. Kicinski and A.J. Kettrup, Chromatographia, 23 (1987) 465.
[6] P. Kolla, J. Kohler and G. Schomburg, Chromatographia, 23 (1987) 465.
[7] G. Bidan, E.M. Genies and M. Lapkowski, J. Electroanal. Chem., 251 (1988) 297.
[8] S. Dong and Z. Jin, J. Chem. Soc., Chem. Commun., (1987) 1871.
[9] B. Keita, D. Bouaziz and L. Nadjo, J. Electroanal. Chem., 279 (1990) 187.
[10] G. Bidan, E.M. Genies and M. Lapkowski, J. Electroanal. Chem., 251 (1988) 297.
[11] M. Lapkowski, G. Bidan and M. Fournier, Synth. Met., 41–43 (1991) 411.
[12] B. Keita and L. Nadjo, J. Electroanal. Chem., 240 (1988) 325.
[13] S. Dong, F. Song, B. Wang and B. Liu, Electroanalysis, 4 (1992) 643.
[14] B. Wang, F. Song and S. Dong, J. Electroanal. Chem., 353 (1993) 43.
[15] S. Dong and W. Jin, J. Electroanal. Chem., 345 (1993) 87.
[16] R.E. Shoup, in High-Performance Liquid Chromatography, Academic, New York, 1986, pp. 91–194.
[17] A. Aaki, T. Matsue and I. Uchida, Anal. Chem., 62 (1990) 2206.
[18] J. Zhou and E. Wang, Talanta, 39 (3) (1992) 235.
[19] L. Jin, T. Liu, X. Sun and Y. Fang, Chem. J. Chin. Univ. 14 (1993) 914.
[20] P.T. Kissinger, K. Bratin, G.C. Davis and L.A. Pachla, J. Chromatogr. Sci., 17 (1979) 137.

ELSEVIER

Analytica Chimica Acta 296 (1994) 181–193

ANALYTICA CHIMICA ACTA

Palladium as a chemical modifier for the determination of mercury in marine sediment slurries by electrothermal atomization atomic absorption spectrometry

P. Bermejo-Barrera *, J. Moreda-Piñeiro, A. Moreda-Piñeiro, A. Bermejo-Barrera

Department of Analytical Chemistry, Nutrition and Bromatology, Faculty of Chemistry, University of Santiago de Compostela, 15706 Santiago de Compostela, Spain

Received 17 January 1994; revised manuscript received 25 April 1994

Abstract

A method for the determination of mercury in marine sediment slurries by electrothermal atomization atomic absorption spectrometry was optimized. It was found that a particle size < 20 μm is sufficient to achieve total atomization of the mercury content in the solid particles of the slurry. This particle size was achieved with simple mechanical grinding, using zirconia beads. The use of different thickening agents, viz., Triton X-100, Viscalex HV30 and glycerol, during the slurry preparation was studied. In addition, an acid predigestion was applied to verify the efficiency of the slurry sampling. The use of palladium at a concentration of 15 mg l^{-1} was found satisfactory for stabilizing mercury at 200°C. Three charring steps, two involving an oxidative process, were studied. The optimum atomization temperature was 1450°C. A limit of detection of 70 μg kg^{-1} was achieved. The standard additions method was used for the determination of mercury in marine sediment samples from the Galician coast, the levels being between 2.2 and 3.2 mg kg^{-1}.

Keywords: Atomic absorption spectrometry; Marine sediments; Mercury; Slurry sampling

1. Introduction

Water quality can be evaluated by studying trace element concentrations in waters, suspended and bed sediments and biota samples. Usually, most water quality investigations have attempted to assess elements in aquatic systems by analysing water samples. Nevertheless, in most aquatic systems, the concentrations of pollutant elements in bed sediments are far greater than the concentrations of trace elements in water [1,2]. The strong association of trace elements, such a Pb, Zn, Cd, As and Hg, with suspended and bottom sediments means that the distribution, transport and availability of these constituents cannot be evaluated solely through the sampling and analysis of the dissolved phase. On the other hand, the study of a sediment column gives information about the element concentration changes over time and thus the area baseline

* Corresponding author.

SSDI 0003-2670(94)00204-Y

levels of several pollutants can be established and the water contamination history can be recorded. In addition, bottom sediment sampling and subsequent chemical analysis can provide fundamental regional geochemical information for use in identifying potential environmental effects due to both point and non-point sources of contamination [1,2]. Therefore, to determine the concentration due to certain trace elements, it is evident that the study of these elements in sediment samples is more suitable than their study in other environmental samples.

Mercury is classified by the US Environmental Protection Agency as a persistent and bioaccumulative element [3] and tends to be concentrated in either sediments (bottom and suspended), biota or even humans, owing to the consumption of marine products. Mercury is a toxic element and the study of mercury contamination is very important.

The determination of mercury by atomic absorption spectrometry (AAS) has usually been performed by the cold vapour technique, and it has been widely applied to the determination of mercury in water, environmental and biological samples [4–11]. However, it is subject to interferences from some metals, such as silver or nickel, and a special accessory is needed to generate the mercury vapour [10]. In addition, when applied to a complex matrix sample, a digestion procedure is needed before the measurement, with the possible loss of mercury owing to its high volatility. Electrothermal atomization AAS (ETAAS) with slurry sampling allows the determination of metals in complex samples, such as environmental samples, by introducing the sample as a solid [12], so the problems related to conventional digestion procedures are avoided.

ETAAS is not recommended for the determination of mercury owing to the possible loss of mercury during the drying and ashing steps. This problem can be minimized with the use of chemical modifiers that stabilize the mercury at higher temperatures. Various substances, such as sulfide, tellurium, permanganate, hydrogen peroxide, silver, selenium, palladium and palladium–magnesium [10,13–19], have been proposed as chemical modifiers for mercury determination. The charring temperatures reported in the literature vary between 100 and 450°C. A temperature of 400°C can be obtained with the use of gold [20], which forms an amalgam with mercury.

In this paper, we propose a method for the determination of mercury in marine sediments by using slurry sampling. This method has the advantage that digestion procedures are not needed because the marine sediment sample is injected into the graphite furnace as a solid, in the form of a slurry. Hence the loss of mercury associated with the conventional digestion methods is avoided and the possible contamination of the sample is removed. To achieve efficient ashing of the sample, without loss of mercury, the use of palladium, magnesium and palladium–magnesium was studied and it was found that palladium is a good chemical modifier, which allows a charring temperature of 200°C. Magnesium, which has been reported as a chemical modifier in conjunction with palladium [10] for the determination of mercury in water and digested sediment samples, depresses the mercury signal, with a consequent decrease in sensitivity.

2. Experimental

2.1. Apparatus

Mercury absorbance was measured with a Perkin-Elmer Model 1100B atomic absorption spectrometer equipped with a deuterium lamp for background correction, an HGA-700 graphite furnace atomizer and an AS-70 autosampler. The source of radiation was a mercury electrodeless discharge lamp operated at 4 W, which provided radiation at 253.7 nm. The spectral bandwidth used was 0.7 nm. Pyrolytic graphite-coated graphite tubes and pyrolytic graphite L'vov platforms were used. For all measurements, integrated absorbance with an integration time of 8 s was used throughout. A Laser Coulter Series LS100, Fraunhofer optical model particle sizer (Coulter Electronics, Hialeah, FL) was used to obtain the particle size distribution. A Vibromatic agitator and an Agimatic magnetic agitator from Selecta (Barcelona) were used in the slurry preparation.

2.2. Reagents

All solutions were prepared from analytical-reagent grade chemicals, unless indicated otherwise, using ultra-pure water of resistivity 18 MΩ cm^{-1}, obtained with a Milli-Q water-purification system (Millipore). Mercury(II) nitrate stock standard solution, 1.000 g l^{-1}, was prepared from the chemical supplied by Panreac (Barcelona). Methylmercury stock standard solution, 1.000 g l^{-1}, was prepared by dissolving 58.22 mg of reference material from the Commission of the European Communities Community Bureau of Reference (BCR) in 50 ml of toluene. Ethylmercury stock standard solution, 1.000 g l^{-1}, was prepared by dissolving 57.74 mg of ethylmercury chloride (Merck, Darmstadt) in 50 ml of toluene. Toluene (Suprapur, 99.5%) was supplied by BDH (Poole). Triton X-100, polyethylene glycol mono(*p*-1,1,3,3-tetramethylbutylphenyl) ether, for gas chromatography, was obtained from Merck. Viscalex HV-30 acrylic copolymer containing carboxyl groups was purchased from Allied Colloids (Bradford). Glycerol (99.4%; ACS reagent-grade) was supplied by Sigma (St. Louis, MO). Palladium stock standard solution, 3.000 g ml^{-1}, was prepared by dissolving 300 mg of palladium (99.999%; Aldrich, Milwaukee, WI) in 1 ml of concentrated nitric acid and diluting to 100 ml with ultra-pure water. If the dissolution was incomplete, 10 μl of hydrochloric acid (Suprapur, 35.0%, with a maximum mercury content of 0.001 μg ml^{-1}; BDH) was added to the cold nitric acid and heated to gentle boiling in order to volatize the excess of chloride. Magnesium nitrate stock standard solution, 2.000 g l^{-1}, was obtained by dissolving 2 g of magnesium nitrate (Suprapur; Merck) in 1 l of ultra-pure water. Nitric acid (Suprapur, 60.0–70.5%, maximum mercury content 0.001 μg ml^{-1}) and hydrochloric acid (Suprapur, 35.0%, maximum mercury content 0.001 μg ml^{-1}) were purchased by BDH. Reference material PACS-1 marine sediment was obtained from the National Research Council of Canada. A pool of marine sediments was obtained from the Galician coast, Spain. Argon of N50 purity (99.999%), used as a sheath gas for the atomizer and for internal purging, was obtained from SEO (Madrid). Synthetic air (C45) and oxygen (C45), used as a sheath gas for the oxidative process in the ashing step of the graphite furnace temperature programme, were supplied by Carburos Metálicos (Barcelona).

2.3. Procedure for slurry preparation

Lyophilized marine sediment samples were ground to reduce them to a particle size of < 250 μm. A 1-g portion of the sample was weighed and placed in a polyethylene vial (Zinsser Analytic, Frankfurt) and 12.5 g of zirconia beads (2–3 mm diameter) (Glen Creston, Stanmore) and 4 ml of water were added. The vials were then mechanically stirred in a flask shaker (Vibromatic, Selecta, Barcelona) for 20 min. The zirconia beads were separated using a sieve funnel (Haldenwanger, Technische Keramic, Düsseldorf). The slurry was then adjusted to a final volume of 50 ml by addition of ultra-pure water.

2.4. Procedure for measurements

A 500-μl portion of the slurry with appropriate volumes of palladium and Triton X-100 solutions to give concentrations of 15 mg l^{-1} and 0.01% (v/v), respectively, was transferred into an autosampler cup, then diluted to 1 ml and stirred magnetically before measurements. A volume of 20 μl was injected twice into the atomizer; between the two injections the drying step of the graphite furnace temperature programme was inserted. A sequential dry–ash–atomize–clean programme of the graphite furnace (Table 1) was run and the integrated absorbance was recorded.

3. Results and discussion

3.1. Particle size and slurry preparation

Particle size reduction with the use of mechanical grinding with zirconia beads involves the optimization of three parameters: the grinding time, the amount of zirconia beads and the volume of water. These experiments were carried out with 1

Table 1
Graphite furnace temperature programme and spectrometer operating conditions

Step	Temperature (°C)	Ramp (s)	Hold (s)	Flow-rate (ml min^{-1})
Injection Drying	90	55	25	Argon 300
Injection Drying	90	55	25	Argon 300
Ashing	200	15	30	Air 300
Atomization	1450	1	7	(read) 0
Cleaning	2000	1	3	Argon 300

Conditions: Hg electrodeless discharge lamp (EDL); Wavelength, 253.7 nm; EDL power, 4 W; spectral bandwidth, 0.7 nm; integration time, 8 s; Peak-area measurements; deuterium lamp background corrector; pyrolytic graphite tubes and platforms (L'vov); injection volume, 40 μl (20+20 μl).

g of a pool of marine sediments from the Galician coast.

The optimum grinding time was determined by measurements on several marine sediment slurry grinding procedures for different times. These measurements were carried out with the use of the optimized graphite furnace temperature programme shown in Table 1. The mean particle size corresponding to each slurry was determined by means of laser diffraction. As can be seen in Table 2, for grinding times longer than 20 min, the mercury absorbance signal remains constant while the mean particle size is gradually decreased. It was concluded that after 20 min the mean particle size reached is sufficient to achieve the atomization of the mercury from the slurry particles, so 20 min was selected as the optimum grinding time.

Table 2
Effect of grinding time on the mercury absorbance signal and the particle size for 1 g of sample, 15 g of Zr beads and 8 ml of water

Grinding time (min)	Mercury absorbance signal	Mean particle size (μm)
0	0.085	41.2
5	0.092	24.8
10	0.086	24.4
15	0.091	23.1
20	0.098	20.7
25	0.104	19.4
30	0.100	18.3
45	0.101	15.4
60	0.102	13.6

Table 3
Effect of the volume of water on the mercury absorbance signal and the particle size for 1 g of sample, a 20-min grinding time and 12.5 g of Zr beads

Volume of water (ml)	Mercury absorbance signal	Mean particle size (μm)
0	0.100	16.6
2	0.105	12.0
4	0.103	11.9
6	0.104	15.6
8	0.104	18.1
10	0.103	20.6
12	0.107	25.0

The effect of different amounts of zirconia beads (between 2.5 and 17.5 g) on the mercury absorbance and mean particle size was studied using the optimum grinding time of 20 min. It was found that for amounts of zirconia beads higher than 12.5 g, the mercury absorbance value remained statistically the same. Although the mean particle size was gradually decreased with larger amounts of zirconia beads, 12.5 g was selected as the optimum because a sufficiently small mean particle size of 20.4 μm was obtained.

The effect of the volume of water on the particle size reduction was studied using the optimum grinding time and amount of zirconia beads of 20 min and 12.5 g, respectively. Table 3 shows that the mercury absorbance signal remains constant throughout the range studied as the mean particle size is < 20 μm in all instances. This means that the most important parameters involved in the slurry preparation are the grinding time and the amount of zirconia beads. The variation of the mean particle size observed is due to the fact that smaller volumes of water are useful for obtaining a good particle size reduction, but when the volume of water is increased, a fuller polyethylene vial causes a decrease in the efficiency of the particle reduction procedure. According to Table 3, 4 ml was selected as the optimum value, giving a mean particle size of 12 μm.

3.2. Effect of thickening agents on particle size

There are different methods for the determination of metals in solid samples from which the slurry is prepared by means of mechanical grinding, adding several stabilizing agents and an adequate amount of zirconia beads. Some authors [21–23] used Triton X-100 and others, e.g., Hoening and co-workers [24,25] and Stephen et al. [26], recomended the use of glycerol and Viscalex HV30, respectively.

To study the effect of these agents on the particle size reduction, several slurries were prepared by introducing the optimum amount of zirconia beads (12.5 g) and different concentrations of these thickening agents between 0 and 0.2% (v/v) for Triton X-100 and Viscalex HV30 and between 0 and 0.2% (w/v) for glycerol. These agents were added in aqueous solution and then the volume was completed to 4 ml with ultra-pure water, following which the slurries were prepared as described.

Table 4 shows the effect of these agents on the mean particle diameter. The mean particle size increased as the concentration of the agents increased, which can be attributed to the increase in the viscosity of the solution due to these agents. In addition, the background signal measured increased with increasing concentration of these thickening agents. Therefore, we do not recommend the use of thickening agents in the particle size reduction procedure as of the efficiency of the process decreases and higher background signals are generated. We prefer to add these agents together with the chemical modifier in the autosampler cup, after the slurry preparation and just before measurements.

Table 4
Effect of Triton X-100, Viscalex HV-30 and glycerol concentrations on the particle size for 1 g of sample, a 20-min grinding time, 12.5 g of Zr beads and 4 ml of water

[Triton X-100] (%, v/v)	ϕ [a] (μm)	[Viscalex HV-30] (%, v/v)	ϕ [a] (μm)	[Glycerol] (%, w/v)	ϕ [a] (μm)
0	12.3	0	12.3	0	12.3
0.04	20.0	0.04	13.5	0.04	18.4
0.08	20.2	0.08	20.5	0.08	19.2
0.12	21.3	0.12	23.4	0.12	20.1
0.16	22.1	0.16	27.2	0.16	19.8
0.20	24.2	0.2	28.0	0.2	20.8

[a] Mean particle size.

3.3. Effect of acid predigestion of the slurry sample

Some workers [27–30] carry out a predigestion of the solid particles in an acid medium to mobilize several elements into solution before the slurry preparation. In this way, a portion of the trace elements remains in the solid phase and the remainder is transfered into aqueous solution. To study this effect, nitric acid concentrations between 0 and 17.5% (v/v) and predigestion times between 0 and 20 h were applied before the slurry preparation. The mercury signals of the slurry and the liquid phase were measured using the temperature programme shown in Table 1.

The results show that with a concentration of nitric acid of 17.5% (v/v) and predigestion times of 10, 15 and 20 h, the mercury signals due to the slurry and the liquid phase are similar. On the other hand, for nitric acid concentrations less than 17.5% (v/v) the mercury absorbance related to the slurry sampling is always higher than that due to the liquid phase sampling, and increases as the concentration of nitric acid and the predigestion time increase. These results indicate that for higher concentrations of nitric acid and longer predigestion times, the mercury mobilization into the solution is increased and a concentration of nitric acid of 17.5% (v/v) with a predigestion time of 10 h is sufficient to transfer into the solution all the mercury content of the solid phase. In this way, the liquid phase can be sampled, which offers a lower background signal in comparison with the slurry without predigestion. Nevertheless, the liquid-phase sampling is not suitable owing to the long predigestion time needed to mobilize the mercury content in the solid particles and because the acidic medium needed also damages the graphite tubes. We therefore prefer sampling of the slurry without acid predigestion for the determination of mercury in marine sediments.

3.4. Comparative study of palladium, magnesium and palladium–magnesium as chemical modifiers

Experiments were carried out to determine the loss of mercury during the charring step of the graphite furnace temperature programme by recording absorbance signals from aqueous standards of 100 $\mu g\ l^{-1}$ of mercury and from slurries prepared from a reference material (PACS-1 marine sediment) containing: (a) 15 mg l^{-1} of Pd, (b) 15 mg l^{-1} of Pd and 8 mg l^{-1} of Mg and (c) 8 mg l^{-1} of Mg.

In Fig. 1a and b are shown the results obtained as absorbance vs. charring temperature. When magnesium is used alone, for aqueous standards of mercury and slurries, it can be seen that mercury is lost, even at the drying temperature. On the other hand, when palladium is used alone or in conjunction with magnesium, at the concentration specified, loss of mercury from the graphite tube is not observed until 400 and 200°C for mercury aqueous standards and slurries, respectively. Owing to this charring temperature difference found between an aqueous standard solution of Hg^{2+} and slurries, the effect of palladium, magnesium and palladium–magnesium at different charring temperatures on methyl- and ethylmercury aqueous standard solutions was studied. It was found that for palladium and palladium–magnesium, a temperature of 400°C is achieved for methyl- and ethylmercury aqueous standard solutions. In addition, and in the same way as for for Hg^{2+} aqueous standard solution and slurries, the use of magnesium alone results in a loss of both organic mercury species at the drying temperatures. Therefore, we conclude that the lower charring temperature obtained for slurries by using palladium and palladium–magnesium, viz., 200°C, is due to the fact that the palladium is reduced by organic matter present in the marine sediments, and therefore it does not form the same Pd matrix as is formed in aqueous mercury standard solutions [31] and so it is not due to the mercury species present in the marine sediment, mainly methylmercury.

Finally, it can be said that magnesium alone does not stabilize the mercury, whereas palladium and palladium–magnesium offer the same stabilization, with a charring temperature of 400°C for aqueous standards of Hg^{2+}, methyl-Hg^{+} and ethyl-Hg^{+} and 200°C for slurries, a study of the optimum concentrations being necessary.

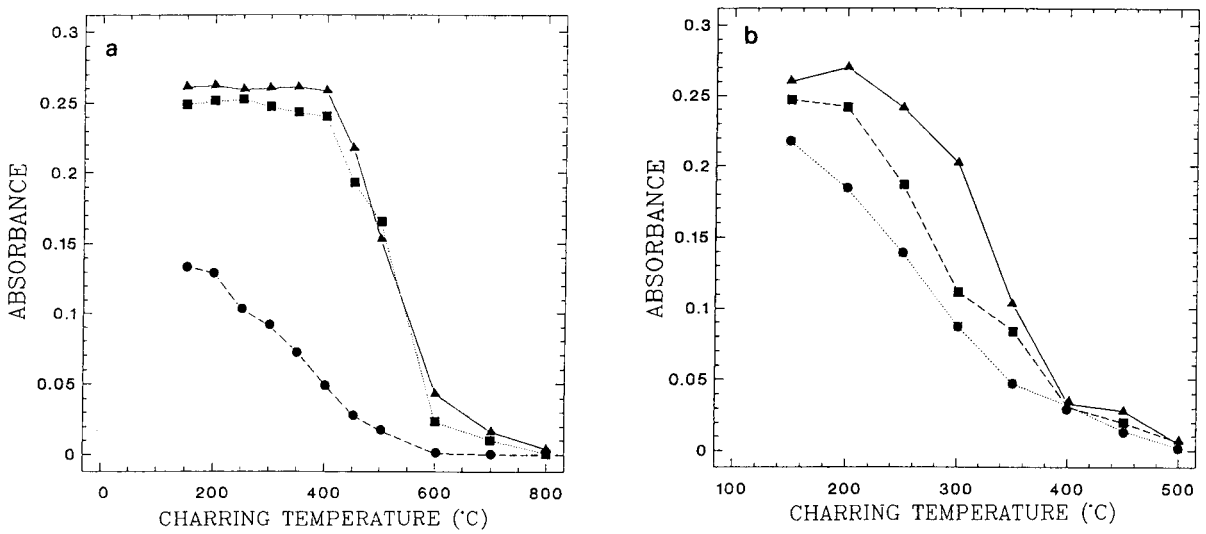

Fig. 1. Charring curves for (a) aqueous standards of 100 $\mu g\ l^{-1}$ of Hg and (b) slurries obtained for (▲) 15 mg l^{-1} of Pd, (■) 15 mg l^{-1} of Pd and 8 mg l^{-1} of Mg and (●) 8 mg l^{-1} of Mg.

3.5. Optimization of the amount of chemical modifier

The effects of various amounts of palladium and magnesium, as chemical modifiers, were studied using different combinations of palladium (0–30 mg l^{-1}) and magnesium (0–15 mg l^{-1}) with an aqueous standard solution of 100 μg l^{-1} of Hg^{2+} and a marine sediment slurry prepared from a reference material. The absorbance was measured in experiments involving differents combinations of magnesium and palladium, by fixing the amount of palladium and varying the amount of magnesium. As shown in Fig. 2a and b, large amounts of magnesium depress the mercury absorbance signal. In addition, the effect of $Mg(NO_3)_2$ at low concentration is different when it is added to a slurry or an Hg^{2+} standard solution, having some beneficial effects when the slurry is present (Fig. 2b), probably owing to the matrix oxidation and the removal the deleterious effects of organic matter, restoring the benefits of using palladium.

On the other hand, when palladium is added, the mercury signal gradually increases until a concentration of 20 and 15 mg l^{-1} for an aqueous Hg^{2+} standard solution of 100 μg l^{-1} and a marine sediment slurry, respectively, and then it remains constant at higher palladium concentrations. Fig. 3 shows the peaks obtained for different concentrations of palladium in the absence of magnesium for a marine sediment slurry. As can be observed, the absorbance peaks increase when palladium is first added, but at higher palladium concentrations the peak heights decrease. In addition, in Fig. 2a and b, it is also seen that larger amounts of magnesium cause lower mercury signals that could not be compensated for by the addition of larger amounts of palladium. On the other hand, when the amount of magnesium was increased, for a fixed amount of palladium of 15 mg l^{-1}, poorer peaks were obtained and the mercury absorbance signal was depressed. Hence

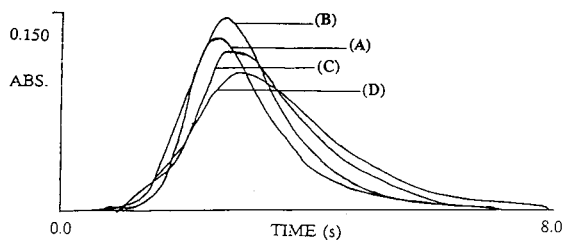

Fig. 3. Effects of 0 mg l^{-1} of Mg and different palladium concentrations on the absorbance peaks corresponding to a slurry. (A) 0 mg l^{-1} of Pd (0.238 A s.); (B) 15 mg l^{-1} of Pd (0.283 A s.); (C) 25 mg l^{-1} of Pd (0.283 A s.); (D) 30 mg l^{-1} of Pd (0.286 A s.).

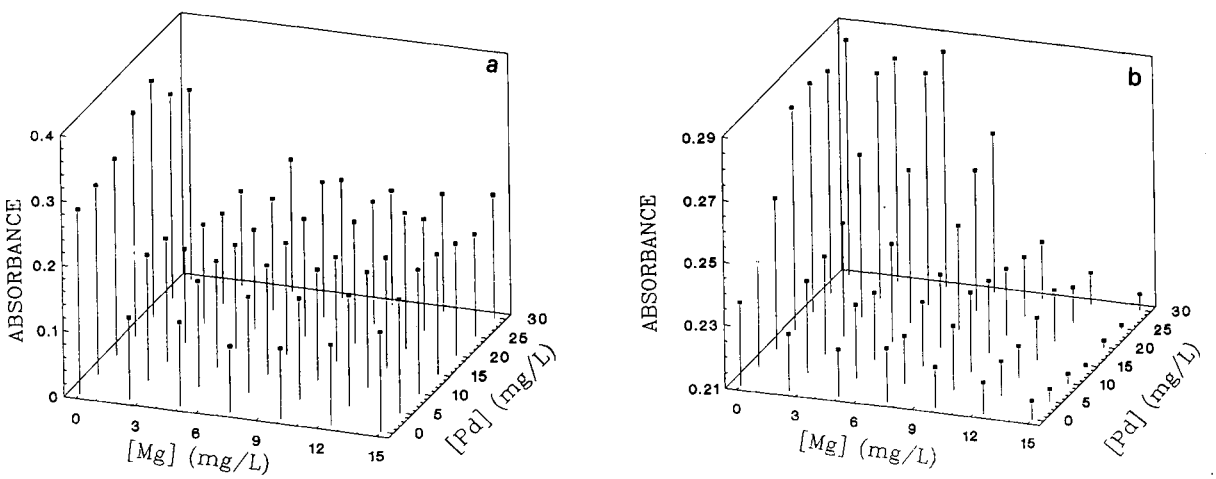

Fig. 2. Dependence of the mercury absorbance signal on the combined effects of various amounts of Mg and Pd added to (a) an aqueous standard solution of 100 μg l^{-1} of Hg^{2+} and (b) a marine sediment slurry.

it can be concluded that the addition of magnesium does not lead to good results.

3.6. Optimization of the graphite furnace temperature programme

Experiments were carried out to determine the optimum temperatures and times for the drying, charring and atomization steps for marine sediment slurry sampling.

With the use of 15 mg l^{-1} palladium as a chemical modifier, an optimum charring temperature of 200°C is achieved. Owing to the low mercury concentration in the marine sediment samples used, preconcentration on the graphite tube was needed in order to achieve a high mercury absorbance signal. Therefore, a slurry volume of 20 μl is injected twice, inserting a drying step between the two injections, as shown in Table 1. Owing to the high viscosity of the slurry, to achieve a satisfactory drying of the slurry a slow ramp rate is required.

The optimization of the charring step was carried out by using argon as the purge gas, and through charring steps converted into an oxidative decomposition process by using synthetic air and oxygen as carrier gases. The use of these oxidative gases is necessary owing to the preconcentration carried out, which gives a high background signal. Therefore, different air and oxygen flow-rates were tried, between 50 and 300 ml min^{-1}, and Fig. 4 shows their effect on the mercury absorbance and background signal. A satisfactory decrease in the background is achieved when a flow-rate of 300 ml min^{-1} of both gases is used, but for flow-rates less than 300 ml min^{-1} good charring is not achieved. On the other hand, when oxygen was used as the carrier gas, a temperature of 150°C during the oxidative process was sufficient, completing the charring step by means of a second charring at 200°C with argon as purge gas. It was shown (Table 5) that when oxygen is used, the temperature programme has two charring steps; the first one with oxygen at 150°C and the second with argon at 200°C. If synthetic air is used as the oxidative gas, in order to obtain a similar decrease in the background, it was necessary to maintain the synthetic air flow throughout the charring step. The ramp and hold times in these oxidative steps were also optimized in order to obtain a better decrease in the background. In Table 5 are shown the different charring steps optimized with the use of argon, synthetic air and oxygen as purge gases. The background signal values obtained for a slurry sample that was measured by using the three different charring stages were 0.434 A s, 0.060 A s and 0.047 A s (A = absorbance) for argon, synthetic air and oxygen, respectively. Hence it can be seen that the conversion of the charring step into an oxidative process generates an important improvement in the decrease of the background

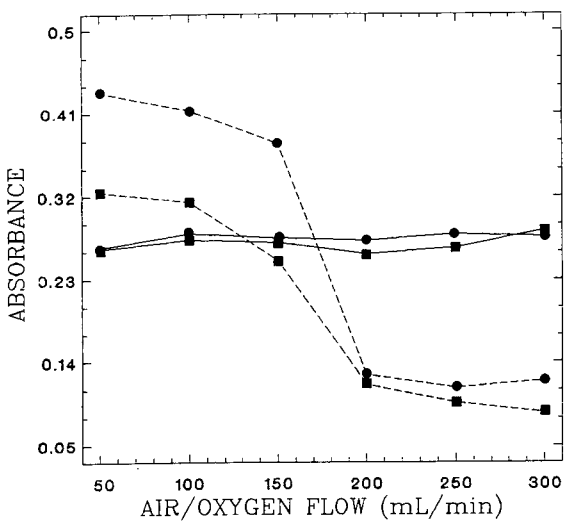

Fig. 4. Effect of different (●) synthetic air and (■) oxygen flow-rates on the mercury absorbance (solid lines) and background (dashed lines) signals.

Table 5
Charring steps corresponding to the use of different purge gases

Purge gas	Temperature (°C)	Ramp (s)	Hold (s)	Flow-rate (ml min^{-1})
Argon	200	15	30	300
Synthetic air	200	15	30	300
Oxygen + argon	150	10	25	300
	200	5	5	300

Slurry prepared from 1 g of sample, with palladium and Triton X-100 at concentrations of 15 mg l^{-1} and 0.01% (v/v), respectively.

signal. On the other hand, the mercury absorbance values obtained are similar in the three cases, and no modification of the peaks was observed. Although the use of oxygen offers the best results, in order to prevent rapid damage to the graphite tubes we prefer to use synthetic air during the charring step.

The determination of the optimum atomization temperature was carried out by studying different atomization temperatures between 1000 and 1700°C for a marine sediment slurry and an Hg^{2+} aqueous standard, using palladium as chemical modifier at its optimum concentration of 15 mg l^{-1}. Fig. 5 shows the atomization curves obtained for a marine sediment slurry and an aqueous Hg^{2+} standard solution. As can be seen, they are very different. The optimum atomization temperature was 1450°C because at this temperature the maximum absorbance value and good peak characteristics are obtained. Fig. 6 shows the mercury peaks obtained with a ramp of 0, 1 and 2 s. It is evident that a ramp time of 1 s gives the highest mercury absorbance value, the maximum power mode not being suitable. This is due to the high volatility of mercury so that, although rapid heating facilitates the release of the analyte from the graphite surface, it also speeds up the dissipation of gaseous analyte atoms within the atomizer through expulsion, and therefore the maximum power is unsuitable for mercury determination [32]. In addition, a hold time of 7 s is necessary to achieve total atomization of the mercury.

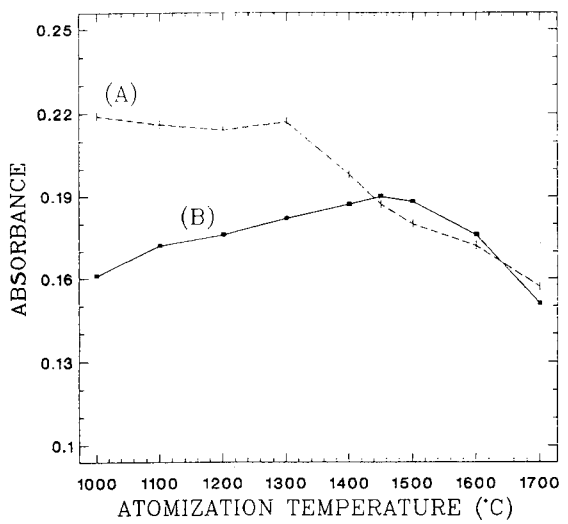

Fig. 5. Atomization curves obtained for (A) an aqueous standard of 100 $\mu g\ l^{-1}$ of Hg and (B) a marine sediment slurry.

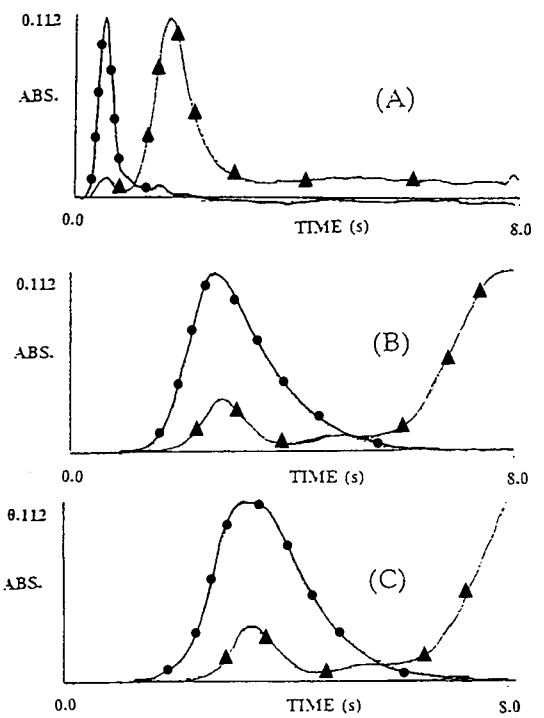

Fig. 6. Effect of the ramp time on (●) mercury and (▲) background absorbance signals. (A) 0 s; (B) 1 s; (C) 2 s.

3.7. Comparative study of thickening agents for stabilizing the slurries

Although the addition of thickening agents during the slurry preparation was not recommended, the use of these agents may be necessary in the introduction of the slurry into the graphite furnace. Therefore, we added these agents to the autosampler cups, together with the optimum concentration of chemical modifier, after the slurry preparation.

A study of the effect of these agents on the stability of the slurries was carried out by determining the within-run precision [relative standard derivation (R.S.D.)] for eleven replicate analyses

Table 6
Within-run precision of the measurements corresponding to the use of different thickening agents

Thickening agent	Mercury absorbance	S.D. [a]	R.S.D. [a] (%)
None	0.181	7.5×10^{-3}	4.1
Triton X-100	0.195	3.7×10^{-3}	1.8
Viscalex HV-30	0.189	1.2×10^{-3}	6.1
Glycerol	0.188	7.4×10^{-3}	3.9

[a] $n = 11$.

of a single sample during the same run. The agents that offers the lowest R.S.D. will be the best agent to stabilize the slurries.

Therefore, 500 μl of the slurry were placed in an autosampler cup, followed by the addition of the chemical modifier (palladium) and suitable volumes of Triton X-100, Viscalex HV30 or glycerol to achieved a concentration of 0.02% (v/v) for Triton X-100 and Viscalex HV30 and 0.02% (w/v) for glycerol, after dilution to 1 ml. Table 6 gives the statistical values obtained for the mercury absorbances related to each thickening agent and for a slurry without addition of a thickening agent. It can be seen that Triton X-100 gives the smallest R.S.D. The use of glycerol does not give good repeatibility and the use of Viscalex HV30 offers a poorer precision than when no stabilizing agent was used. This has been reported previously by other workers [23,26,30], who attribute it to sample solution adhering to the outside of the autosampler capillary.

Finally, the use of these thickening agents does not increase the background signal; 0.055, 0.044 and 0.063 A s were obtained using Triton X-100, Viscalex HV30 and glycerol, respectively. The background signal obtained without the use of stabilizing agents was 0.032 A s. These increases are not important. On the other hand, the best peak was obtained with the use of Triton X-100. In addition, when this agent is used, the mercury absorbance is higher than those obtained with the use of the other agents.

Finally, a concentration of 0.01% (v/v) of Triton X-100 was found to be optimum for achieving a good stabilizing effect of the slurry.

3.8. Calibration and standard additions graphs

To obtain a calibration graph, standard aqueous solutions containing mercury at concentrations in the 0–40 $\mu g\ l^{-1}$ range were mixed with suitable volumes of solutions of palladium and Triton X-100 to give concentrations of 15 mg l^{-1} and 0.01% (v/v), respectively. The blank of the calibration was 0.006 A s. The standard additions method was used in the same range of concentrations added by using a slurry prepared from PACS-1 reference material. The equations obtained were as follows:

calibration graph:

$$\text{absorbance} = -9\times10^{-4} + 1.4\times10^{-3}\,[\text{Hg}];\quad r = 0.997$$

standard additions graph:

$$\text{absorbance} = 0.22 + 3.4\times10^{-3}\,[\text{Hg}];\quad r = 0.999$$

where absorbance refers to integrated absorbance and the mercury concentration [Hg] is in $\mu g\ l^{-1}$. As can be seen, the two graphs shown very different slopes. This is due to the organic matter content and the combined effect of the different interfering elements. Therefore, aqueous calibration is not a real possibility.

3.9. Sensitivity

The sensitivity was studied through three parameters, the limit of detection (LOD), the limit of quantification (LOQ) and the characteristic mass (m_0) [33]. By performing the necessary measurements, the results obtained were LOD = 0.7 $\mu g\ l^{-1}$, LOQ = 2.3 $\mu g\ l^{-1}$ and m_0 = 123.9 pg.

The limit of detection and quantification for the marine sediment sample, using 1 g of sediment sample, diluting the slurry to 50 ml and taking 500 μl to prepare the final solution with the modifier and thickening agent (1000 μl), were 70 and 230 $\mu g\ kg^{-1}$, respectively. These limits can be improved by taking a larger volume of the slurry of marine sediment to prepare the final solution.

In addition, to obtain the lowest detection and quantification limits using the slurry procedure, it

is necessary to increase the concentration of the sample suspended in the slurry, but an increase in sample concentration is related to an increase in viscosity, which may impair the precision of sample introduction. Because of this, the effect of sample concentration on the precision of mercury signals was studied by preparing slurries that contained 2, 4 and 6% (w/v) of marine sediment sample. An amount of mercury aqueous standard solution was added to each type of slurry to obtain similar absorbances. Eleven replicate injections of each slurry were performed and the R.S.D. values were calculated. The results obtained are given in Table 7. There is no effect on the precision due to the slurry concentration and, moreover, the use of higher slurry concentrations offers no problems with respect to the background signal. The detection and quantification limits using a slurry marine sediment sample of 6% (w/v) and taking 40 μl (20 + 20 μl) of this solution are 23 and 77 μg kg^{-1} of mercury, respectively.

3.10. Precision

The within-batch precision of the method, obtained for eleven replicates of four slurry samples from PACS-1 reference material with different concentration of Hg^{2+} added, was investigated. To study the within-batch precision, four slurry samples with 0, 10, 20 and 30 μg l^{-1} of Hg^{2+} added were used and the results were 0.8, 1.5, 1.3 and 1.6%, respectively.

The repeatibility of the overall procedure was studied by measuring eleven different slurries of the same pool of marine sediments from the Galician coast. The R.S.D. obtained was 12.4%.

Table 7
Variation of the LOD with the concentration of the slurry

Concentration of slurry (%, w/v) [a]	Mercury absorbance	R.S.D. [b] (%)	LOD (μg kg^{-1})	LOQ (μg kg^{-1})
2.0	0.204	1.1	70	230
4.0	0.217	1.7	35	115
6.0	0.225	2.4	23	77

[a] Slurries prepared with 1, 2 and 3 g of reference material (PACS-1) as indicated in the procedure.
[b] $n = 11$.

Table 8
Analytical recovery of the method

Mercury concentration added (μg/l) [a]	Mercury concentration measured (μg/l)	Analytical recovery (%)	S.D. [b] (%)
10	9.9	98.8	7.1×10^{-3}
20	19.6	98.1	5.3×10^{-3}
30	29.4	97.8	2.1×10^{-3}
40	40.3	100.7	5.7×10^{-3}

[a] Hg^{2+} standard concentration in the autosampler cup added to a slurry prepared from a reference material.
[b] $n = 11$.

3.11. Accuracy

The accuracy of the method was studied by determining the analytical recovery and by analysis of a PACS-1 marine sediment reference material with a certified content of mercury of 12.3 ± 0.9 μg g^{-1}.

The values obtained for the analytical recovery are given in Table 8; they were close to 100% for all the mercury concentrations studied. The result obtained by analysing the reference material, expressed as the mean ± S.D./$\sqrt{n}$, was 12.9 ± 0.04 μg g^{-1}.

In addition, a study of the accuracy with various amounts of marine sediment sample was also carried out. Slurries containing 1, 2 and 3 g of the reference material were prepared and diluted to 50 ml [2.0, 4.0 and 6.0% (w/v)]. The results obtained for the three slurries were similar, and for slurries containing 2.0, 4.0 and 6.0% (w/v), mercury contents in the reference material of 12.9, 13.0 and 13.0 μg g^{-1}, respectively, were obtained.

3.12. Interferences

The effects of foreign elements that are present in the marine sediments on the determination of 75 μg l^{-1} of Hg^{2+} from an aqueous standard solution and slurries prepared with

PACS-1 reference material were studied by using the optimum amounts of Pd and Triton X-100. We assume that a species begins to interfere at a concentration when the mercury absorbance signal is increased or decreased by 10% of the signal value in its absence.

Numerous cations, such as Ag^+, Al^{3+}, As^{3+}, Cd^{2+}, Co^{2+}, Cr^{3+}, Cu^{2+}, Fe^{3+}, Mg^{2+}, Mn^{2+}, Ni^{2+}, Pb^{2+}, Se^{2+} and Zn^{2+}, and anions such Br^-, Cl^-, F^-, I^-, S^{2-}, $S_2O_3^{2-}$, SO_4^{2-} and SCN^- start to interfere at concentrations higher than those usually found in this kind of sample. Table 9 gives the lowest concentrations of various cationic and anionic species that interfere. As can be seen, this interference behaviour is smaller (except for Cd^{2+} and Cu^{2+}) in slurries than in aqueous standard solutions, probably owing to the matrix effects, which are very different in the two cases. The cationic species Cd^{2+}, Co^{2+} and Pb^{2+} and the anionic species Cl^- and F^- show the highest interfering effects at concentrations lower than 120 mg kg^{-1}.

Table 9
Effect of different elements on the mercury absorbance signal

Interferent	Lowest concentration [a] for standard solutions (mg kg^{-1})	Lowest concentration [a] for slurry (mg kg^{-1})
Ag^+	50	100
Al^{3+}	360	500
As^{3+}	40	1000
Cd^{2+}	80	70
Co^{2+}	50	200
Cr^{3+}	200	2000
Cu^{2+}	500	600
Fe^{3+}	40	800
Mg^{2+}	500	500
Mn^{2+}	700	1000
Ni^{2+}	30	1000
Pb^{2+}	40	150
Se^{2+}	400	400
Zn^{2+}	120	1500
Br^-	60	400
Cl^-	120	240
F^-	70	200
I^-	160	500
S^{2-}	400	800
$S_2O_3^{2-}$	200	700

[a] The lowest concentration that produced a variation of 10% in the mercury signal.

Table 10
Mercury levels in several marine sediment samples

Sample	Mercury concentration (mg kg^{-1})	S.D. [a] (mg kg^{-1})	R.S.D. [a] (%)
1	3.2	0.05	1.6
2	2.2	0.09	4.1
3	2.7	0.12	4.4
4	2.2	0.02	0.9
5	2.6	0.05	1.9
6 [b]	2.3	0.12	5.2
7 [c]	12.5	0.09	0.7

[a] $n = 4$.
[b] Pool of marine sediments from the Galician coast.
[c] PACS-1 marine sediment reference material.

To conclude, some interferences effects were observed, but as the concentrations of the ions concerned in the samples analysed (that is, the samples for which the method has been developed) are not high, we can assume that for many practical analytical applications there will be no interferences in the method. However, the standard additions method is needed, owing to the matrix effect.

3.13. Applications

The method was applied to the determination of mercury in marine sediment samples from the Galician coast (Ría de Pontevedra), north-western Spain. Two subsamples taken from each sediment sample were prepared in the form of slurries, and two subsamples from each were subjected to AAS. The mercury concentrations obtained are given in Table 10, together with the R.S.D.s for four analyses of each marine sediment sample. The values obtained are ten times higher than the mercury levels found in uncontaminated areas.

4. Conclusions

Slurry sampling for the determination of mercury in a complex sample, such as marine sediments, by ETAAS is advantageous because the loss of mercury during the wet digestion proce-

dures required in other methods is avoided. With the proposed procedure for slurry preparation, a particle size less than 20 μm was shown to be sufficient to obtain total atomization of the mercury content in the slurry particles. Palladium was found to be a good chemical modifier, providing stabilization of mercury up to 200°C, but magnesium was not satisfactory. In addition, the use of Triton X-100 as a thickening agent has provided good stabilization of the slurry. Finally, aqueous calibration is not considered adequate and calibration by the standard additions method must be used.

References

[1] U. Förstner, Contaminated Sediments, Springer, Berlin, 1989.
[2] A. Horowitz, A Primer on Sediment Trace Element Chemistry, Lewis, MI, 1991.
[3] P. Chapman, G. Romberg and G. Vigers, J. Water Pollut. Control Fed., 54 (1982) 292.
[4] S. Omang, Anal. Chim. Acta, 33 (1971) 415.
[5] S. Omang and P. Paus, Anal. Chim. Acta, 56 (1971) 393.
[6] S. Omang, Anal. Chim. Acta, 63 (1973) 247.
[7] R. Lutze, Analyst, 104 (1979) 979.
[8] G. Knaver, Mar. Pollut. Bull., 7 (1976) 6.
[9] N. Mikac, Z. Kwokai and M. Branica, Mar. Chem., 28 (1989) 109.
[10] B. Welz, G. Schlemmer and J. Mudakavi, J. Anal. At. Spectrom., 7 (1992) 499.
[11] W. Van Delf and G. Vos, Anal. Chim. Acta, 209 (1988) 147.
[12] C. Bendicho and M. De Loos-Vollebregt, J. Anal. At. Spectrom., 6 (1991) 353.
[13] D. Littlejohn, J. Egila, R. Gosland, V. Kunwar and C. Smith, Anal. Chim. Acta, 250 (1991) 71.
[14] H. Issaq and W. Zielinski, Anal. Chem., 48 (1976) 787.
[15] K. Fujiwara, K. Sato and K. Fuwa, Bunseki Kagaku, 26 (1977) 773.
[16] R. Ediger, At. Absorpt. Newsl., 14 (1975) 127.
[17] X. Shan and Z. Ni, Acta Chim. Sin., 37 (1979) 261.
[18] Z. Grobenski, W. Erler and V. Voellkopt, At. Spectrosc., 6 (1985) 91.
[19] L. Ping, K. Fuwa and K. Matsumoto, Anal. Chim. Acta, 171 (1985) 279.
[20] G. Lindsted and I. Skare, Analyst, 96 (1971) 223.
[21] Y. Madrid, M. Bonilla and C. Cámara, J. Anal. At. Spectrom., 4 (1984) 167.
[22] Y. Madrid, M. Bonilla and C. Cámara, Analyst, 115 (1990) 563.
[23] P. Bermejo-Barrera, M. Aboal-Somoza, R. Soto-Ferreiro and R. Domínguez-González, Analyst, 118 (1993) 665.
[24] M. Hoening and P. Van Hoeyweghen, Anal. Chem., 58 (1986) 2614.
[25] M. Hoening, P. Regnier and R. Wollast, J. Anal. At. Spectrom., 4 (1989) 631.
[26] S. Stephen, J.M. Ottaway and D. Littlejohn, Fresenius' Z. Anal. Chem., 328 (1987) 346.
[27] N. Miller-Ihli, Fresenius' Z. Anal. Chem., 337 (1990) 271.
[28] L. Ebdon and A. Lechotycki, Microchem. J., 34 (1986) 340.
[29] N. Miller-Ihli, Spectrochim. Acta, Part B, 44 (1989) 1221.
[30] N. Miller-Ihli, J. Anal. At. Spectrom., 3 (1988) 73.
[31] M.W. Hinds and K.W. Jackson, J. Anal. At. Spectrom., 5 (1990) 199.
[32] X.-P. Yan, Z.-M. Ni and Q.-L. Guo, Anal. Chim. Acta, 272 (1993) 105.
[33] L.H. Keith, W. Crummett, J. Deegan, R.A. Libby, J.K. Taylor and G. Wentler, Anal. Chem., 55 (1983) 2210.

ELSEVIER

Analytica Chimica Acta 296 (1994) 195–203

ANALYTICA CHIMICA ACTA

Determination of ruthenium in organic solutions by flame atomic absorption spectrometry, with ethanol and methyl isobutyl ketone as solvents

Matti Kauppinen *, Kimmo Smolander

Department of Chemistry, University of Joensuu, P.O. Box 111, SF-80101 Joensuu, Finland

Received 27 January 1994; revised manuscript received 31 March 1994

Abstract

A flame atomic absorption spectrometric method is described for the determination of ruthenium in organic solutions containing toluene, 1-hexene, 1-heptanol and 1-heptanal. Ethanol and methyl isobutyl ketone (MIBK) were tested as solvents. In addition to burner position and acetylene flow, the composition of the organic solution significantly affected the absorbance. Ethanol has several advantages over MIBK as a solvent: sensitivity is better and the detection limit lower, the smell is less unpleasant, the burner and chamber assembly keep cleaner and the burner position is less critical. Ethanol is an excellent solvent for the analysis of hydroformulation solutions containing more than 50 μg/ml of ruthenium. Synthetic and real hydroformulation solutions containing 50–2000 μg/ml Ru were successfully analysed after dilution with appropriate amounts of ethanol and toluene.

Keywords: Ruthenium; Flame atomic absorption spectrometry; Methyl isobutyl ketone (MIBK); Ethanol; Hydroformulation

1. Introduction

Besides playing a significant role in nuclear technology [1], ruthenium is an important component of catalysts and as such has been intensively studied in recent years [2–6]. The literature dealing with the determination of ruthenium is nevertheless quite meagre. Allan [7] published limits for the detection of ruthenium by flame atomic absorption spectrometry (AAS) in 1962, and Guerin [8] introduced the flameless (electrothermal) AAS method for the determination of ruthenium ten years later. Fabec and Ruschak [9] have reported the use of an inductively coupled plasma atomic emission spectrometer for the determination of Al, Co, La and Ru on alumina-based catalysts, while Gregoire [10] and Sen Gupta and Gregoire [11] have applied inductively coupled plasma mass spectrometry (ICP-MS) to the determination of ruthenium in geological materials.

In all the studies noted above, the matrix has been geological [10–12] or biological [13] material, plating solutions [14] or a synthetic aqueous solvent [15–21]. To prevent the numerous interferences associated with ruthenium determina-

* Corresponding author.

SSDI 0003-2670(94)00207-3

tion by flame AAS, the use of various masking, releasing or buffering agents has been recommended. El-Defrawy et al. [21] added 1 M KCN, concentrated HCl and 2 M H_2SO_4 to eliminate interferences from various metal ions and complex forming agents. Harrington and Bramsted [22] used titanium–potassium matrix solution as releasing agent, and Heinig and Mauersberger [15] buffered synthetic purex waste solutions with lanthanum nitrate and reported that cerium was then the only source of interference in the air acetylene flame. The use of uranium to mask interferences was investigated by Scarborough [23] and Montford and Cribbs [20]. Urbain and Cattenot [17] preferred nitrous oxide–acetylene flame to air–acetylene flame, and as a means of overcoming and stabilizing the interferences, they used lanthanum sulphate buffer. Fabec [24] chose nitrous oxide–acetylene flame as well, and 2000 μg/ml aluminium to eliminate the interferences of Al, Na, Ti, Co and La. Smolander et al. [25] determined Ru, Rh and Fe in cluster compounds by flame AAS after decomposition by two different methods. Lanthanum sulphate or $KHSO_4$ was added to eliminate interferences caused by foreign metal ions and phosphorus.

Only a few of the methods reported in the literature describe the determination of ruthenium in organic solvents. Young and Baldwin [26] tested various dithiocarbamates, in combination with a range of solvents and found ammonium pyrrolidinedithiocarbamate (APCD) in amyl acetate to give a good recovery of Ru when measured by flameless AAS. Aihara and Kiboku [27] used potassium xanthates as complexing agents and MIBK as the extracting medium. Braca et al. [28] determined ruthenium in organometallic compounds by dissolving samples of 20–40 mg in MIBK and analysing solutions by flame AAS with ruthenium tris-acetylacetonate, $Ru(C_5H_7O_2)_3$, as standard. Dornemann and Kleist [29] isolated traces of ruthenium in brines by extracting the hexamethylenedithiocarbamate chelate with a mixture of diisopropyl ketone and xylene.

In the work described here, we developed a method for the determination of ruthenium in simple organic solutions (methyl isobutyl ketone and ethanol) and in organic solutions containing toluene, 1-hexene, 1-heptanol and 1-heptanal. Mixtures like the latter are found in hydroformulation processes where ruthenium cluster compounds are used as catalysts. Finally, we tested the method on synthetic and real hydroformulation solution in conjunction with hydroformulation experiments being carried out in our laboratory.

2. Experimental

2.1. Apparatus

For all measurements we used a Varian SpectrAA-400 atomic absorption spectrometer equipped with a Varian Mark 5 A burner and the new spray chamber assembly model 99 100611 00, which is made of fluorinated high density polyethylene (FHDPE). Instrumental parameters are given in Table 1.

2.2. Reagents

All chemicals were of analytical reagent grade. 1-Hexene, 1-heptanol and 1-heptanal were from Sigma (St. Louis, CA); methyl isobutyl ketone (MIBK) was from Baker (Deventer), toluene from Riedel de Häen (Seelze) and ethanol from Alko (Rajamäki).

Standards for the determination of ruthenium in organic solvents were prepared using sublimed triruthenium dodecacarbonyl $[Ru_3(CO)_{12}]$ synthesised at the University of Joensuu. Analysis:

Table 1
Instrumental parameters

Wavelength	349.9 nm
Lamp current	10 mA
Slit width	0.2 nm
Air flow	13.5 l/min
Acetylene flow	2.0 l/min
Delay time	1 s
Time constant	0.05 s
Measurement time	3 s
Replicates	3
Burner height	5–7
Sample uptake	8.9 ml/min
Background corrector	Off

Calculated for $Ru_3(CO)_{12}$ (MW 639.335): Ru, 47.43%, C, 22.54%. Found: Ru, 48.6%, C, 22.72%. IR (CH_2Cl_2): ν(CO), 2061 vs, 2029 s, 2010 m.

Glassware and polypropylene tubes were acid washed with a solution containing 2 mol/l HNO_3 and 1.6 mol/l HCl and rinsed with deionized water (17.5 MΩ cm^{-1}).

250 μg/ml or 100 μg/ml Ru standard stock solutions were prepared daily by dissolving 52.71 mg or 21.09 mg of $[Ru_3(CO)_{12}]$ in 100 ml of toluene in a water bath. Additional standard stock solutions were prepared by using as solvents pure MIBK, ethanol with 25% of toluene, or ethanol with 10% of MIBK. The yellow solutions prepared in MIBK grew dark in a few hours, whereas the solutions prepared in toluene and in ethanol with 25% of toluene remained unchanged for several days. The lack of colour change, which confirms the stability of the solution, is one good reason for choosing toluene as solvent when preparing standard stock solutions. A second reason is that toluene is used as solvent in hydroformulation reactions and therefore is naturally present in samples.

2.3. Samples

We prepared standard series containing sublimed triruthenium dodecacarbonyl in toluene, MIBK or ethanol and samples containing 80% toluene and 20% 1-hexene, 1-heptanol, 1-heptanal or their mixtures and 12–200 μg/ml of ruthenium. Solvents were pure MIBK, MIBK–ethanol mixture (50 + 50, w/w) and absolute ethanol. The ratio of solvent to sample was mostly 3 : 1, so that concentrations in final solutions were 3–50 μg/ml of rhodium, 75% solvent, 20% toluene and 5% 1-hexene, 1-heptanol, 1-heptanal or their mixtures. All standard and sample solutions were made by weighing.

Many studies were done on 20 μg/ml Ru solutions containing 75–85% solvent (MIBK, ethanol or their mixtures), 20% or 10% toluene, 5–0% hexene, and 0–5% 1-heptanol, 1-heptanal or their mixtures; but we also tested stronger solutions up to 100 μg Ru/ml.

Hydroformulation solutions were diluted with ethanol and toluene to get a toluene concentration of 20%, which was the toluene concentration used in blanks and standards.

3. Results and discussion

3.1. Selecting the solvent

We tested MIBK and ethanol as solvents for toluene in the ratio 20% toluene and 80% solvent. As can be seen in Fig. 1 and Table 2, the sensitivity was better, the linear dynamic range broader and the detection limit lower in ethanol. In addition the burner height was less critical

Table 2
Comparison of ethanol and MIBK as solvents in the determination of ruthenium in toluene solutions at burner height 6

Solvent	Ethanol	MIBK
Sensitivity [a]	0.0068	0.0051
Characteristic concentration [b] (μg/ml)	0.65	0.86
Linear range (μg/ml)	0–20	0–10
Detection limit [c] (μg/ml)	0.27	0.85
Detection limit [d] (μg/ml)	0.62	1.66
Recommended working range (μg/ml)	3–50	10–50
R.S.D.%, 5–50 μg/ml, $n = 15$	< 3	

[a] Absorbance unit/ppm with 10 μg/ml Ru solution.
[b] The concentration corresponding to an absorbance of 0.0044 AU.
[c] Calculated as $\frac{2 \times \text{st.dev.}(A_{(2.5\text{ppm})} - A_{(\text{blank})}) \times 2.5\mu\text{g/ml}^{-1}}{\text{average}(A_{(2.5\text{ppm})} - A_{(\text{blank})})}$
[d] Calculated as 3σ according to IUPAC recommendations.

when ethanol rather than MIBK was the solvent (Fig. 2). Addition of toluene had an affect on the absorbances: the blank with 20% toluene in MIBK absorbs were strongly at low burner positions (Fig. 2, curve C), and at burner positions lower than 5 the absorbance is even greater than the absorbance of 20 μg/ml Ru in pure MIBK (Fig. 2, curve E). Toluene has a similar but much weaker effect on the absorbance of blanks containing ethanol as solvent, and the effect varies less with burner position (Fig 2, curve A).

The absorbance of 20 μg/ml Ru solution in pure MIBK varied only slightly with burner height (Fig. 2, curve E), but in any case such solutions were not studied further; for in practice toluene is always present in hydroformulation solutions, and for these ethanol was found to be a better solvent than MIBK. The solvent mixture 50% MIBK + 50% ethanol proved to have no advantage over absolute ethanol.

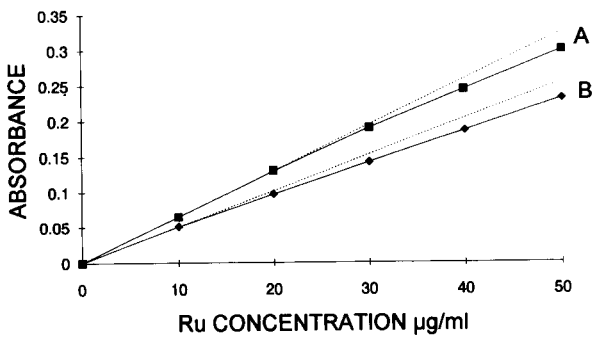

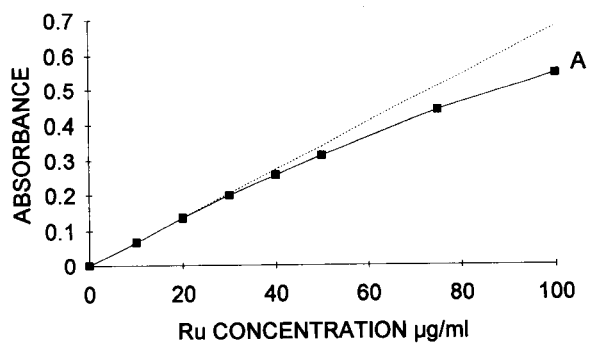

Fig. 1. Calibration graphs of ruthenium in organic solutions measured at burner position 6. (A) 80% ethanol + 20% toluene, (B) 80% MIBK + 20% toluene.

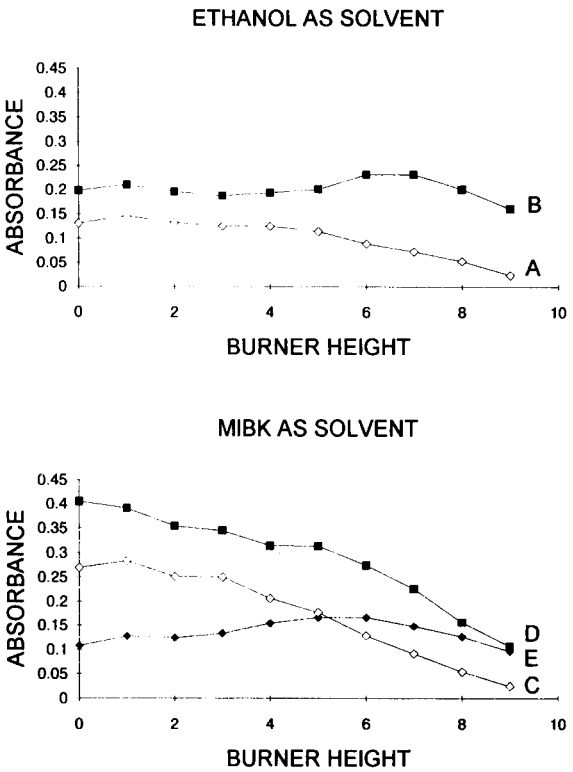

Fig. 2. Effect of burner height on absorbances of blanks in (A) 80% ethanol + 20% toluene, (C) 80% MIBK + 20% toluene, and on absorbances of 20 μg/ml Ru solutions in (E) pure MIBK, (B) in ethanol with 20% of toluene, (D) in MIBK with 20% of toluene.

3.2. Optimization

The instrument was optimized according to the manufacturer's instructions. After adjustment of the lamp to give maximum energy the burner was adjusted horizontally, vertically and rotationally so that the centre of the burner slot was aligned with the light beam. After that the flame was ignited, ethanol was aspirated for 10 min to stabilize the burner and the instrument zero was adjusted during the aspiration. A 20 μg/ml Ru solution was exchanged for ethanol, and the position of the burner, the flame composition and the position of the glass bead were adjusted to obtain maximum absorbance consistent with minimum noise.

After optimizing on sensitivity, different flame compositions were tested and the position of the

burner was varied to optimize for lack of interference.

3.3. Effect of acetylene flow

Using the optimum air flow of 13.5 l/min, which was also the minimum permitted air flow, the acetylene flow was varied from the optimum

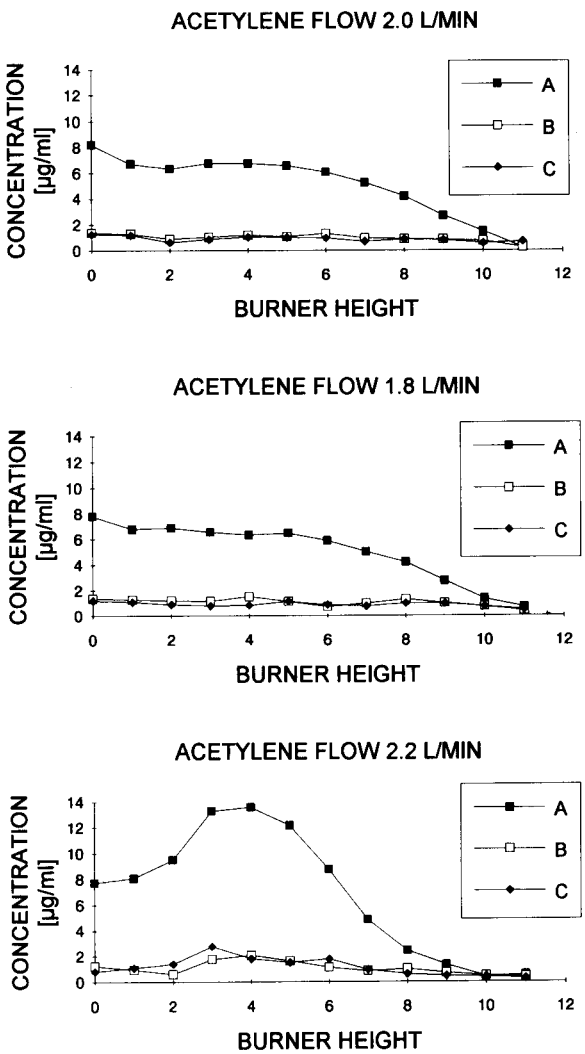

Fig. 3. Effect of burner height position on equivalent analyte concentrations of blanks under constant air flow (13.5 l/min) and different acetylene flows in different matrices. (A) 75% ethanol + 20% toluene + 5% hexene, (B) 75% ethanol + 20% toluene + 5% heptanol, (C) 75% ethanol + 20% toluene + 5% heptanal.

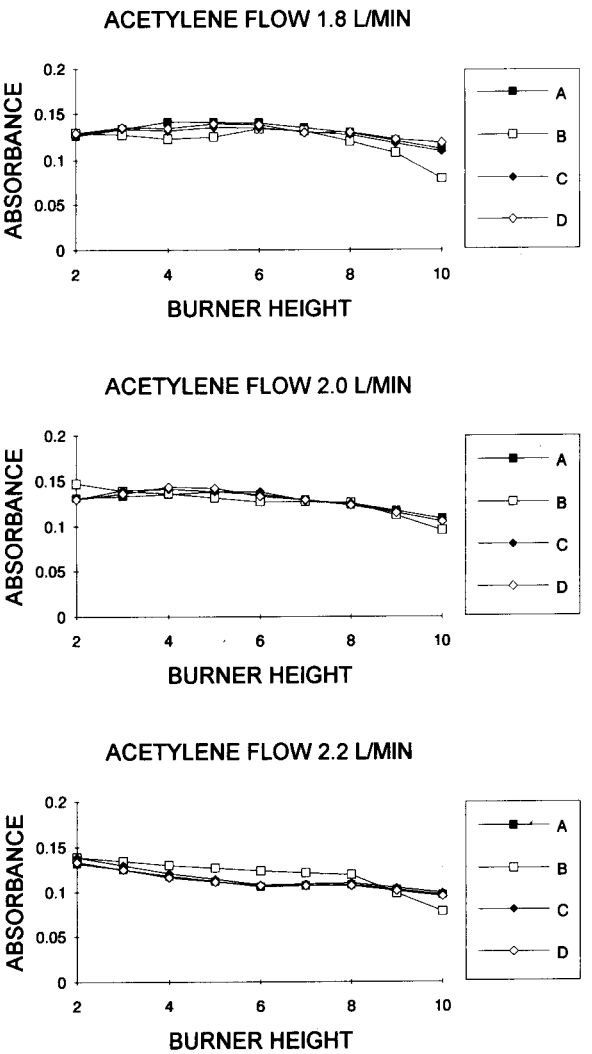

Fig. 4. Effect of burner height position and acetylene flow on absorbances of 20 µg/ml Ru solutions in different matrices. (A) 80% ethanol + 20% toluene, (B) 75% ethanol + 20% toluene + 5% hexene, (C) 75% ethanol + 20% toluene + 5% heptanol, (D) 75% ethanol + 20% toluene + 5% heptanal.

2.0 l/min to 1.8 l/min and 2.2 l/min. Relative to flows of 1.8 and 2.0 l/min, the flow of 2.2 l/min gave higher equivalent analyte concentrations of blanks, especially those containing 5% of 1-hexene (Fig. 3 curve A), poorer sensitivity and greater differences between the absorbances of 20 µg/ml Ru solutions in different matrices (Fig. 4). With an acetylene flow of 1.8 l/min the flame was slightly too lean and liable to go out when no

organic solution was aspirating into the flame. Thus 2.0 l/min was confirmed to be the optimum acetylene flow.

3.4. Effect of burner height

The burner height is critical for solutions containing 20% toluene when MIBK is used as solvent, but less critical when ethanol is used as solvent (Fig. 2). As the burner height was raised from 0 to 6, the absorbance of 20 μg/ml Ru solution containing 80% ethanol and 20% toluene (Fig. 4, curve A) increased slightly with acetylene flows of 1.8 l/min and 2.0 l/min and decreased with an acetylene flow of 2.2 l/min. As the burner height was raised from 6 to 10 the absorbances decreased with all three acetylene flows. Best sensitivity was obtained with the acetylene flow 2.0 l/min on burner positions 4–6, while the differences between the absorbances of 20 μg/ml Ru solutions in different matrices were smallest on burner positions 7–8.

3.5. Effect of organic matrix

Addition of 5% 1-hexene, 1-heptanol or 1-heptanal did not significantly affect the absorbances of 20 μg/ml Ru solutions in ethanol with 20% of toluene on burner positions 3–9 (Table 3). At low burner positions (0–2), 1-hexene increased the absorbances and at high burner positions (10–12) it decreased the absorbances. As 1-hexene also affected the absorbance of a blank containing 75% ethanol, 20% toluene and 5% hexene (Fig. 3, curve A), it would clearly interfere with the determination of ruthenium in diluted solutions. At burner positions 0–6, equivalent analyte concentration of the hexene blank was over 6 μg/ml, compared with less than 2 μg/ml in blanks containing 5% of 1-heptanol or 1-heptanal.

Table 3
Recovery of 20 μg/ml of Ru in solutions containing 75% ethanol, 20% toluene, and 5% 1-hexene, 1-heptanol or 1-heptanal

Burner height	Recovery (%)		
	Hexene	Heptanol	Heptanal
0	119	101	99
1	121	105	103
2	110	104	101
3	103	105	101
4	99	104	104
5	96	101	102
6	97	103	101
7	102	101	100
8	103	102	101
9	97	101	100
10	87	100	97
11	77	99	97
12	76	97	94

The effect of hexene is also clearly seen in Fig. 5, where twenty solutions were measured at vari-

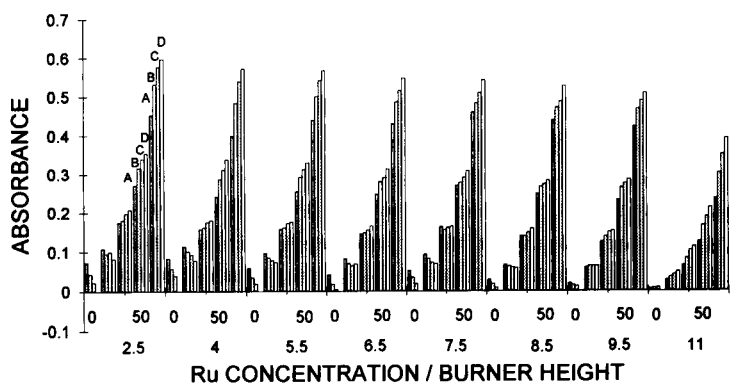

Fig. 5. Effect of hexene concentration on the absorbances of 0, 10, 25, 50 and 100 μg/ml ruthenium solutions in ethanol containing 20% of toluene. Hexene concentrations in each pattern of five at different burner heights are (A) 5%, (B) 2.5%, (C) 1% and (D) 0%.

ous burner heights. Ruthenium concentrations in the solutions were 0, 10, 25, 50 and 100 μg/ml and they contained 0, 1, 2.5 and 5% of hexene. Hexene increased the absorbances of blanks and the dilute solutions but decreased the absorbances of solutions containing 25 μg/ml or more of ruthenium. Background correction with a deuterium lamp did not remove the interference.

Toluene has a clear effect on the absorbances; we tested 20 μg/ml Ru solutions and blanks containing 10, 15, 20 and 25% of toluene. As can be seen in Fig. 6, the effect is stronger at low burner positions. However the net absorbances (A_s–A_b) differ little at burner positions 2–5. The same solutions measured with background correction supplied by a deuterium lamp gave results comparable to the net absorbances, which shows that the interference of toluene can be removed by using a background corrector. Because toluene is not the only interfering substance and because the background corrector does not remove the interference of hexene we nevertheless recommend measuring Ru without the background corrector and instead keeping the toluene concentration constant. To eliminate the inteferences of other organic substances, standards need to be prepared that are identical with the samples, or the samples need to be diluted.

3.6. Buffering agents in ethanol

We tested uranyl nitrate [$UO_2(NO_3)\cdot 6H_2O$] and lanthanum nitrate [$La(NO_3)_3\cdot 6H_2O$] in concentrations of 1% in the final ethanol solution containing 20% of toluene. Neither compound increased the sensitivity or otherwise improved the determination of ruthenium, but instead both caused a salt to accumulate in the burner.

3.7. Determination of ruthenium in hydroformulation solutions

Ruthenium cluster compounds bound to a carrier are used as heterogeneous catalysts in hydroformulation reactions, but they work only on a carrier and lose their power if released into the solution. For this reason a reliable method has been sought for the determination of ruthenium in organic solvents.

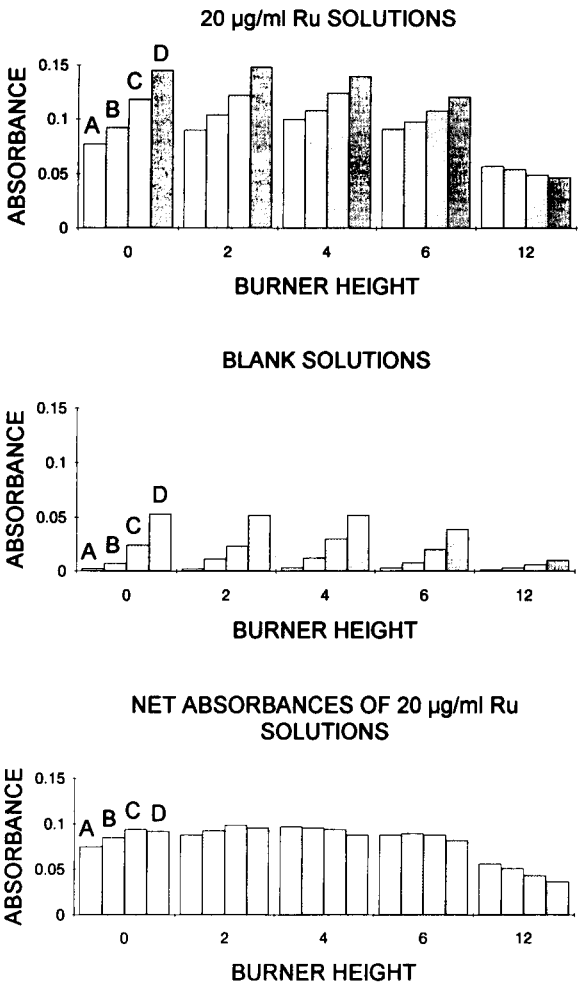

Fig. 6. Effect of toluene concentration on absorbances of 20 μg/ml Ru solutions and blanks at different burner heights. Toluene concentrations: (A) 10%, (B) 15%, (C) 20% and (D) 25%.

The main component in hydroformulation solutions is toluene, which is used as the solvent in concentrations of 88–91%. After reaction, the solution contains 2–9% hexenes, 0.5–5% heptanol and small amounts of other compounds. As we have shown, toluene affects the absorbances of Ru solutions in two ways: it increases the absorbances of blanks and diluted solutions and decreases the absorbances of concentrated solutions. The effect of the interference can be elimi-

Table 4
Composition and calculated and determined ruthenium concentrations of five synthetic hydroformulation solutions at their final dilutions

Sample	Toluene (%)	Hexene (%)	Heptanol (%)	Ru (μg/ml) calculated	Ru (μg/ml) determined [a]
S1	22.0	1.9	0.4	15.1	15.2±0.2
S2	21.9	1.9	0.4	24.9	24.3±0.2
S3	21.9	1.7	0.6	24.8	24.5±0.3
S4	21.8	1.9	0.4	34.7	34.0±0.6
S5	21.8	1.7	0.6	34.7	35.6±1.8

[a] Mean of five measurements ± 95% confidence interval.

nated, however, by keeping the toluene concentration constant in blanks, standards and samples.

Synthetic hydroformulation solutions in toluene were tested, where Ru concentrations were 60–200 μg/ml and where 1-hexene and 1-heptanol were present in concentrations of 7.6–6.8% and 1.6–2.4%, respectively. These solutions were diluted with a threefold amount of ethanol and analysed by flame AAS, using standards with a matrix nearly identical to that of the samples. The concentrations of toluene, 1-hexene and 1-heptanol in standards were 22.0, 1.9 and 0.6%, respectively. The slight differences in hexene and heptanol concentrations did not affect the measurement and the results were very satisfactory (Table 4).

When the dilution was 25 times or more, the concentrations of other organic substances were less than 0.5% and did not affect the absorbances. Table 5 shows the dilutions of real hydroformulation solutions. At all three dilutions the concentration of toluene was 20%, as it was in the blanks and standards. The analytical results in Table 6 show that when the concentration of Ru in the original solution was low (sample 1),

Table 5
Preparation of hydroformulation sample dilutions

Dilution (times)	Total volume (ml)	Sample volume (ml)	Toluene in sample (ml)	Toluene added (ml)	Toluene total (%)
25	10	0.40	0.352	1.648	20
50	25	0.50	0.440	4.560	20
100	25	0.25	0.220	4.780	20

Table 6
Absolute Ru contents of 6.2 ml of hydroformulation solution and Ru concentrations in final dilutions and original hydroformulation solutions, calculated according to different dilutions

Sample (times)	Dilution	μg/ml in final dilution	μg/ml in original solution	mg Ru in 6.2 ml orig. sol.
	25	5.11	128	0.79
1	50	2.78	139	0.86
	100	0.84	84	0.52
	25	10.09	252	1.56
2	50	5.70	285	1.77
	100	2.32	232	1.44
	25	38.43	961	5.96
3	50	23.55	1178	7.30
	100	11.60	1160	7.19
	25	53.01	1325	8.22
4	50	36.26	1813	11.24
	100	17.75	1775	11.01
	25	43.08	1077	6.68
5	50	28.65	1433	8.88
	100	14.82	1482	9.19
	25	27.65	691	4.29
6	50	18.73	937	5.81
	100	8.32	832	5.16

the results were most reliable with lower dilutions. When the Ru concentration in the original solution was relatively high, the lowest dilution gave too low results, while the higher dilutions gave accurate results. Note that the usual volume of the solution in the hydroformulation experiments being carried out in this laboratory is 6.2 ml per reaction, and thus the last column in Table 6 presents the absolute amount of ruthenium in 6.2 ml of hydroformulation solution.

To determine the stability of the sample dilutions, we analysed the solutions after two and four hours. The absorbances of the samples were decreased about 20% in two hours and about 50% in four hours, while the absorbances of the standards were decreased by less than 10% in four hours. Evidently, to obtain reliable results one must prepare various dilutions and carry out the determinations immediately.

We tested the standard addition method as well, but found it unsatisfactory. The amounts of real samples available were small and the stability of samples at room temperature was poor. At the

same time, the present method requires prior information about the approximate ruthenium concentration.

4. Conclusions

No problems occur in the determination of ruthenium in pure organic solutions such as MIBK or ethanol, or when solutions and standards contain the same amounts of toluene. However, problems do arise when solutions and standards contain different amounts of toluene or the samples contain additional organic substances, since toluene and other organic substances affect the absorbances of solutions even when they are present in concentrations of only a few per cent. In these cases standards need to be prepared that are identical with the samples, or the samples need to be diluted. We prefer ethanol to MIBK as solvent when analysing organic solutions, for the following reasons: the sensitivity is better and the detection limit lower, the smell is less unpleasant, the burner and chamber assembly keep cleaner and the burner position is less critical.

Ethanol is also an excellent solvent when analysing hydroformulation solutions; and when samples are diluted with ethanol and toluene in a ratio of at least 1:10 the final solutions will contain not more than 1% total of 1-hexene, 2-hexene, heptanol and other organic substances. At such low concentration, at optimum burner height and acetylene flow, their effect on the absorbance will be insignificant. In the present case, dilutions as great as 1:25 or even 1:100 were appropriate, and the concentrations of organic substances, except toluene, were then less than 0.5%. In conclusion, when hydroformulation solutions are analysed using ethanol as solvent, standards prepared in ethanol with 20% of toluene will be suitable without the addition of other compounds. However, to avoid any decrease in the absorbance, the determination must be done immediately after dilution.

References

[1] H.A. Hamid, At. Spectrosc., 10 (1989) 16.
[2] M. Bressan, A. Morvillo and G. Romanello, J. Mol. Catal., 77 (1992) 283.
[3] W.P. Griffith, Chem. Soc. Rev., (1992) 179.
[4] M. Tanaka, T. Hayashi and Z.-Y. Mi, J. Mol. Catal., 81 (1993) 207.
[5] C. Crotti, S. Cenini, F. Ragaini and F. Porta, J. Mol. Catal., 72 (1992) 283.
[6] T. Venäläinen, T.A. Pakkanen, T.T. Pakkanen and E. Iiskola, J. Organometall. Chem., 314 (1992) C49.
[7] J.E. Allan, Spectrochim. Acta, 18 (1962) 259.
[8] B.D. Guerin, J. South Afr. Chem. Inst., 25 (1972) 230.
[9] J.L. Fabec and M.L. Ruschak, Anal. Chem., 55 (1983) 2241.
[10] D.C. Gregoire, J. Anal. At. Spectrom., 3 (1988) 309.
[11] J.G. Sen Gupta and D.C. Gregoire, Geostand. Newslett., 13 (1989) 197.
[12] J.G. Sen Gupta, Talanta, 36 (1989) 651.
[13] R.G. Megarrity and B.D. Siebert, Analyst, 102 (1977) 95.
[14] T.Y. Kometani and L.D. Blizer, Plating and Surface Finishing, 67 (1980) 57.
[15] W. Heinig and K. Mauersberger, Talanta, 32 (1985) 145.
[16] V.N. Pichykov and O.V. Rudnitskaya, J. Anal. Chem. USSR, 39 (1985) 250.
[17] H. Urbain and M. Cattenot, Analusis, 7 (1979) 196.
[18] R. Iwata and I. Ogata, Bull. Chem. Soc. Jpn., 47 (1974) 2611.
[19] W.B. Rowston and J.M. Ottaway, Anal. Lett., 3 (1970) 411.
[20] B. Montford and S.C. Cribbs, Anal. Chim. Acta, 53 (1971) 101.
[21] M.M.M. El-Defrawy, J. Posta and M.T. Beck, Anal. Chim. Acta, 102 (1978) 185.
[22] D.E. Harrington and W.Z. Bramsted, Talanta, 22 (1975) 411.
[23] J.M. Scarborough, Anal. Chem., 41 (1969) 250.
[24] J.L. Fabec, At. Spectrosc., 4 (1983) 46.
[25] K. Smolander, I. Mustonen, J. Pursiainen, T. Saari, T. Venäläinen and T.A. Pakkanen, Fresenius' Z. Anal. Chem., 329 (1987) 27.
[26] C.M. Young and J.M. Baldwin, Microchem. J., 23 (1978) 265.
[27] M. Aihara and M. Kiboku, Buseki Kagaku, 30 (1981) 390.
[28] G. Braca, R. Cioni, G. Sbrana and G. Scandiffio, At. Absorp. Newslett., 14 (1975) 39.
[29] A. Dornemann and H. Kleist, Fresenius' Z. Anal. Chem. 313 (1982) 319.

ELSEVIER

Analytica Chimica Acta 296 (1994) 205–211

ANALYTICA CHIMICA ACTA

On-line preconcentration and determination of trace platinum by flow-injection atomic absorption spectrometry

A. Cantarero, M.M. Gómez, C. Cámara, M.A. Palacios *

Departamento de Química Analítica, Facultad de Química, Universidad Complutense, Madrid 28040, Spain

Received 20th December 1993

Abstract

The analytical performance of a platinum preconcentration method using a 0.01 M HNO_3 carrier solution and an alumina microcolumn is discussed. On-line preconcentration is followed by flame atomic absorption spectrometry (FAAS), and off-line preconcentration by graphite furnace atomic absorption spectrometry (GFAAS). The preconcentration factors were 600 for FAAS (25 μl elution volume) and 30 for GFAAS (500 μl elution volume), both with a 15-ml sampling volume. The detection limits in these conditions were 0.02 mg l^{-1}, and relative standard deviation (R.S.D.) of 9% (0.1 mg l^{-1} solution, $n = 5$) for FAAS and 0.33 μg l^{-1}, and a R.S.D. of 7% (5 μg l^{-1} solution $n = 5$) for GFAAS. The proposed method is suitable for platinum determination in natural water samples.

Keywords: Atomic absorption spectrometry; Flow injection; Alumina; Microcolumns; Platinum; Preconcentration; Waters

1. Introduction

Platinum has gained enormously in importance as a result of technological developments in motor car catalytic converters, catalysts for the petrochemical, chemical and pharmaceutical industries, and anti-cancer therapy [1]. So far platinum compounds have had little impact on the environment because its industrial manipulation is performed in closed systems, effective filters are employed and the metal is usually recycled. Thus, the average natural concentration of platinum in the environment is around the ng kg^{-1} level [2]. However, localized platinum contamination in areas such as roadsides [2,3] has increased to μg kg^{-1} and even to mg kg^{-1} levels. Since platinum has a high toxicity (close to that of lead), and approximately 2 μg of Pt per km travelled is released into the environment from motor car catalytic converters [2], there is a need for methods to determine very low platinum concentrations in environmental samples in order to redress our poor knowledge of the biological effects of platinum and its compounds.

Some platinum compounds, such as cisplatin and carboplatin, are usually employed as anticancer drugs. The need to check the possible toxicity of these compounds and determine their effect on the human body has aroused considerable interest in developing fast analytical meth-

* Corresponding author.

SSDI 0003-2670(94)00211-4

ods for platinum quantification in different biological fluids at different stages of treatment [4,5].

Finally, there is a demand for rapid and sensitive methods for the determination of platinum, and precious metals in general, in natural waters owing to their potential use in geochemical prospecting, because of the possibility that streams in platinum-rich areas will be enriched in the element [6,7].

The determination of trace levels of platinum requires sensitive analytical techniques, such as graphite furnace atomic absorption spectrometry (GFAAS) [8], neutron activation analysis (NAA) [9] and inductively coupled plasma mass spectrometry (ICP-MS) [4]. A separation/preconcentration step is often required prior to determination in order to achieve the necessary detection limits and remove matrix interferences. The preconcentration/separation methods proposed include liquid–liquid extraction [10], preconcentration on silica gel Separon SGX C_{18} in the presence of cationic surfactants [11], preconcentration as the bis(carboxylmethyl)dithiocarbamate chelate on XAD-4 [3], preconcentration of the platinum pyrrolidinedithiocarbamate (Pt–PCDT) complex on C_{18}-bonded silica gel [12] and preconcentration on silica gel functionalized with aminopropyltriethoxysilane [13]. Most preconcentration methods are off-line and require considerable sample manipulation and long analysis times.

With the advent of flow-injection analysis (FIA) [14] there has been considerable interest in developing on-line sample preconcentration procedures for flame atomic absorption spectrometry (FAAS) in an attempt not only to enhance sensitivity but to decrease analysis time, McLeod et al. [15,16] have demonstrated the suitability of activated alumina microcolumns for on-line preconcentration-matrix removal by flow-injection inductively coupled plasma atomic emission spectrometry (FI-ICP-AES) of various cations (Cr^{3+}, Pb^{2+}, Cd^{2+}, Co^{2+}, Fe^{3+}, Mn^{2+}, Ni^{2+} and Zn^{2+}) and oxyanions (PO_4^{3-}, SO_4^{2-}, CrO_4^{2-} etc.), with high preconcentration factors, little sample manipulation and a high sample throughput.

In this work activated alumina microcolumns for on-line trace enrichment of Pt(IV) in its chlorocomplex ($PtCl_6^{2-}$) and final determination by FAAS or GFAAS were studied for application to environmental and clinical samples.

2. Experimental

2.1. Reagents and materials

Stock standard Pt(IV) solution (865 mg l^{-1}) was prepared by dissolving the metal in a minimum volume of aqua regia and evaporation just to dryness. The residue was treated with 5 ml of conc. HCl and 0.1 g of NaCl and the solution was again evaporated just to dryness. The residue was dissolved in 20 ml of (1 + 1) HCl and diluted to 1000 ml with deionized water. Working standard solutions of platinum were prepared daily by appropriate dilution of the stock standard Pt(IV) solution. Milli-Q water was used throughout for preparing sample solutions (stored in pre-cleaned polypropylene (Nalgene) containers). Nitric acid (0.01 M) and ammonia solution (2 M) were prepared from concentrated reagents (Merck, Aristar grade). Anion effects were studied in solutions of analytical-reagent grade products from Merck.

2.2. Preparation of activated alumina microcolumns

The activated alumina (Merck, Brockman Grade I, basic form, particle size 63–200 μm) was sieved, a particle size position of 160–200 μm was selected and a small amount (about 0.025 g) was packed evenly into a PTFE tube (7 cm × 1.5 mm i.d.).

2.3. Instrumentation and operating procedures

A Perkin-Elmer 3100 atomic absorption spectrometer with an air–acetylene flame (12–2 ml min^{-1}) and equipped with an impact bead was employed. A platinum hollow cathode lamp (λ = 265.9 nm) of 0.7 nm spectral band pass was used. An integration time of 20 s was used to evaluate transient signals. A 1100B Perkin-Elmer atomic absorption spectrometer with a deuterium lamp background-correction system and equipped with

a HGA 400 Perkin-Elmer furnace atomiser with a pyrolytic graphite tube was also employed.

2.4. Operating procedure for on-line platinum preconcentration and FI-FAAS determination

The FI manifold (Fig. 1), which consisted of a peristaltic pump, a rotatory injection valve and a microcolumn, was connected directly to the spectrometer via the nebulizer inlet tubing. Nitric acid (0.01 M) served as the carrier stream.

Sample solutions and standards were adjusted to about pH 2.5 by the addition of hydrochloric acid, pumped into the carrier stream and passed through the microcolumn at 3 ml min^{-1} for specified time periods for retention of platinum. The adsorbed platinum was eluted by injection into the carrier solution of 25 μl of 2 M ammonia solution at 1 ml min^{-1} and measured by FAAS. Two further injections of eluent were made to ensure complete removal of residual platinum and prevent sample cross-contamination. The carrier solution had to be pumped alone for 1 min to re-establish microcolumn acidity before commencing the next retention–elution cycle.

2.5. Operating procedure for platinum preconcentration and GFAAS determination

Carrier solution (0.01 M HNO_3) was pumped through the microcolumn at 3 ml min^{-1} for 2 min to activate the alumina. Sample solutions of about pH 2.5 were passed through the microcolumn at 3 ml min^{-1} for specified time periods for retention of platinum, and then the carrier solution was passed for 30 s to eliminate residual platinum adsorbed on the tubes. The platinum retained on the microcolumn was eluted into a small vial by pumping 0.5 ml of 2 M ammonia solution at 1 ml min^{-1}. The introduction of a bubble between the carrier and the ammonia solution allowed the platinum eluted from the microcolumns to be distinguished for collection. The carrier solution had to be pumped alone for 1 min to re-establish microcolumn acidity before commencing the next retention–elution cycle. Aliquots of eluted platinum (20 μl) were injected into the graphite furnace for analysis. Table 1 shows the graphite furnace temperature program used.

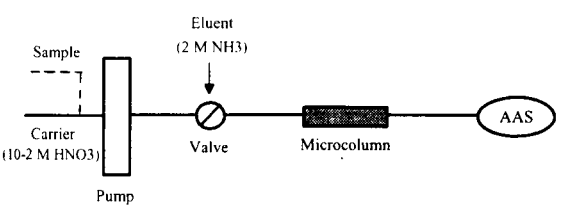

Fig. 1. Flow injection manifold for platinum preconcentration by FI-FAAS.

Table 1
Temperature program for the determination of platinum by GFAAS

Step	T(°C)	Ramp (s)	Hold (s)	Ar flow (ml min^{-1})
Dry	110	10	30	300
Mineralization	1300	10	30	300
Atomization	2500	0	3	stop flow
Clean	2600	1	2	300

3. Results and discussion

3.1. Preconcentration–elution parameters for alumina microcolumn

Activated alumina can function as either a cation or an anion preconcentrator depending on the pH [15]. Since the acidic form of alumina has a high affinity for a range of oxyanions and Pt(IV) occurs in natural waters predominantly as the chlorocomplex anion $PtCl_3^{2-}$, the on-line trace enrichment of platinum on activated alumina microcolumns is theoretically possible. FAAS has been used to study the suitability of an alumina microcolumn for platinum preconcentration at the low mg l^{-1} level.

Because of the low concentrations of platinum in natural waters, the suitability of alumina microcolumns for platinum preconcentration was checked at the low μg l^{-1} level. GFAAS detection was used because FAAS lacks sensitivity for platinum at the low μg l^{-1} level, and off-line preconcentration/elution was used because of

the non-flow-through nature of the graphite furnace atomizer.

The behaviour of the alumina microcolumn in quantitative preconcentration of Pt(IV) at the mg l^{-1} and $\mu g\ l^{-1}$ levels was studied using 1 mg l^{-1} and 7 $\mu g\ l^{-1}$ of Pt(IV) as $PtCl_6^{2-}$, respectively.

The acidity of the carrier stream, alkalinity of the eluant and sample pH were critical variables that were studied in order to maximise Pt(IV) recovery. The efficiency of the preconcentration/elution process was studied by comparing the peak areas of the signals for the analyte eluted from the microcolumn with that of the same analyte mass injected in the carrier stream flowing through an empty PTFE tube of the same dimensions as the alumina microcolumn.

Pt(IV) retention was quantitative for carrier streams within the 0.01–0.1 M HNO_3 range. However, the nitric acid concentration in the carrier affected the subsequent elution by the basic eluent. Satisfactory performance was achieved using a 0.01 M HNO_3 carrier. A relatively high concentration (2 M) of ammonia was required for efficient elution of Pt(IV) in one injection.

Sample pH was another critical factor in the retention process, as seen in Fig. 2. The best results were obtained at about pH 2, which is similar to the pH of the carrier solution. Thus, 10^{-2} M HNO_3 and 2 M NH_3 were chosen as the carrier and eluent, respectively, for sample solutions of platinum at pH 2.5.

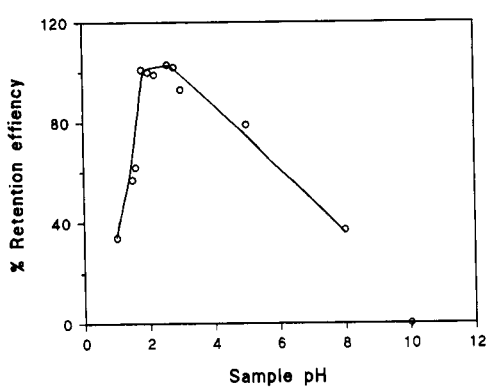

Fig. 2. Influence of sample pH on retention efficiency. Sample: 6 μg of Pt(IV).

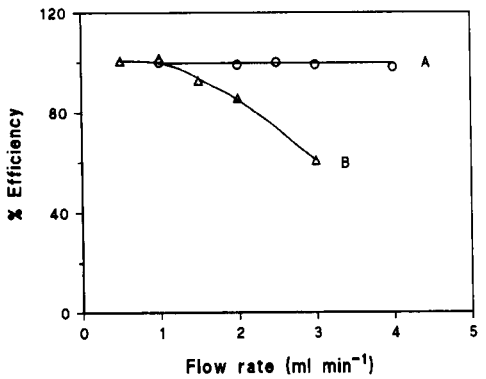

Fig. 3. Effect of reagents flow on preconcentration and elution: (A) retention using 0.01 M HNO_3 carrier, (B) elution with 2 M NH_3 eluent. Sample: 6 $\mu g\ l^{-1}$ Pt(IV).

The study of the effect of flow rate on sample retention and elution (Fig. 3) revealed that relatively high flow rates up to a maximum of 4 ml min^{-1} in the sampling mode could be used without impairment of retention efficiency. A preconcentration flow rate of 3 ml min^{-1} was chosen for subsequent work to avoid back-pressure problems in the FI manifold and leakage at joints. In contrast, the elution flow rate study done on 2 M NH_3 eluent showed that the maximum flow rate for complete removal of platinum was 1 ml min^{-1}. This behaviour is consistent with other studies [17] and indicates the importance of eluant contact time in the FI system.

Elution volume strongly affects the preconcentration factor, defined as the ratio of sample volume to elution volume. The elution efficiency for 6 μg of Pt(IV) was calculated using volumes in the 25–500 μl range. The results showed that for a small elution volume, such as 25 μl of 2 M NH_3, maximum efficiency was achieved, with constant peak areas for all elution volumes tested. However, peak height increased with decreasing elution volume, and the analytical peaks were narrower and more perfect for smaller elution volumes. Thus, a 25-μl elution volume was selected for subsequent work, requiring an integration time of 20 s.

Fig. 4a shows a typical peak given by the alumina preconcentration microcolumn system described in the experimental section, and Fig. 4b is a typical absorbance versus time response for

the same amount of platinum and the same system without a microcolumn. The relatively sharp transient signal (peak width at half-height = 6 s) in Fig. 4a is indicative of relatively rapid desorption, while, the corresponding peak without a microcolumn in Fig. 4b is much wider (peak width at half-height = 16 s).

3.2. Interferences

The possibility of interferences in samples due to competition between platinum and co-existing anions for available sites was examined at the high and low Pt levels. Table 2 shows that a high ionic strength medium (1000 mg l^{-1} chloride as NaCl) significantly decreases platinum retention, and that chloride concentrations as high as 5000 mg l^{-1} completely prevent platinum retention on the microcolumn. Bromide and iodide interfere more than chloride, but do not interfere at the concentrations of these anions normally found in natural waters. These findings suggest that the proposed method might be suitable for the trace enrichment of platinum at the low mg l^{-1} and μg l^{-1} levels in natural waters.

Table 2
Recovery of platinum in the presence of co-existing anions [a]

Spike	Concentration (mg l^{-1})	Pt recovery, % [b]	Pt recovery, % [c]
Cl^-	10	105±3	99±4
(as NaCl)	100	77±1	–
	200	–	105±8
	1000	69±3	–
	5000	7±2	–
Br^-	0.2	–	98±6
(as KBr)	0.5	–	89±7
	1	100±4	75±4
	10	77±5	–
I^-	0.5	99±3	103±7
(as KI)	1	76±1	62±8
F^-	10	102±3	107±6
(as NaF)			
PO_4^{3-}	20	–	103±4
(as NaH_2PO_4)	100	98±2	–
SO_4^{2-}	50	–	99+3
(as Na_2SO_4)	100	90±2	–
	200	–	50±8
	1000	16±4	–

[a] Mean ± S.D (n = 3).
[b] Preconcentrated platinum, 6 μg.
[c] Preconcentrated platinum, 42 ng.

3.3. Analytical performance

The breakthrough capacity of the alumina microcolumn under the working conditions was > 1.24 mg Pt(IV) per g of alumina. This high value suggested high performance by the microcolumn even in the presence of competing anions.

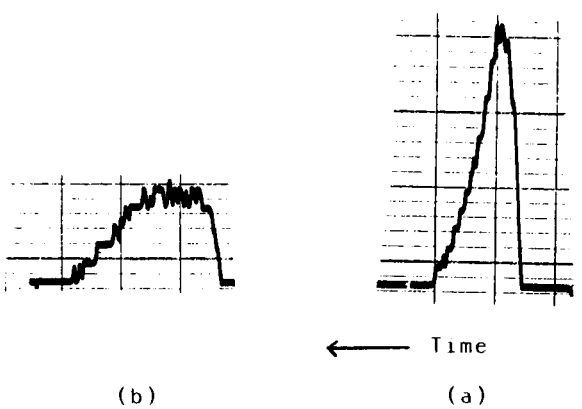

Fig. 4. Absorbance versus time responses for (a) preconcentration of 6 μg Pt(IV), 250 μl elution volume, (b) injection of 250 μl of Pt(IV) solution containing 6 μg Pt without microcolumn.

3.4. On-line FI-FAAS method

Standard solutions were processed (in triplicate) for 5 and 10 min at a sampling rate of 3 ml min^{-1} and the absorbance (as peak area) versus platinum concentration graphs were linear over the 0–5 mg l^{-1} range (Fig. 5a, and b). The signal obtained for 1 mg l^{-1} of Pt(IV) preconcentrated for various times up to 10 min also increased linearly with time (Fig. 5c). This linearity demonstrates the good preconcentration ability of the proposed FI-FAAS method. Preconcentration factors of 600 and 1200 for 5 and 10 min sampling times, respectively, make the method very promising for the low μg l^{-1} level. The relative standard deviation (R.S.D.) at the 100 μg l^{-1} and 5 mg l^{-1}

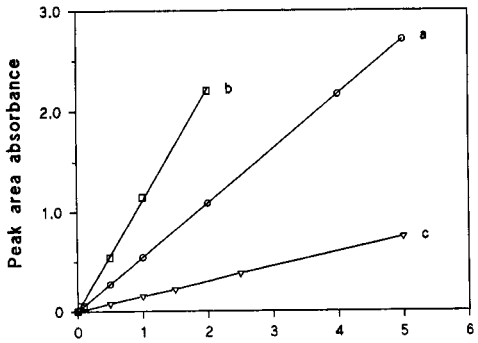

Fig. 5. Pt(IV) Calibration graphs for FI-FAAS: (a) 5 min preconcentration time, abscisa scale in mg l^{-1}; (b) 10 min preconcentration time, abscisa scale in mg l^{-1}; (c) 1 mg l^{-1} Pt(IV), preconcentrated, abscisa scale × 2 in (min).

levels and 5 min sampling time were 9% and 2% ($n = 5$), respectively. The limit of detection, defined as three times the S.D. of the blank (3σ) for 5 and 10 min sampling times was 20 and 10 μg l^{-1}, respectively.

The study of microcolumn reproducibility did not detect any significant differences between the five randomly chosen microcolumns tested. The alumina microcolumns could be used for at least six months with no deterioration in column performance. A sample throughput of nine samples per hour was achieved for a 5-min sampling time.

3.5. Off-line GFAAS method

Platinum standard solutions in the 0–15 μg l^{-1} range were preconcentrated for 5 min and eluted with 500 μl of 2 M NH_3. An eluate volume of 20 μl was injected into the graphite furnace. The calibration graph obtained was compared with those for unpreconcentrated standard platinum solutions; the results showed a preconcentration–elution efficiency close to 100%. This means that a real sample can be preconcentrated on the alumina microcolumn and its platinum concentration directly read from the 0.2% HNO_3 calibration graph, taking into account the relevant preconcentration factor without the need for standard addition. The R.S.D. at the 5 μg l^{-1} level and a 5 min sampling time was 9% ($n = 5$). The limit of detection (3σ) was 0.33 μg l^{-1} for a 5-min sampling time.

Table 3
Recovery of Pt(IV) spiked into tap water at the mg l^{-1} level

Pt spike (mg l^{-1})	Preconcentration		μg Pt_{total}	μg $Pt_{measured}$ [a]	% Recovery
	t (min)	Flow (ml/min)			
1	3	3	9	9.1 ± 0.9	101
1	5	3	15	14.5 ± 0.3	97
4	5	3	60	60.4 ± 1.4	101

[a] Mean ± S.D. ($n = 3$).

Table 4
Recovery of Pt(IV) spiked into tap water at the μg l^{-1} level

Sample	Preconcentration		Pt_{spike} (μg l^{-1})	$Pt_{measured}$ (μg l^{-1}) [a]	Recovery (%)
	t (min)	Flow (ml/min)			
M_1	5	3	7	6.9 ± 1.0	99
M_2	5	3	7	7.2 ± 1.5	103
M_1	5	3	15	14.8 ± 1.1	99
M_1	5	3	15	14.6 ± 1.2	97

[a] Mean ± S.D. ($n = 3$).

3.6. Natural water Pt(IV) recoveries by FI-FAAS and GFAAS

The suitability of the proposed method for natural water samples was checked by spiking tap water with 0.5 and 4 mg l^{-1} of platinum (as $PtCl_6^{2-}$) for on-line preconcentration and 7 and 15 μg l^{-1} for the off-line procedure. The results, given in Tables 3 and 4, show that the proposed method is suitable for the trace enrichment of platinum at the mg l^{-1} to μg l^{-1} level in natural waters.

4. Conclusions

The proposed flow-injection system incorporating activated alumina microcolumns enables effective on-line platinum preconcentration and final determination by FAAS. Sample volumes of 15 ml (5 min sampling time) resulted in an enrichment factor of about 600 and permitted the determination of platinum in natural waters at the sub-mg l^{-1} level. The application of the pro-

posed FI system to off-line platinum preconcentration and final determination by GFAAS permitted the determination of platinum in natural waters at the sub-μg l^{-1} level. The proposed preconcentration method is transferable to ICP-MS spectrometry and a companion paper will assess its suitability for the determination of platinum in natural waters at the ng l^{-1} level.

Acknowledgements

The authors wish to thank Max Gorman for revision of the manuscript, and the DGICYT for financial support (PB91-0376).

References

[1] H. Renner and C. Schmuckler, in E. Merian (Ed.), Metals and Their Compounds in the Environment, VCH. Weinheim, 1991, p. 1135.
[2] A.J. Martin, L. Martin, J. Orea and N. Soufi, Ing. Quim., 255 (1990) 183.
[3] M.L. Lee, G. Tölg, E. Beinrohr and P. Tschöpel, Anal. Chim. Acta, 272 (1993) 193.
[4] B. Casetta, M. Roncadin, G. Montanari and M. Furlanut, At. Spectrosc., 12 (1991) 81.
[5] S. Caroli, A. Alimonti, F. Petrucci, F. La Torre, C. Dominici and M.A. Castello, Ann. Ist. Super. Sanita, 25 (1989) 487.
[6] D. Vlassopoulos, S.A. Wood and A. Mucci, Abstracts of the Goldschmidt Conference, Geochemical Society Meeting, Baltimore, MD, May, 1988, p. 81.
[7] S.A. Wood and A. Mucci, Abstracts of the Goldschmidt Conference, Geochemical Society Meeting, Baltimore, MD, May, 1988, p. 83.
[8] J.E. Cantle (Ed.), Atomic Absorption Spectrometry, Elsevier, 1982, p. 366.
[9] C.H. Wang, D.L. Willis and W.D. Loveland, Radiotracer Methodology in the Biological, Environmental and Physical Sciences, Prentice-Hall, Englewood Cliffs, NJ, 1975.
[10] S.A. Wood, D. Vlassopoulas and A. Mucci, Anal. Chim. Acta, 229 (1990) 227.
[11] V. Otruba, M. Strnadova and B. Skalnikova, Talanta, 40 (1993) 221.
[12] N.K. Shah and C.M. Wai, J. Radioanal. Nucl. Chem., 130 (1989) 451.
[13] A. Tong, Y. Akama and S. Tanaka, Anal. Chim. Acta, 230 (1990) 179.
[14] J. Ruzicka and E.H. Hansen, Flow Injection Analysis. Wiley-Interscience, New York, 2nd edn., 1981.
[15] C.W. McLeod, Y. Zhang, I. Cook, A. Cox, A.R. Date and Y.Y. Cheung, J. Res. National Bureau of Standards, 93 (1988) 462.
[16] C.W. McLeod and J. Wei, Spectrosc. World, 2 (1990) 32.
[17] M.M. Gomez and C.W. McLeod, J. Anal. At. Spectrom., 8 (1993) 461.

ELSEVIER

Analytica Chimica Acta 296 (1994) 213–218

ANALYTICA CHIMICA ACTA

Direct determination of aluminium in biological materials by electrothermal vaporization–inductively coupled plasma atomic emission spectrometry with polytetrafluoroethylene as chemical modifier

Hu Bin, Jiang Zucheng *, Zeng Yun'e

Department of Chemistry, Wuhan University, 430072, Wuhan, China

Received 12th October 1993; revised manuscript received 28th March 1994

Abstract

A method for the determination of aluminium in biological materials with electrothermal vaporization and inductively coupled plasma atomic emission spectrometry is described, in which polytetrafluoroethylene (PTFE) is used as chemical modifier to improve the vaporization of aluminium. The absolute detection limit of aluminium is 5.0 pg and the R.S.D. is 2.2% at an aluminium concentration of 0.2 μg ml^{-1} ($n = 9$). The reliability of the entire procedure was confirmed by analyses performed on three standard reference biological materials.

Keywords: Atomic emission spectrometry; Inductively coupled plasma; Aluminium; Biological materials

1. Introduction

It is well established that aluminium plays an important role in the pathogenesis of a number of clinical disorders that can develop in patients with chronic renal failure undergoing long-term dialysis. Aluminium is believed to be a possible pathogenic factor in Alzheimer's dementia [1]. Consequently, the determination of aluminium in biological materials has attracted considerable interest. Unfortunately, reliable results for the determination of Al in biological samples are difficult to obtain and improvements in analytical performance are imperative. Approaches to trace aluminium determinations in biological materials include neutron activation analysis [2], atomic emission spectrometry (AES) [3–5] and atomic absorption spectrometry [6,7].

Success has been achieved using graphite furnace atomic absorption spectrometry (GFAAS), especially at low aluminium levels, because GFAAS is one of the most cost-effective, sensitive technique, available. In addition, GFAAS can also be used for the direct analysis of solid samples. Recently, approaches to solid sampling for the direct determination of aluminium in biological materials have been described. The results reported by Frech and Baxter [8] using both atomic emission and absorption measurements

* Corresponding author.

SSDI 0003-2670(94)00159-J

with an ideal but not commercially available constant-temperature furnace show very good agreement for analyses of sample materials as solids and after dissolution. Nordahl et al. [7] determined aluminium in human biopsy and necropsy specimens by direct solid-sampling cup-in-tube GFAAS. Although there are many advantages of solid sampling over conventional sample decomposition procedures (acid digestion or fusion), such as a shorter sample preparation time, decreased analyte loss, lower sample contamination and increased sensitivity, some obvious drawbacks still exist. There are errors that can arise during the weighing of the solid sample; the transfer operation and the sample introduction.

The slurry sample-introduction technique can overcome problems associated with direct solid sampling mentioned above, as it combines the advantages of both liquid and solid sampling and permits sample introduction using micropipettes and autosamplers which are routinely used in liquid sampling. Another advantageous feature of slurry introduction is that the same atomizers that are used for liquid sampling can be successfully used for atomization of slurries. Recent developments in direct solid sample analysis by GFAAS have been reviewed by Miller-Ihli [9] and Bendicho and de Loos-Vollebregt [10].

By combining the benefits of the increased sensitivity and microsampling ability of GFAAS with the simultaneous multi-element capability and ease of operation of the inductively coupled plasma (ICP), Baxter *et al.* [3] and Sanz-Medel *et al.* [4] determined traces of aluminium in biological fluids. Compared with conventional pneumatic nebulization ICP-AES, the detection limit could be lowered to 5.0 ng ml^{-1}. Long and Snook [11] also developed a slurry sampling electrothermal vaporization (ETV)–ICP-AES method for the direct determination of the major element composition of multimineral, multivitamin capsules, the analytical results were in good agreement with those of the pneumatic nebulization ICP-AES method.

Here, we report on studies to determine aluminium directly in biological materials by slurry sampling ETV–ICP–AES using a polytetrafluoroethylene (PTFE) slurry as chemical modifier.

2. Experimental

2.1. Instrumentation

The ICP source system and the graphite furnace sample introduction device used in this study were identical with those reported previously [12]. A commercial 27 ± 3 MHz argon ICP source (Beijing Broadcast Instrument Factory, Beijing) with a 2-kW plasma generator was interfaced to a WDG 500-1A monochromator (Beijing Second Optics, Beijing). The output of the photomultiplier (R456, Hamamatsu) was amplified and registered on a strip-chart recorder (L23-104, Sichuan Fourth Meters, Sichuan).

A WF-1 heating device with a matching graphite furnace (Beijing Second Optics) was used as the electrothermal vaporization unit. The instrumental operating conditions and wavelength used are given in Table 1.

2.2. Standard solution and reagents

A stock standard solution of Al with a concentration of 1 mg ml^{-1} was prepared by dissolving 0.1000 g of high-purity aluminium from which the surface oxides had just been removed in dilute hydrochloric acid with heating. After cooling, the resulting solution was diluted to 100 ml. A 60% (w/v) PTFE slurry (viscosity 7×10^{-3}–15×10^{-3} Pa s) was purchased from Shanghai Insti-

Table 1
ETV–ICP-AES operating conditions

ICP-AES:			
Incident power	1.0 kW		
Carrier gas (Ar) flow-rate	0.5 l min^{-1}		
Coolant gas (Ar) flow-rate	15 l min^{-1}		
Auxiliary gas (Ar) flow-rate	0.8 l min^{-1}		
Observation height	12 mm		
Al emission line	309.27 nm		
ETV settings:	Dry	Ash	Vaporize
Temperature (°C)	100	1200	2240
Ramp time (s)	15	25	0
Hold time (s)	25	15	3
Injection volume	10 μl		
PTFE concentration	6% (w/v)		

tute of Organic Chemistry. Except for Na_2SiO_3 (analytical-reagent grade, Shanghai Reagent Factory), the other reagents (NaCl, KCl, $CaCO_3$, MgO, CuO, Fe_2O_3 and ZnO) were all of Specpure grade. Hydrochloric acid and nitric acid were of Suprapur grade. Doubly distilled, deionized water was used throughout.

2.3. Contamination control

Aluminium is a ubiquitous element, and therefore biological samples with low concentrations of aluminium are easily contaminated. In order to avoid this problem, a strictly operational procedure was followed, similar to those suggested by other workers [13–15]. Distilled, deionized water was used throughout, all containers were soaked in 5% HNO_3 for at least 48 h before rinsing throughly with a large amount of distilled, deionized water and all containers were tested for blanket aluminium levels.

2.4. Preparation of slurry samples

Serum samples

Human serum samples were stored in polyethylene bottles until used. Four different amounts of Al with 12% (w/v) PTFE were prepared by pipetting 0, 20, 60 and 200 μl of 1 μg ml^{-1} Al standard solution together with 0.2 ml of 60% PTFE into four solutions of 1% (v/v) Triton X-100 in 0.1% (v/v) nitric acid and diluting to 1 ml. Four aliquot serum samples (0.2 μl) were diluted with the above slurries in a ratio of 1 : 1. The resulting slurries contained 0, 10, 30 and 100 ng ml^{-1} of Al in the presence 6% PTFE, respectively.

NIST SRM 1577a bovine liver

A 0.5000 g portion of lyophilized sample was weighed and carbonized in a quartz crucible at low temperature until no further smoke appeared and then ashed at 550°C in a muffle furnace for 1 h. The ash was transferred quantitatively into a PTFE bottle and 2 ml of 6% (w/v) PTFE slurry were added. The suspension was homogenized with an ultrasonic processor for 30 min.

BCR No. 278 mussel tissue

A 0.5000 g of sample was weighed and pretreated according to the method described above. The ash was dispersed in 2.0 ml of distilled-deionized water with an ultrasonic processor for 40 min. A 0.4 ml volume of the suspension mentioned above was taken and 0.2 ml of 60% PTFE slurry added, then diluted to 2.0 ml. The suspension was dispersed with an ultrasonic processor for 30 min, after which the bottles were shaken vigorously prior to sampling. For standardation by the standard additions technique, the slurries were spiked with aqueous standard solutions.

2.5. Recommended procedure

After ignition and stabilization of the plasma, 10 μl of sample were pipetted manually into the graphite furnace with a microsyringe. The graphite furnace was sealed with a graphite cylinder before the graphite furnace heating cycle was started. The desolvated, vaporized sample was carried into the plasma by the argon carrier gas. Under the selected conditions the relative emission intensity of aluminium was recorded by the strip-chart recorder. The calibration graph was constructed using peak-height measurements.

3. Results and discussion

3.1. Optimization of the ICP discharge parameters

The ICP discharge parameters were established using a standard slurry of 0.2 μg ml^{-1} of Al containing 6% PTFE, and the signal-to-background ratios were used. The results are given in Table 1.

3.2. Study of ashing and vaporization parameters

The drying temperature and hold time were selected by observing directly the vaporization of the slurry sample on to the wall of the tube; the process has to be smooth enough to avoid sputtering of the liquid. A drying temperature of 100°C and the desolvation time of 40 s were used.

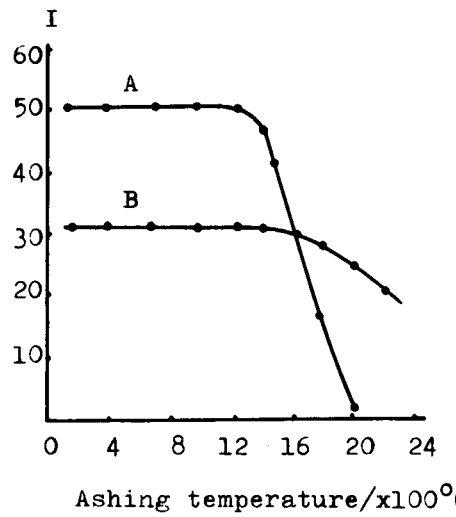

Fig. 1. Dependence of Al emission signal on ashing temperature for (A) 10 μl of 0.2 μg ml^{-1} Al standard solution containing 6% PTFE and (B) 10 μl of 1 μg ml^{-1} Al standard solution without PTFE.

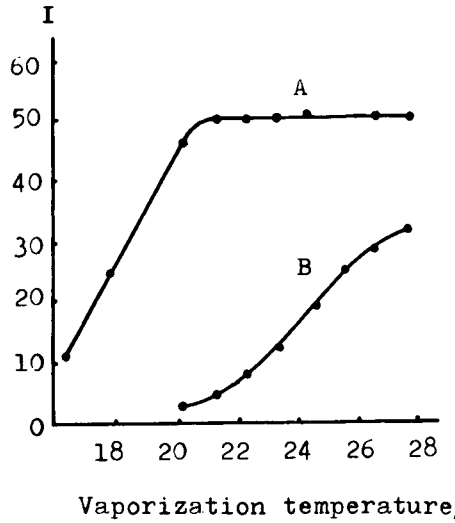

Fig. 2. Dependence of Al emission signal on vaporization temperature for (A) 10 μl of 0.2 μg ml^{-1} Al standard solution containing 6% PTFE and (B) 10 μl of 1 μg ml^{-1} Al solution without PTFE.

In order to optimize the ashing and vaporization temperature, ashing and vaporization curves were constructed for a 0.2 μg ml^{-1} standard slurry of Al containing 6% PTFE, and the results are shown in Figs. 1 and 2. When PTFE was present decreases in the Al analytical signal occurred at ca. 1200°C, whereas without PTFE decreases were found at ca. 1600°C. This indicates that on addition of PTFE, Al reacted with it in the graphite furnace and vaporized in the form of AlF_3 (b.p. 1291°C). The optimum ashing temperature was 1200°C. It is obvious from Fig. 2 that the presence of PTFE greatly affected the vaporization behaviour of Al and the vaporization curve reached a constant value at ca. 2200°C. This meant that the fluorination reaction between Al and PTFE was complete. In contrast, without PTFE, no constant level was found in the temperature range tested. In subsequent experiments, a vaporization temperature of 2240°C was chosen.

3.3. Choice of PTFE concentration

Fig. 3 demonstrates the dependence of the Al emission intensity on the concentration of PTFE. The Al emission intensity increased with increase in PTFE concentration up to 5% (w/v). The maximum emission intensity achieved with this concentration remained constant up to the highest amount studied (10%), but the stability of the plasma discharge decreased owing to vigorous decomposition of PTFE. Considering that some

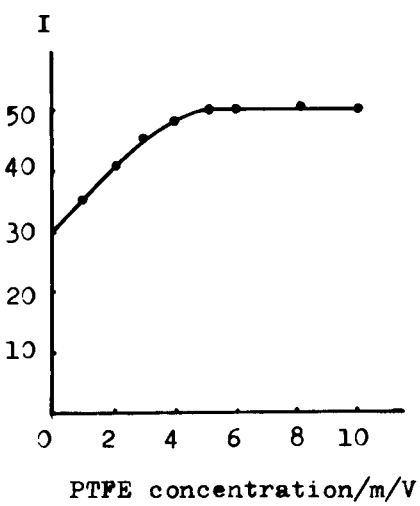

Fig. 3. Dependence of Al emission signal on PTFE concentration for 10 μl of 0.2 μg ml^{-1} Al solution.

PTFE was consumed by coexisting elements in real sample analysis, the PTFE concentration was selected as 6%.

3.4. Effects of matrix elements on determination of Al

The influence of the matrix on the determination of Al was investigated. The interfering elements studied were Ca, Cu, Fe, K, Mg, Na, Si and Zn with an Al concentration of 0.2 μg ml^{-1}. It was found that by using PTFE as a chemical modifier, amounts of Ca, Fe, K, Na and Zn up to 5 mg ml^{-1} and Cu up to 2 mg ml^{-1} did not affect the determination of Al. Magnesium did not interfere with the determination of Al at concentrations below 3 mg ml^{-1}. However, with large amounts of Mg the emission intensity of Al was considerably enhanced. This was due to the Mg 309.3-nm spectral interference caused by evaporation of Mg. When the Si concentration was higher than 1 mg ml^{-1}, the Al signal decreased significantly because a large amount of Si reacted with PTFE and inhibited the vaporization of Al.

3.5. Analytical figures of merit

According to the recommendations of the American Chemical Society Committee of Environmental Improvement, the detection limit, the lowest concentration level that can be determined to be statistically different from a blank, is defined as three times the within-batch standard deviation of a single blank determination, corresponding to a 99% confidence level. Using a PTFE slurry as chemical modifier, the detection limit for Al determined by ETV–ICP-AES was 0.5 ng ml^{-1}, whereas without PTFE the detection limit was 6 ng ml^{-1}. The detection limit was improved twelvefold with the use of PTFE as chemical modifier. The relative standard deviation (R.S.D.) of this method, obtained for nine replicate determinations at a concentration of 0.2 μg ml^{-1}, was 2.2%. Fig. 4 shows the calibration graph for the determination of Al by ETV–ICP-AES with the use of PTFE as chemical modifier. The graph is linear over a concentration range of three orders of magnitude.

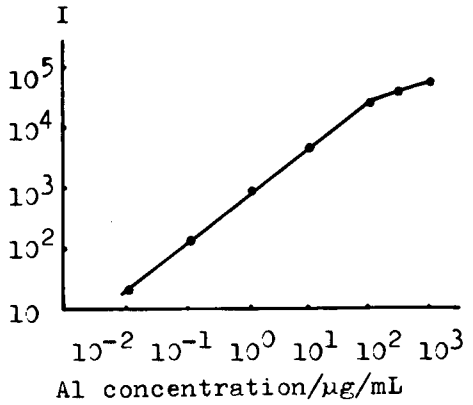

Fig. 4. Calibration graph for Al with PTFE as chemical modifier.

3.6. Determination of aluminium in biological materials

The proposed method was applied to various types of biological materials for the determination of Al. The results obtained using the standard additions procedure are given in Table 2.

Table 2
Results for the determination of Al by ETV–ICP-AES with PTFE as chemical modifier

Sample	Determined value	Indicative value	Literature value
Human serum (ng ml^{-1}) [a] S 8741 [a]	20.0 ± 1.0	20.0	–
Standard serum (ng ml^{-1})	29.0 ± 1.6	30.0	–
NIST SRM 1577a bovine liver (μg g^{-1})	0.86 ± 0.10	2.0	1.0 [8], 1.2 [7], 0.6 [16]
BCR No. 278 mussel tissue (μg g^{-1})	63.2 ± 3.9	68.5, 71.9	–

[a] Both samples and the indicative values were supplied by Hubei Medical College.

The agreement with the reference values was satisfactory.

Acknowledgements

This work was supported by the National Natural Science Foundation and the Education Commission Foundation of China.

References

[1] A.S. Prasad (Ed.), Essential and Toxic Trace Elements in Human Health and Disease, Alan R. Liss, New York, 1988, p. 645.
[2] J. Versieck and R. Cornelis, Anal. Chim. Acta, 116 (1980) 217.
[3] D.C. Baxter, W. Frech and E. Lundberg, Analyst, 110 (1985) 475.
[4] A. Sanz-Medel, R. Rodriguez Roza, R.G. Alonso, A.N. Vallina and J. Cannata, J. Anal. At. Spectrom., 2 (1987) 177.
[5] M.R. Pereiro Garcia, A. Lopez Garcia, M.E. Diaz Garcia and A. Sanz-Medel, J. Anal. At. Spectrom., 5 (1990) 15.
[6] E.A. Nater, R.G. Burau and M. Akeson, Anal. Chim. Acta, 225 (1989) 233.
[7] K. Nordahl, B. Radziuk, Y. Thomassen and R. Weberg, Fresenius' J. Anal. Chem., 337 (1990) 310.
[8] W. Frech and D.C. Baxter, Fresenius' Z. Anal. Chem., 328 (1987) 400.
[9] N.J. Miller-Ihli, Anal. Chem., 64 (1992) 964A.
[10] C. Bendicho and M.T.C. de Loos-Vollebregt, J. Anal. At. Spectrom., 6 (1991) 353.
[11] S.E. Long and R.D. Snook, At. Spectrosc., 3 (1982) 171.
[12] Hu Bin, Jiang Zucheng and Zeng Yun'e, Fresenius' J. Anal. Chem., 340 (1991) 435.
[13] N.J. Miller-Ihli, Spectrochim. Acta, Part B, 44 (1989) 1221.
[14] D.C. Manning and W. Slavin, Appl. Spectrosc., 37 (1983) 1.
[15] D.C. Manning, W. Slavin and G.R. Carnrick, Spectrochim. Acta, Part B, 37 (1982) 331.
[16] J.-P. Schmit, M. Youla and Y. Gelinas, Anal. Chim. Acta, 249 (1991) 495.

ELSEVIER

Analytica Chimica Acta 296 (1994) 219–222

ANALYTICA CHIMICA ACTA

Book Reviews

Alan G. Howard and P.J. Statham, *Inorganic Trace Analysis: Philosophy and Practice*, Wiley, Chichester, 1993 (ISBN 0 471 94144 1). xii + 182 pp. Price £89.95.

Information on inorganic ultra-trace analysis and how to solve the different problems and difficulties which arise when the concentration of the analytes decreases are very rare. In addition they are scattered in the literature and therefore very difficult to find. This book is a very valuable contribution to overcome the severe lack of comprehensive literature and reviews on this topic.

The book concentrates on inorganic trace and ultra-trace analysis for metals and describes the thinking approach to this science, its principles, the philosophy and general strategy, handling techniques, problems and possibilities. It does not provide detailed procedures or specific details of trace analytical techniques. The emphasis in each of the 8 chapters (chapter headings: Introduction, Working Environment, Laboratory Materials, Storage, Reagents, Water Supply, Working Practices, Trouble Shooting) is on the description of the problems and errors inherent in the different sections and steps of an analytical procedure. The huge concentration of information can only be summarized by listing some of the most important key words such as hazards, gains and losses in sampling, sample pretreatment, storage, dissolution and decomposition, separation, preconcentration and determination; sources of contamination, sorption, adsorption and volatilization; materials, tools, handling, cleaning and purification.

The subjects are thoroughly treated, clearly described and illustrated by many examples. Fundamental remarks are highlighted in special text boxes. The presentation of the book is excellent with very clear and well chosen illustrations. Somewhat disappointing is only the fact that the references at the end of each chapter are very limited and in some cases not very well chosen.

This book offers a very valuable reference for all scientists involved in trace and ultra-trace analysis and will be very useful for those readers who are coming to the subject for the first time, wanting a good, broad, up-to-date coverage of this topic.

P. Tschöpel

R.F.M. Herber and M. Stoeppler, *Trace Element Analysis in Biological Specimens* (Techniques and Instrumentation in Analytical Chemistry, Vol. 15), Elsevier, Amsterdam, 1994 (ISBN 0-444-89867-0). xiii + 576 pp. Price Dfl. 475.00/US$271.50.

The determination of trace elements in human organs, tissues and fluids is an essential means of studying the chemical and biological interactions of these elements. This is of direct importance for clinical and toxicological studies, with implications for the environment and epidemiology. This book describes, in individual chapters, the techniques that find most use for trace element determinations in biological samples, viz. flame AAS and furnace AAS, AES, voltammetry, neutron activation analysis and isotope dilution MS. However, the emphasis has shifted from simply high sensitivity to the importance of the reliability of the analytical results. To this end, there are chapters on sampling, sample storage and treatment, inter- and intralaboratory surveys, reference methods and materials, and statistics

SSDI 0003-2670(94)00307-6

and data evaluation. There is also a useful chapter on chemical speciation.

The second part of the book deals with the elements in alphabetical order; Al, As, Cd, Cr, Cu, Pb, Mn, Hg, Ni, Se, Tl, V and Zn. There is a subject index, and each chapter has an extensive bibliography. All the chapters are written by celebrated practitioners. The overall text thus provides an authoritative and comprehensive account of reliable trace element analysis in (of?) biological specimens, and should be available to all workers in the field. The only minor complaint is that Chapter 8 is consistently referred to as Chapter 7 in the running head.

Alan Townshend

Fabrizio Bruner, *Gas Chromatographic Environmental Analysis*, VCH, New York, 1993 (ISBN 1-56081-011-4). xii + 233 pp. Price DM 98.00/£40.00.

The growing interest in environmental analysis has seen a significant increase in the number of generalist and specialist textbooks on the subject. This monograph is aimed particularly at graduate students who wish to study environmental analysis and chemists and technicians who need to be aware of the scientific basis for official analytical methods.

The preface states the authors opinion that gas chromatography is still the most widely used technique for environmental analysis and the best way to introduce analysts to the particular way of thinking required to solve environmental analytical problems. The contents are therefore primarily devoted to gas chromatographic instrumentation (including GC–MS) but there are "flashes" of liquid chromatographic (LC) instrumentation and applications.

The first half of the book is devoted to an overview of basic chromatographic theory and gas chromatography and mass spectrometry instrumentation. It is clearly presented, with good diagrams, but much of this information is available in general analytical textbooks. One is left with the impression that the author would have liked to include more on LC but was constrained by the title.

From a practitioner's point of view the second half of the book contains more directly relevant information, with chapters on the analysis of volatile air and water pollutants and simple preparation and analysis of organic micropollutants from complex matrices. The latter is such an important aspect of the overall procedure that it could have been expanded to include topics such as supercritical fluid extraction, coupling of LC and GC and the handling of photosensitive compounds. Nonetheless issues such as contamination from solvents, solid and liquid phase extraction from complex environmental matrices, preconcentration and procedures for selected classes of compounds, e.g., chlorofluorocarbons, are covered in some detail.

This book contains some useful coverage of environmental analysis by gas chromatography and is well written, but the overall impression is that it falls between the details expected from the title and the desire to appeal to a more general graduate student readership.

Paul J. Worsfold

Jaroslava Turková, *Bioaffinity Chromatography*, Second, completely revised edition, Journal of Chromatography Library, Vol. 55, Elsevier, Amsterdam, 1993 (ISBN 0-444-89030-0). xvii + 800 pp. Price Dfl. 495.00/US$282.75.

After the publication of the first edition of the book *Affinity Chromatography* in 1978 the interest in separation methods such as affinity chromatography suitable for the isolation of specific bioactive compounds from very complicated biorganic matrices has increased enormously. In the last fifteen years many new techniques have appeared and the refinement of the existing methods has been continuous. *Bioaffinity Chromatography* is a worthy successor to its forerunner, *Affinity Chromatography*, which has been regarded by both beginner and experienced chromatographers as a highly comprehensive work. The present book is entirely devoted to techniques used in this special field consisting of 15 chapters that cover both theory and practice. Most of the techniques and theoretical aspects are well enumerated and are compiled with adequate references at the end of each chapter. Many examples are given of how affinity chromatography can be used in health sciences and in biotechnological industry. In view of the fact that many modern laboratories use highly automated chromatographs some more reference to

the instrumentation, automated sample handling and data evaluation could have been included.

In conclusion, this book is very useful with information that will be valuable to any scientist initiating work in the area of affinity chromatography and as a reference book for more experienced research workers.

Tibor Cserháti

Trends in Analytical Chemistry (TrAC), Reference Edition, Vol. 12, Elsevier, Amsterdam, 1993 (ISBN 0-444-81805-7). viii + 601 pp. Price Dfl. 675.00/US$387.75.

As always, the Reference Edition of TrAC is bursting with up to date accounts of recent advances in analytical science, including the "computer corner" articles, as published in the monthly edition of TrAC. Articles on capillary electrophoresis and chiral analysis are accompanied by determination of rare earths in rocks, and of mycotoxins in foods, and single cell analysis by glow discharge mass spectrometry. This year, the volume is made considerably larger by the inclusion of the "Directory of Capillary Electrophoresis" (CE), which comprises full details of > 200 scientists who have published in this field (77 pp.), a geographical index of these authors, an index of 18 companies manufacturing CE equipment, and an index of authors listed by techniques and areas of applications.

D. Stevenson and I.D. Wilson (Eds.), *Sample Preparation for Biomedical and Environmental Analysis*, Plenum, New York, 1994 (ISBN 0-306-44663-4). x + 246 pp. Price US$75.00.

Sample preparation is one of the key areas of the analytical process; improper or inappropriate sample preparation will make subsequent analytical measurements difficult or invalid. Yet it is a subject that does not receive its due attention from researchers and funding bodies. It is particularly gratifying, therefore, that a symposium was dedicated to this subject in 1991, and that papers presented at the symposium have been made available to a wider audience in this book, albeit three years later. There are 24 papers covering several topics, especially solid phase extraction, on-line and automated sample treatment and supercritical fluid extraction. Many well-known authors are included (e.g., Brinkman, R.M. Smith, I.D. Wilson, Novotny). The presentation of all articles is in a uniform style and format. There is a subject index, a compound index, and a list of authors.

David H. Russel (Ed.), *Experimental Mass Spectrometry*, Plenum, New York, 1994 (ISBN 0–306-44457-7). xiii + 311 pp. Price US$79.50.

This is the first of a series of volumes intended to describe the extensive developments in mass spectrometry (MS) that have taken place in the 1980s and 1990s. The present volume is "a guide for the non specialist", comprising 8 chapters, written by 21 authors, all but one (Gaümann, who has written on multiple pulses and dimensions in FT Ion cyclotron resonance (ICR) MS) from the USA. The subjects covered include the fragmentation of $(M - H)^-$ ions, alkali adducts, colission-induced dissociations, experimental FTICRMS, protein structure elucidation by time-of-flight MS, liquid chromatography/FAB and electrospray ionisation MS, and tandem MS of large biomolecules. Volume 2 will be devoted entirely to matrix-assisted laser desorption ionisation of biomolecules.

S. Görög (Ed.), *Advances in Steroid Analysis '93, Proceedings of the 5th Symposium on the Analysis of Steroids*, Akadémia Kiadó, Budapest (ISBN 963-05-6721-0). xiii + 623 pp. Price US$85.00.

As with the previous triennial symposia in the series, the last being at Pécs in 1990, this volume presents, in camera ready format, 65 of the papers presented at the Szombathely Conference, May 3–5, 1993. They are classified under receptor binding studies (9 papers), immunoassays (13), chromatography (10), spectroscopy (3), biosynthesis and metabolism (8), clinical studies (13), environment steroids and cancer (7) and miscellaneous (2). There is a subject index.

George Socrates, *Infrared Characteristic Group Frequencies. Tables and Charts*, 2nd edn., Wiley,

Chichester, 1994 (ISBN 0-471-94230-8). xii + 249 pp. Price £60.00.

In this new edition of the original 1980 text, there has been appreciable inclusion of new data, particularly in the "Inorganic Compounds and Coordination Complexes" chapter. A section on spurious bands has also been included. The result is a text full of tables and charts which are readily accessible, and will be welcomed by all scientists who need to interpret infrared spectra.

Send your article on floppy disk!

All articles may now be submitted on computer disk, with the eventual aim of reducing production times and improving the reliability of proofs still further. Please follow the guidelines below.

With revision, your disk plus one final, printed and exactly matching version (as a printout) should be submitted together to the editor. **It is important that the file on disk to be processed and the printout are identical.** Both will then be forwarded by the editor to Elsevier.

The accepted article will be regarded as final and the files will be processed as such. Proofs are for checking typesetting/editing: only printer's errors may be corrected. No changes in, or additions to the edited manuscript will be accepted.

Illustrations should be provided in the usual manner and, if possible, on a **separate** floppy disk as well.

Please follow the general instructions on style/arrangement and, in particular, the reference style of this journal as given in the "Guide for Authors".

The preferred storage medium is a 5¼ or 3½ inch disk in MS-DOS or Macintosh format, although other systems are also welcome.

Please label the disk with your name, the software & hardware used and the name of the file to be processed.

For further information on the preparation of compuscripts please contact:

Elsevier Science B.V.
Analytica Chimica Acta
P.O. Box 330
1000 AH Amsterdam, The Netherlands
Phone: (+31-20) 5862 791 Fax: (+31-20) 5862459

ELSEVIER SCIENCE

Analytical Applications of Circular Dichroism

Edited by **N. Purdie** and **H.G. Brittain**

Techniques and Instrumentation in Analytical Chemistry Volume 14

Circular dichroism is a special technique which provides unique information on dissymmetric molecules. Such compounds are becoming increasingly important in a wide variety of fields, such as natural products chemistry, pharmaceutics, molecular biology, etc. The content of this book has been selected in order to feature the unique aspects of circular dichroism, and how these strengths can be of assistance to workers in the field.

Substantial discussions have been provided regarding the particular phenomena associated with dissymmetric compounds which give rise to the circular dichroism effect. Reviews are also given of the type of instrumentation available for the measurement of these effects. A number of chapters cover the wide range of applications illustrating the power of the method.

Owing to its broad appeal, the book will be of interest to workers in all areas of chemistry and pharmaceutical science.

Contents:

© 1994 360 pages Hardbound
Price: Dfl. 355.00 (US $ 202.75)
ISBN 0-444-89508-6

ORDER INFORMATION

For USA and Canada
ELSEVIER SCIENCE INC.
P.O. Box 945
Madison Square Station
New York, NY 10160-0757
Fax: (212) 633 3880

In all other countries
ELSEVIER SCIENCE B.V.
P.O. Box 330
1000 AH Amsterdam
The Netherlands
Fax: (+31-20) 5862 845

US$ prices are valid only for the USA & Canada and are subject to exchange rate fluctuations; in all other countries the Dutch guilder price (Dfl.) is definitive. Customers in the European Community should add the appropriate VAT rate applicable in their country to the price(s). Books are sent postfree if prepaid.

ELSEVIER SCIENCE B.V.

PUBLICATION SCHEDULE FOR 1994

	J	F	M	A	M	J	J	A	S	O	N	D
Anal. Chim. Acta	284/3 285/1–2 285/3	286/1 286/2 286/3	287/1–2 287/3 288/1–2	288/3 289/1 289/2	289/3 290/1–2 290/3	291/1–2 291/3 292/1–2	292/3 293/1–2 293/3	294/1 294/2 294/3	295/1–2 295/3 296/1	296/2 296/3 297/1–2	297/3 298/1 298/2	298/3 299/1 299/2
Vib. Spec.	6/2		6/3		7/1		7/2		7/3		8/1	

INFORMATION FOR AUTHORS

Detailed "Instructions to Authors" for *Analytica Chimica Acta* was published in Volume 289, No. 3, pp. 381–384. Free reprints of the "Instructions to Authors" of *Analytica Chimica Acta* and *Vibrational Spectroscopy* are available from the Editors or from: Elsevier Science B.V., P.O. Box 330, 1000 AH Amsterdam, The Netherlands. Telefax: (+31-20) 5862 459.

Manuscripts. The language of the journal is English. English linguistic improvement is provided as part of the normal editorial processing. Authors should submit three copies of the manuscript in clear double-spaced typing on one side of the paper only. *Vibrational Spectroscopy* also accepts papers in English only.

Rapid publication letters. *Letters* are short papers that describe innovative research. Criteria for letters are novelty, quality, significance, urgency and brevity. Submission data: max. of 2 printed pages (incl. Figs., Tables, Abstr., Refs.); short abstract (e.g., 3 lines); *no* proofs will be sent to the authors; submission on floppy disc; *no* revision will be possible.

Abstract. All papers, reviews and letters begin with an Abstract (50–250 words) which should comprise a factual account of the contents of the paper, with emphasis on new information.

Figures. Figures should be suitable for direct reproduction and as rich in contrast as possible. One original (or sharp glossy print) and two photostat (or other) copies are required. Attention should be given to line thickness, lettering (which should be kept to a minimum) and spacing on axes of graphs, to ensure suitability for reduction in size on printing. Axes of a graph should be clearly labelled, along the axes, outside the graph itself.

All figures should be numbered with Arabic numerals, and require descriptive legends which should be typed on a separate sheet of paper. Simple straight-line graphs are not acceptable, because they can readily be described in the text by means of an equation or a sentence. Claims of linearity should be supported by regression data that include slope, intercept, standard deviations of the slope and intercept, standard error and the number of data points; correlation coefficients are optional.

Photographs should be glossy prints and be as rich in contrast as possible; colour photographs cannot be accepted. Line diagrams are generally preferred to photographs of equipment. Computer outputs for reproduction as figures must be good quality on blank paper, and should preferably be submitted as glossy prints.

Nomenclature, abbreviations and symbols. In general, the recommendations of IUPAC should be followed, and attention should be given to the recommendations of the Analytical Chemistry Division in the journal *Pure and Applied Chemistry* (see also *IUPAC Compendium of Analytical Nomenclature, Definitive Rules*, 1987).

References. The references should be collected at the end of the paper, numbered in the order of their appearance in the text (*not* alphabetically) and typed on a separate sheet.

Reprints. Fifty reprints will be supplied free of charge. Additional reprints (minimum 100) can be ordered. An order form containing price quotations will be sent to the authors together with the proofs of their article.

Papers dealing with vibrational spectroscopy should be sent to: Dr J.G. Grasselli, 150 Greentree Road, Chagrin Falls, OH 44022, U.S.A. Telefax: (+1-216) 2473360 (Americas, Canada, Australia and New Zealand) or Dr J.H. van der Maas, Department of Analytical Molecular Spectrometry, Faculty of Chemistry, University of Utrecht, P.O. Box 80083, 3508 TB Utrecht, The Netherlands. Telefax: (+31-30) 518219 (all other countries).

0003-2670/94/$07.00

CHEMOMETRICS TUTORIALS II

edited by **R.G. Brereton**, University of Bristol, Bristol, UK, **D.R. Scott**, U.S. Environmental Protection Agency, Research Triangle Park, NC, USA, **D.L. Massart**, Vrije Universiteit Brussel, Brussels, Belgium, **R.E. Dessy**, Virginia Polytechnic Institute, Blackburg, VA, USA, **P.K. Hopke**, Clarkson University, Potsdam, NY, USA, **C.H. Spiegelman**, Texas A&M University, College Station, TX, USA and **W. Wegscheider**, Universität Graz, Graz, Austria

The journal Chemometrics and Intelligent Laboratory Systems has a specific policy of publishing tutorial papers (i.e. articles aiming to discuss and illustrate the application of chemometric and other techniques) solicited from leading experts in the varied disciplines relating to this subject. This book comprises reprints of tutorials from Volumes 6-11 of this journal, covering the period from mid 1989 to late 1991. The authors of the papers include analytical, organic and environmental chemists, statisticians, pharmacologists, geologists, geochemists, computer scientists and biologists, which reflects the strong interdisciplinary communication. The papers have been reorganized into major themes, covering most of the main areas of chemometrics.

This book is intended both as a personal reference text and as a useful background for courses in chemometrics and laboratory computing.

1992 x + 314 pages
Paperback
Price: US $ 156.50 / Dfl. 250.00
ISBN 0-444-89858-1

ORDER INFORMATION

For USA and Canada
ELSEVIER SCIENCE

Judy Weislogel
P.O. Box 945
Madison Square Station,
New York, NY 10160-0757
Tel: (212) 989 5800
Fax: (212) 633 3880

In all other countries
ELSEVIER SCIENCE

P.O. Box 211
1000 AE Amsterdam
The Netherlands
Tel: (+31-20) 5803 753
Fax: (+31-20) 5803 705

US$ prices are valid only for the USA & Canada and are subject to exchange rate fluctuations; in all other countries the Dutch guilder price (Dfl.) is definitive. Books are sent postfree if prepaid.

ELSEVIER
SCIENCE

414\143\0036

0003-2670(19941010)296:2;1-A